The Relation of Sensory Adaptation and Stimulus Perception in the Rat Whisker-System

Dissertation

zur

Erlangung der naturwissenschaftlichen Doktorwürde
(Dr. sc. nat.)

vorgelegt der

Mathematisch-naturwissenschaftlichen Fakultät

der

Universität Zürich

von

Simon Musall

aus

Deutschland

Promotionskomitee

Prof. Dr. Fritjof Helmchen (Vorsitz)

Prof. Dr. Bruno Weber

Prof. Dr. Kevan Martin

Zürich, 2015

Für Lisa. In Liebe.

Zusammenfassung

Die Abnahme neuronaler Antworten bei wiederholter Präsentation eines sensorischen Stimulus ist eine weit verbreitete Eigenschaft, sowohl im peripheren als auch im zentralen Nervensystem. Diese sensorische Adaptation tritt in nahezu allen sensorischen Modalitäten auf und wird durch eine Vielzahl verschiedener Mechanismen, z.B. biophysikalische Effekte sensorischer Rezeptoren, inhibitorische Rückopplungen, intrinsische Zellmechanmismen oder Depression von Projektionssynapsen bedingt. Zahlreiche psychophysikalische Studien haben außerdem gezeigt das Adaptation einen signifikanten Einfluß auf die sensorische Wahrnehmung hat. Die anhaltende Präsentation eines sensorischen Stimulus reduziert hierbei die Wahrnehmung eines anschließend präsentierten Teststimulus, während die Unterschiede zwischen verschiedenen Stimuli verstärkt werden. Der genaue Zusammenhang zwischen neurophysiologischer und perzeptueller Adaptation ist jedoch weitgehend unbekannt. Das Ziel der vorliegenden Studie ist die Herstellung einer direkten Verbindung zwischen der Adaptation kortikaler Neuronen und der daraus resultierenden sensorischen Wahrnehmung. Hierzu wurde eine Kombination von elektrophysiologischen Ableitungen, optogenetischer neuronaler Stimulation und Verhaltensversuchen in dem somatosensorischen System der Ratte eingesetzt.

In **Kapitel 1** gebe ich eine Einführung über sensorische Adaptation und bespreche verschiedene Nachweise für seine physiologischen Ursachen, funktionellen Auswirkungen und Bedeutung für Stimuluswahrnehmung. Der erste Teil dieses Kapitels konzentriert sich auf generelle Adaptation die in einer Vielzahl verschiedener neuronaler Netzwerke auftritt. Der zweite Teil behandelt die Bedeutung von stimulus-spezifischer Adaptation (SSA), die einen Spezialfall darstellt und vor Allem im sensorischen Cortex auftritt. Der letzte Teil bietet eine Übersicht über die verschiedenen experimentalen Ansätze und Ziele der Arbeit.

Kapitel 2 behandelt die Hauptergebnisse meiner Arbeit und liegt in Form eines wissenschaftlichen Aufsatzes vor, der in dem wissenschaftlichen Magazin Nature Neuroscience veröffentlich wurde. Im Rahmen dieser Studie habe ich ein neuartiges Verhaltensparadigma zur psychophysikalischen Prüfung einzelner Schnurrhaarstimulationen genutzt und zusätzlich die Aktivität einzelner Neurone im Barrelfeld der Ratte

aufgezeichnet. Durch den Einsatz verschiedener theoretischer Modelle konnte ich das Verhalten trainierter Ratten auf Basis der stimulus-induzierten Aktivität kortikaler Neurone zutreffend beschreiben. Um einen kausalen Zusammenhang zwischen kortikaler Adaptation und Stimuluswahrnehmung herzustellen, induzierte ich die kortikale Expression des Blaulicht sensitiven Ionenkanals Channelrhodopsin-2. Im Gegensatz zur Stimulation einzelner Schnurrhaare, die frequenzabhängige Adaption auslöst, erzeugte die direkte Stimulation kortikaler Neurone adaptationsfreie, lichtinduzierte Antworten. Der direkte Vergleich der Verhaltensperformance mit Schnurrhaar- oder Lichtstimulation zeigte, dass die Umgehung der kortikalen Adaptation die interhemisphärische Diskrimierung von Stimulusfrequenzen stark verbessert aber gleichzeitig die Wahrnehmung von Intensitätsveränderungen einschränkt. Dies zeigt, dass die Adaptation kortikaler Neurone von kritischer Bedeutung für die Sinneswahrnehmung ist und die Wahrnehmung konstanter Reize reduziert um die perzeptuelle Intensität abweichender Stimuli zu verstärken.

Kapitel 3 beinhaltet die zweite Studie die ich während meines Doktorats durchgeführt habe und zurzeit zur Begutachtung bei dem wissenschaftlichen Magazin Cerebral Cortex vorliegt. Im Rahmen dieser Studie erweiterte ich unser Verhaltensparadigma durch eine Kombination verschiedener Stimulationsmerkmale und studierte so die perzeptuelle Bedeutung von SSA. Ich konnte zeigen, dass die gezielte Veränderung verschieden Stimulationsmerkmale, wie die Richtung einer Schnurhaar-Auslenkung oder Stimulation eines benachbarten Schnurrhaares, die Wahrnehmung eines abweichenden sensorischen Stimulus deutlich steigert. Änderungen der gleichen Merkmale induzierten außerdem einen Anstieg im Antwortverhalten einzelner Neurone im cortikalen Barrelfeld. Die Analyse der neuronalen Antworten in verschiedenen cortikalen Tiefen ergab, dass die Antworten auf abweichende Stimuli in spezifischen Schichten des Cortex verstärkt werden. Dies legt nahe, dass die stimulus-spezifische Detektion abweichender sensorischer Reize ein Merkmal intracorticaler Informationsverarbeitung ist.

In **Kapitel 4** diskutiere ich wie die verschiedenen Ergebnisse meiner Arbeit das bestehende Wissen über sensorische Adaptation erweitern und ihre Bedeutung für das Verständnis cortikaler sensorischer Verarbeitung.

Abstract

The attenuation of neuronal responses to repeated sensory stimulation is an omnipresent feature in both the peripheral and central nervous system. Such sensory adaptation occurs in virtually all sensory modalities and is caused by a variety of different mechanisms, including biophysical effects on sensory receptors, inhibitory feedback loops, intrinsic cellular mechanisms and short-term depression of projection synapses. Numerous psychophysical studies also showed that adaptation has a significant influence on sensory perception. Here, prolonged presentation of an adaptor stimulus reduces the perception of a subsequently presented test stimulus while markedly increasing the discriminability between different stimuli. However, the precise relation between these neurophysiological and behavioral results is widely unknown. The main objective of this thesis is to establish a direct relation between adaptation of cortical neurons and stimulus perception. To achieve this goal, I applied a combination of electrophysiological recordings, optogenetic neural stimulation and animal behavior in the rat whisker-system.

In **chapter 1**, I will provide an introduction to sensory adaptation and review the evidence for its physiological origins, functional implications for stimulus processing and importance for sensory perception. The first part of chapter 1 will focus on general adaptation that is widely observed in a variety of different neuronal circuits. The second part will focus on stimulus-specific adaptation (SSA), a special case of adaptation that mainly occurs in sensory cortex. The last part gives an overview of the experimental approaches and specific aims of the thesis.

Chapter 2 contains the main results of my project and is presented in the form of a research article that has been published in the scientific journal Nature Neuroscience. In this study, I used a novel behavioral paradigm for psychophysical testing of single-whisker stimuli and recorded the activity of sensory neurons in the rat barrel cortex. Using different theoretical models, I could closely describe the behavioral performance of trained rats based on stimulus-evoked activity of cortical neurons. To establish a causal relation between cortical adaptation and stimulus perception, I then induced the cortical expression of the blue light sensitive ion-channel channelrhodopsin-2. In contrast to whisker stimulation, which causes

frequency-dependent adaptation, direct light activation of cortical neurons resulted in non-adapting stimulus-evoked responses. The comparison of behavioral performance with either whisker or light stimulation revealed that circumventing adaptation strongly improves cross-hemispheric discrimination of stimulus frequency while reducing the detection of changes in stimulus intensity. This shows that sensory adaptation critically governs the perception of sensory stimuli, decreasing fidelity under steady-state conditions in favor of change detection.

Chapter 3 contains the second study that I conducted during my project, which is currently under revision at the scientific journal Cerebral Cortex. Here, I addressed the importance of SSA for stimulus perception by expanding our behavioral paradigm to a set of different stimulus features. I found that changes in specific stimulus features, such as whisker deflection direction or identity of a stimulated whisker robustly enhances detection of deviant stimuli. Changes in the same features also evoked stronger stimulus responses of single neurons in the barrel cortex. Analysis of neural responses in different cortical depths revealed that deviant responses are enhanced in specific cortical layers, suggesting that stimulus-specific deviance detection is a feature of intracortical information processing.

In **Chapter 4,** I discuss how the different results of the thesis expand the current knowledge on sensory adaptation and their implications for the understanding of sensory processing in cortex.

Contents

Chapter 1 : Sensory adaptation

1.1. Mechanisms, function and behavior

1.1.1. Introduction

The efficient encoding of sensory information to generate an according behavioral output is crucial for survival. As different organisms evolved, they developed a wide array of sensors to sample their environment and intricate neural systems to read-out the resulting sensory input. In virtually all these systems, an overarching theme is the ability to dynamically change the representation of physical events, based on contextual factors such as stimulus history or the behavioral state of the organism. A main feature that promotes this ability is sensory adaptation, the attenuation of neural responses to persistent stimulation (Adrian and Zotterman 1926). Sensory adaptation occurs in a variety of different forms and has wide-ranging implications for stimulus processing and behavior. In this first part of chapter one, I will provide an overview of the different sources for adaptation, the theoretical background on how adaptation improves sensory information flow and stimulus coding and eventually the psychophysical evidence on how adaptation affects stimulus perception in humans.

My doctoral thesis focuses on understanding the relation between neural adaptation in the somatosensory cortex and stimulus perception. This chapter will therefore focus on adaptation in the rodent somatosensory system to provide a background for the first study of my thesis that is described in detail in chapter two.

1.1.2. Subcortical adaptation in the rodent whisker-pathway

Sensory adaptation is particularly well studied in the rodent whisker-pathway, a part of the somatosensory system that conveys physical information from the facial whiskers. Rodents rely heavily on their whiskers for spatial navigation and object recognition and the whisker-pathway is a popular model to study sensory processing due its distinctive anatomical and functional structure (Diamond et al. 2008). Here, each individual whiskers represent a de-

fined stimulation area that has a one-to-one somatotopic representation from the whisker snout via several subcortical areas up to a specialized part of the primary sensory cortex, the so called barrel cortex (**Fig. 1.1.1a**) (Erzurumlu et al. 2010; Bosman et al. 2011). Adaptation occurs at various stages of this pathway and is first seen at the level of individual mechanical receptors in the whisker follicle. Here, cutaneous receptors are innervated by primary sensory neurons in the trigeminal ganglion (TG) that exhibit strong response depression to a continuous sinusoidal stimulus sequence, applied to a single whisker (Erzurumlu et al. 2010). The degree of response adaptation depends on specific properties of whisker stimulation and is particularly strong when facial muscles are paralyzed. It is also affected by other physiological factors that affect the viscoelacity of the skin (Fraser et al. 2006). Adaptation is therefore not exclusively a neuronal phenomenon but can also arise from mechanical effects that influence the signal transduction to individual receptors. Nerve endings from TG neurons have two types of mechanical receptors at the whisker base. Merkel discs are formations of Merkel cells and afferent nerve fibers (also known as Merkel-cell-neurite-complexes) while lanceolate endings are specialized mechanoreceptors that are part of the TG neurons. Both are sensitive to mechanical stimulation but convey largely different neural responses. Merkel discs elicit slowly adapting responses in their corresponding nerve fibers and thus faithfully represent changes of ongoing whisker movements (Bosman et al. 2011; Ikeda et al. 2014). They are mainly associated with encoding of objects in space (Fraser et al. 2006). In contrast, fibers with lanceolate endings exhibit rapidly adapting responses and thus predominately signal transient whisker deflections but remain inactive upon slow, continuous movements (Lumpkin et al. 2010; Bosman et al. 2011). TG neurons usually receive exclusive inputs from a single whisker and the majority are slowly adapting, based on their responses to single whisker deflections (Leiser and Moxon 2006).

Two trigemincal nuclei in the brainstem are the main projection target for whisker inputs from the TG: The principal trigeminal nucleus (PrV) and the spinal trigeminal nucleus (SpV) (Bosman et al. 2011). In both nuclei, projections from different whiskers are visible in barrelettes, cluster of neurons that receive input from the same whisker that can be visualized by cytochrome oxidase staining (Erzurumlu et al. 2010). Neurons in the brainstem show little response adaptation and generally resemble stimulus responses in the TG (Fraser et al.

2006; Ganmor et al. 2010a). Interestingly, adaptation in PrV neurons is less pronounced with increasing deflection velocity while the opposite is observed in TG neurons (Ganmor et al. 2010a). The exact mechanism behind this effect is not yet understood but has important implications for encoding of sensory stimuli. An increase in adaptation with stimulus intensity (as in TG neurons) could result in neural responses that fall below low-intensity responses during repeated stimulation. The resulting coding ambiguity of stimulus intensity during adaptation is prevented by reversing intensity-dependent response adaptation in PrV neurons (Ganmor et al. 2010a). This effect is not observed in the SpV, suggesting that its downstream targets encode different whisker-related information (Mohar et al. 2013).

Neurons in the brainstem project to different nuclei in the thalamus, the ventral posteromedial nucleus (VPM) and the posteromedial nucleus (POm). Furthermore, the reticular nucleus (RT), an aggregation of GABAergic interneurons, forms a sheet-like structure that surrounds the thalamus and provides intrathalamic inhibition to both VPM and POm. The RT has been attributed to significantly contribute to thalamic adaptation due to buildup of inhibition, thereby controlling the information flow from brainstem to the somatosensory cortex (Hartings and Simons 2000; Hirata et al. 2009).

There are three major pathways from the brainstem to the somatosensory thalamus and eventually the cortex (**Fig. 1.1.1b**). The lemniscal pathway originates in the PrV and projects to the dorsomedial section of the VPM (VPMdm). It conveys mostly single-whisker information to the barreloids in VPM, whisker-specific structures that are analogous to the barrelettes in PrV (Erzurumlu et al. 2010; Bosman et al. 2011). VPM neurons then project to the whisker-specific barrels in barrel-cortex layer IV, as well as layer Vb. They also form intrathalamic connections to RT neurons that project back to VPM, thus creating a negative feed-back loop (Ganmor et al. 2010a). However, because RT neurons adapt more strongly than VPM neurons, sustained stimulation can lead to subsequent disinhibition of the VPM. Overall, the degree of adaptation in the lemniscal thalamus is relatively low and mainly occurs at stimulation frequencies above 12 Hz (Hartings et al. 2003; Khatri et al. 2004a). The paralemniscal pathway originates in the whisker unspecific area of the SpV and projects to the POm. POm neurons target several cortical areas including the barrel cortex, the second-

ary somatosensory cortex (S2) and the primary motor cortex (M1) (Bosman et al. 2011). In the barrel cortex they terminate in cortical layers I and Va and additionally project to layer IV in the area between cortical barrels, the septa (Meyer et al. 2010). POm neurons also exhibit moderate adaptation that is slightly more pronounced as in the VPM (Landisman and Connors 2007). Most probably, POm neurons show the same adaptation behavior as in the SpV and therefore adapt more strongly at higher stimulus intensities, although this has not yet been experimentally confirmed. The third pathway, the extralemniscal pathway, also originates in the SpV but conveys a mixture of whisker-specific and multi-whisker information and targets the ventrolateral part of the VPM (VPMvl) that has less distinct tuning to individual whiskers (Diamond et al. 2008; Bosman et al. 2011). Thalamocortical projections in the extralemniscal pathway target mainly S2 and only weakly project to layer IV barrels (Bosman et al. 2011). Sensory adaptation in the extralemniscal pathway is not well characterized but it may relate more closely to adaptive behavior in the paralemniscal pathway as they both arise from neurons in the SpV.

Each of the three pathways is assumed to convey different information about whisker movements. A prominent hypothesis is that the paralemniscal pathway conveys information about whisker kinematics during active whisker movement, the extralemniscal pathway the exact timing of object contacts and the lemniscal pathway detailed information on both whisker movement and touch (Bosman et al. 2011; Diamond et al. 2008). However, the functional role of each pathway has not yet been directly tested and is still subject of future research. Aside of the lemniscal, paralemniscal and extralemniscal pathway, there are at least three additional pathways that all convey multi-whisker information but are not yet fully characterized (Bosman et al. 2011). The functional role of these pathways and their respective degree of adaptation is currently unknown.

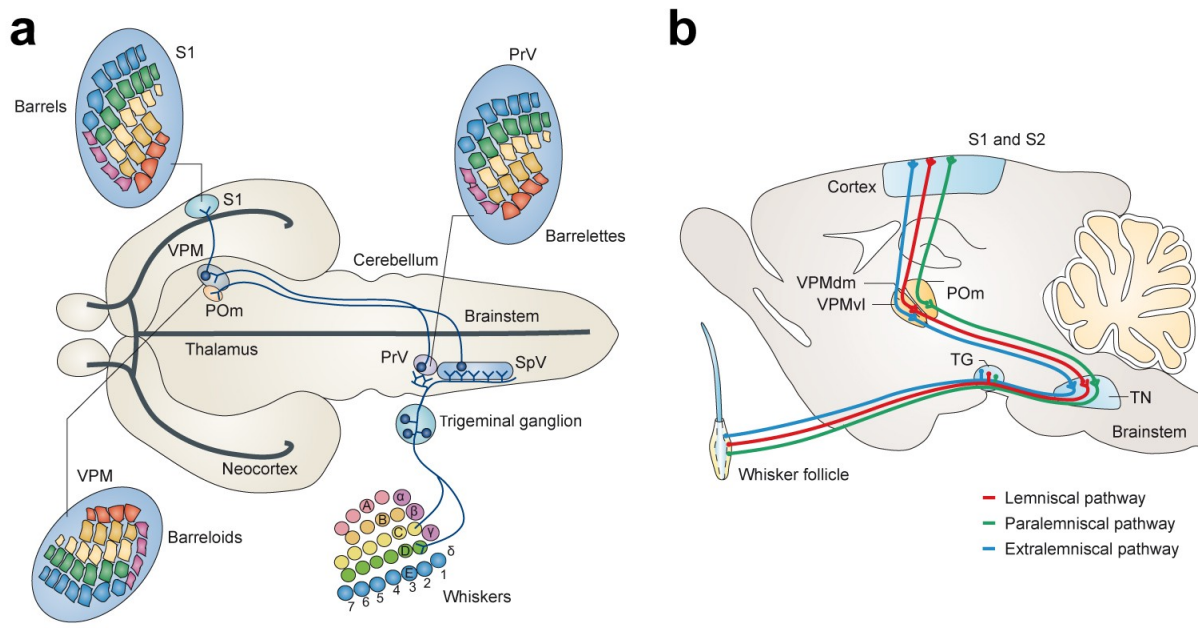

Figure 1.1.1. Overview of the rodent whisker-pathway

a, The highly ordered structure of individual whiskers on the whisker pad (bottom right) is somatotopically conserved along different stages of the rodent whisker pathway. In the brainstem, an anatomical representation of the whiskers are the barrelettes that are particularly pronounced in the PrV (top right). The thalamic VPM contains the so called barreloids (bottom left) that are transmitted in a one-to-one fashion to the barrels in layer IV of the somatosensory cortex (top left). Panel modified after Erzurumlu et al. 2010 **b**, Whisker specific information is transmitted from the TG, to the trigeminal nuclei (TN) and via different nuclei in the thalamus to the primary and secondary somatosensory cortex. Projections are separated into three major pathways: The lemniscal (red), paralemniscal (green) and extralemniscal pathway (blue). The lemniscal and extralemniscal pathway are relayed through different parts of VPM (VPMdm and VPMvl) respectively. The paralemniscal pathway is gated through the POm and innervates different layers of S1 and S2. Panel modified after Diamond et al. 2008.

1.1.3. Adaptation in somatosensory cortex

In contrast to the moderate adaptation in the thalamus, several studies showed that neural responses in layer IV of the barrel cortex are highly adaptive to repeated whisker stimulation (Chung et al. 2002; Khatri et al. 2004b; Katz et al. 2006). The most common explanation for this increase in adaptation is the frequency-dependent, short-term depression of thalamocortical synapses (Chung et al. 2002). In contrast to general firing-rate adaptation, e.g. signal generation at the receptor level or inhibitory buildup, cortical adaptation is therefore mainly attributed to input depression rather than the inability of cortical neurons to generate spikes.

Cortical adaptation is highly related to changes in behavioral state and most prominent in quiescent states, such as sleep, anesthesia or awake immoblity (Castro-Alamancos 2002). Conversely, adaptation is suppressed in more active states, such as active exploration (Fanselow and Nicolelis 1999) or learning (Castro-Alamancos 2004a). The relationship between cortical adaptation and arousal is mostly explained by changes in the spontaneous activity of thalamic neurons. The degree of thalamic excitability is controlled by the reticular formation in the brainstem (Castro-Alamancos 2004a) but also modulated by feedback projections from cortical layer VI in S1 (Mease et al. 2014). Thalamic firing increases during arousal (Castro-Alamancos and Oldford 2002) and therefore results in a higher degree of activity-dependent depression of thalamocortical synapses (Fanselow and Nicolelis 1999; Castro-Alamancos 2004a). Such pre-adapted thalamocortical signal transmission results in lower stimulus-evoked responses in cortex (Castro-Alamancos and Oldford 2002), that shows only weak adaptation to repeated stimulation. This effect is further amplified by different firing modes of thalamic neurons that respond to sensory stimulation in either a burst of 2-10, high-frequency spikes or by tonic firing where only a single stimulus-evoked spiking response is generated (Sherman 2001). Bursting mainly occurs in quiescent states and thalamic neurons rapidly shift to tonic firing with sustained sensory stimulation (Fanselow et al. 2001). Switching between bursting and tonic firing is therefore a way to dynamically change the sensory information that is transmitted to the cortex.

Cortical neurons also adapt more strongly to stimulation of whiskers that are adjacent to their respective barrel (Katz et al. 2006) and changes in behavioral state as well as sustained stimulation therefore result in a spatial sharpening of neural responses in S1 (Moore et al. 1999; Ollerenshaw et al. 2014). It has been suggested that this increase in both temporal and spatial precision during adaptation is advantageous for perceptually challenging tasks such as fine texture and object recognition (Fanselow and Nicolelis 1999; Castro-Alamancos 2004a). However, increased perceptual precision comes at the cost of reduced awareness of sensory stimuli in general. Adaptation therefore represents a trade-off between detection and discrimination of sensory information that is adjusted depending on behavioral demands. This was confirmed by a recent study in trained rats, showing that previous presentation of an adapting stimulus sequence reduces the animals sensitivity to

detect a single test stimulus while increasing the ability to identify which whisker was stimulated (Ollerenshaw et al. 2014).

Cortical adaptation may additionally depend on intrinsic mechanisms, such as prolonged hyperpolarization of cortical neurons observed in cat visual cortex after sustained visual stimulation (Carandini and Ferster 1997; Sanchez-Vives et al. 2000). However, later studies in the rodent somatosensory cortex were unable to reproduce these earlier findings (Chung et al. 2002; Katz et al. 2006). A potential reason for this mismatch could be that adaptation operates on multiple timescales and intrinsic mechanisms only account for effects after substantial stimulus exposure in the range of tens of seconds and longer (Chung et al. 2002).

1.1.4. Functional roles of adaptation

Adaptation is a key mechanism to adjust the gain of a sensory stimulus to modulate the dynamic range of a given sensory system (Wark et al. 2007). This is important because sensory neurons are believed to primarily encode external stimuli by the rate at which they generate spikes. However, the range of firing rates that a neuron can produce is very limited compared to the range of physical stimuli that can be encountered in the external world. Adaptation provides an efficient solution for this problem by adjusting the neural representation of a given sensory stimulus depending on the statistics of the environment (Dean et al. 2005; Maravall et al. 2007). As described above, a sensory stimulus that is presented in the absence of ongoing stimulation will trigger a strong neural response. However, if a stimulus occurs after presentation of an adaptor sequence, the respective neural response amplitude will be reduced in accordance to the background intensity (**Fig. 1.1.2a**) (Adibi et al. 2013). Moreover, a sensory stimulus still evokes the maximal neural response amplitude if it is strong enough relative to the adaptor intensity. Adaptation is therefore not a subtractive mechanism that generally reduces neuronal response amplitude but adjusts the threshold for neural responses to remain above the intensity of ongoing background stimulation (**Fig. 1.1.2b**). In case of a uniform adaptor sequence, the shift in neural tuning curves occurs relative to the background intensity which is defined as mean stimulus velocity over a given period of time. Naturalistic stimulus sequences however are usually non-uniform and there-

fore additionally fluctuate in other statistical properties such as the variance of the stimulus distribution (Wark et al. 2007). By presenting Gaussian white noise stimuli of periodically changing variance (**Fig. 1.1.2c)**, Maravall et al. found that changes in variance also induce a scaling of neural tuning curves (Maravall et al. 2007). Here, tuning curves were not shifted but stretched out with higher compared to lower stimulus variance, thus covering the full range of presented stimulus velocities (**Fig. 1.1.2d)**. Notably, this adaptation to variance occurred over rather long timescales (in the range of several seconds) compared to intensity adaptation which usually occurs after about 100 miliseconds (Fairhall et al. 2001; Wark et al. 2007). It is possible that adaptation to different statistical properties is due to independent physiological mechanisms, namely fast adaptation due to depression of synaptic inputs (Chung et al. 2002; Katz et al. 2006) and adaptation over longer timescales due to changes in intrinsic cellular mechanisms (Carandini and Ferster 1997; Sanchez-Vives et al. 2000). The implementation of such different timescales for adaptation may be beneficial to optimize the time required for an adaptive system to accurately estimate changes in the statistical properties of a stimulus distribution.

1.1.5. Perceptual implications of adaptation

As expected from the widespread response adaptation in different sensory systems, adaptation has important implication for stimulus perception and behavior. Most of the studies that focused on the perceptual role of adaptation were done in humans and applied the experimental framework of psychophysics. Within psychophysics, a standard set of experimental designs and analysis tools has been developed to infer how physical properties of a test stimulus relate to stimulus perception (Green and Swets 1989). Here, two classical concepts are the laws by Weber and Fechner which describe how sensory stimulus perception changes relative to stimulus intensity. Weber's law states that the minimal discernible difference (also known as the just noticeable difference or JND) between to stimuli is proportional to stimulus magnitude. The JND for a given sensory stimulus is therefore a fraction of its intensity; in case of somatosenstation a change in three percent or more in applied skin pressure (Green and Swets 1989). Fechner's law states that sensory perception is not linear-

ly proportional to stimulus intensity but follows a logarithmic scale, also known as Fechner's scale. Both principles combined are sometimes referred to as the Weber-Fechner law.

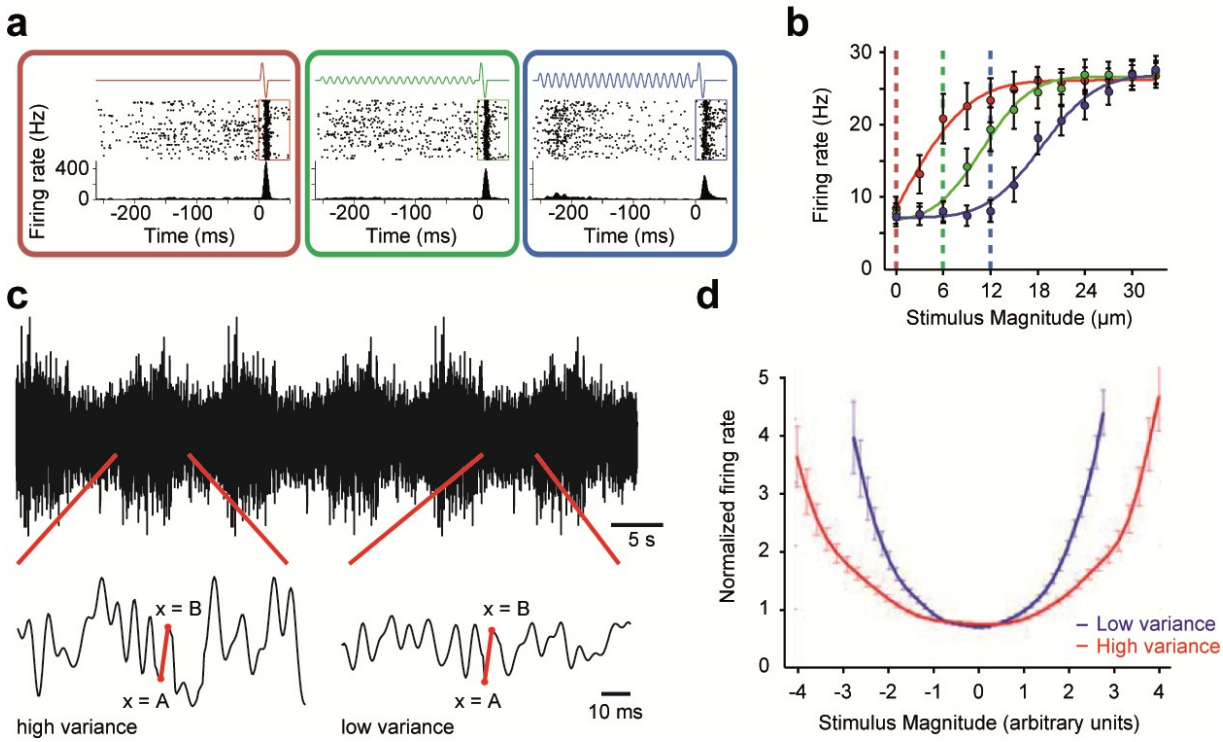

Figure 1.1.2. Adaptation alters neuronal response functions
a, Neural responses to a test stimulus after presentation of a uniform adaptor stimulus sequence. Neural responses are highest when the test stimulus is presented without any adaptor sequence (red square) and successively reduced with increasing adaptor intensity (green and blue squares). **b,** Responses to the test stimulus are shifted in accordance to the intensity of the adaptor sequence (dashed lines). In all three cases, neurons only respond to stimuli of higher intensity as the adaptor sequence but reach the same response amplitude if the stimulus intensity is sufficiently high. Panels **a** and **b** modified after Adibi et al. 2013. **c,** Example of a Gaussian noise stimulus sequence with alternating variance. The stimulus sequence consists of episodes of either high or low variance and neural tuning curves were computed by comparing events where a change from position A to subsequent position B was the same in both conditions (marked in red). **d,** The neural response function scales with stimulus variance. At higher stimulus variance, the neural response function is not shifted but stretched out (red) compared to low variance stimulation (blue). Panels **c** and **d** modified after Maravall et al. 2007.

To study how stimulus detection and discrimination is affected by adaptation, an adaptor sequence is presented prior to a test stimulus, usually applied to the fingertip or the back of the hand, and human subjects report their respective stimulus perception by choosing one out of two possible response options. This is known as a two-alternative forced choice (2-AFC) paradigm. In accordance with reduced neural responsiveness during adaptation, pre-

exposure of an adaptor sequence has been shown to reduce the perceived intensity of a subsequent stimulus (Laskin and Spencer 1979; Gescheider et al. 1995). This effect, known as forward masking, depends on both the amplitude and duration of the adaptor sequence (Gescheider et al. 1995). Conversely, adaptation increases subject's ability to discriminate various stimulus properties, such as stimulus location (Tannan et al. 2006), amplitude (Goble and Hollins 1993; Tannan et al. 2007) or stimulation frequency (Tommerdahl et al. 2005). Overall, these psychophysical studies are in good agreement with neurophysiological results of adaptation. However, it remains unclear which physiological mechanisms are decisive for the observed behavioral effects. Due to the widespread occurrence of adaptation it may be that adaptation in either the peripheral or the central nervous system is more important to shape sensory perception.

A more direct approach to establish a relation between neural stimulus response behavior and perception is the psychophysical testing of trained animals, which was classically done in primates (Talbot et al. 1968; Mountcastle et al. 1972; Romo et al. 1998). More recently, psychophysical testing has been extended to rodents where most of the neurophysiological research on sensory adaptation had been conducted (Carandini and Churchland 2013). As part of this new line of study, Ollerenshaw et al. were the first to show a relation between adaptation-induced spatial sharpening of cortical representations in somatosensory cortex and discrimination of the location of a single-whisker stimulus (Ollerenshaw et al. 2014). Furthermore, they found that the perceptual intensity of whisker stimuli was reduced after adaptation. In line with earlier psychophysical results, they suggested that adaptation reflects a trade-off between stimulus detectability and discriminability that is mainly driven by adaptation of cortical neurons in somatosensory cortex. Using a theoretical model of thalamocortical circuitry, they suggested that cortical adaptation is mainly a result of thalamic firing behavior and depression of thalamocortical synapses.

1.2. Stimulus-specific adaptation

1.2.1. Feature selectivity

The hypothesis that cortical adaptation mainly depends on short-term depression of thalamocortical synapses has wide-ranging implications for stimulus processing and perception. Aside of the ones already discussed, it may account for an important feature of adaptation that has been described in several sensory modalities, especially the visual (Movshon and Lennie 1979; Müller et al. 1999; Reches et al. 2010; Dhruv and Carandini 2014) and auditory (Ulanovsky et al. 2003; von der Behrens et al. 2009; Farley et al. 2010; Mill et al. 2011; Taaseh et al. 2011; Hershenhoren et al. 2014) but also the somatosensory (Katz et al. 2006) system: stimulus specificity. Stimulus-specific adaptation or SSA is also defined by a reduction of neural responses to highly repetitive stimulation but in contrast to firing-rate adaptation or neural fatigue, SSA does not generalize towards other stimulus features (Nelken 2007). A sensory neuron that adapts to a highly repetitive stimulus therefore retains its responsiveness when a different low-probability stimulus is presented. SSA thus represents a more complex form of adaptation and has been proposed as a single-cell correlate of the psychological phenomenon of habituation (Netser et al. 2011; Gutfreund 2012). Habituation is a behavioral phenomenon that describes the ability of many organisms to widely ignore a sensory scene while remaining responsive to specific stimuli that break the background regularity (Rankin et al. 2009). For example when a student is working in a noisy environment and subconsciously ignores loud noises from his coworkers but immediately responds to his professor when he enters the room. Importantly, such unexpected events do not have to be of higher intensity as the ongoing background (as might be expected with general adaptation) but convey deviating stimulus features or irregularities to evoke sensory perception. Habituation is also considered as the simplest form of learning (Dudai 2004; Rankin et al. 2009) and has been described behaviorally in numerous species (Thompson 2009).

The following sections will summarize the implications of stimulus-specificity for the framework of sensory adaptation. I review the available evidence for the functional anatomy of SSA in the mammalian sensory pathway and different physiological mechanisms that

may account for the generation of SSA. Most of this evidence is derived from studies in the auditory system, on which the following chapter therefore will focus. However, the available evidence from other sensory areas suggests that SSA is in fact a general mechanism of sensory processing, especially in the neocortex. Also, different data in favor of or against SSA as a correlate of mismatch negativity (MMN) (Näätänen 1992), a deviant-specific signal component in human electroencephalographic (EEG) measures (Näätänen 2009) are provided. This second part of chapter one should give an extended perspective on adaptation in sensory systems and forms the basis for the second study of my doctoral project that focuses on SSA in somatosensory cortex and will be presented in chapter three.

1.2.2. Experimental background

The first feature-selective adaptation of single neurons was observed by Movshon and Lennie who studied adaptation of single neurons in the visual cortex (Movshon and Lennie 1979). Here, prolonged presentation of a specific grating stimulus selectively reduced neural response amplitude which could be rescued by presenting gratings of similar contrast but different orientation. They concluded that the observed single-cell adaptation was selective for grating orientation and coined the term stimulus-specific adaptation to describe this effect. Later, this notion was expanded to even more complex visual stimuli (Müller et al. 1999) and similarly observed in auditory neurons, responding to pure tones of different frequency (Ulanovsky et al. 2003, 2004), duration (Umbricht et al. 2005) or amplitude (Ulanovsky et al. 2004). In all these studies, the hallmark of SSA was an increased neural response to a low-probability deviant compared to a high-probability standard stimulus.

To measure such deviant-standard differences a commonly used experimental approach is the oddball paradigm that was originally designed to study MMN in humans (Squires et al. 1975a) (see also subchapter 1.2.6). In this paradigm, a sequence of repeatedly presented identical stimuli (‘standard’) is randomly interrupted by a deviant stimulus (‘deviant’) that differs in a given stimulus feature, such as tone frequency or duration. Usually, deviant stimuli are presented at low probabilities of about 10 % and deviant-standard differences decrease with increasing deviant presentation probability (Ulanovsky et al. 2003). After a first stimulation sequence, the corresponding features of standard and deviant stim-

uli are swapped and a second sequence of equal length is presented (**Fig. 1.2.1a**). By analyzing standard and deviant responses to the same stimulus feature (being standard in one sequence and deviant in the other), the oddball paradigm allows to study the influence of stimulus presentation probability on neural response amplitude to a given sensory stimulus (Ulanovsky et al. 2003; Nelken 2007). This setting of the oddball paradigm is sometimes also referred to as a 'flip-flop' design (Harms et al. 2014). The oddball paradigm was first applied to study SSA by Ulanovsky et al. who found significant SSA to different tone frequencies in single neurons in cat auditory cortex (Ulanovsky et al. 2003) (**Fig. 1.2.1b**). SSA in single neurons is even evoked in sequences with a 50-50 % feature distribution when comparing stimulus responses that were preceded by a different stimulus feature with those that were preceded by an identical stimulus. This rapid, local-context effect is called the '1-trial effect' (Ulanovsky et al. 2004).

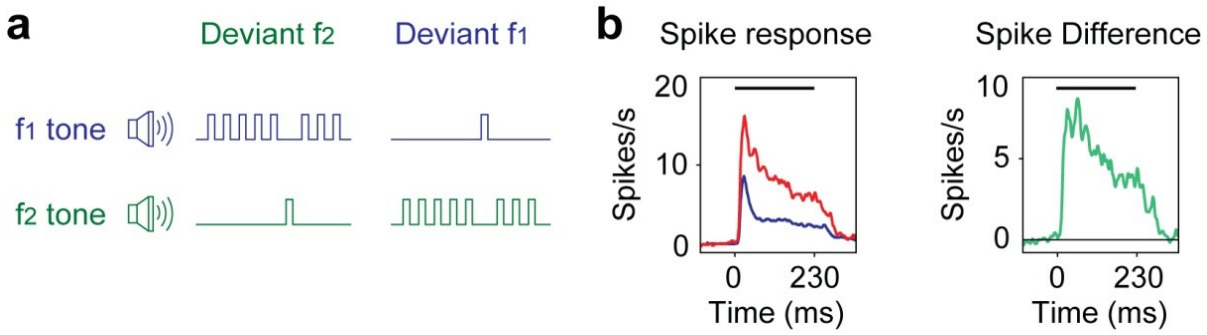

Figure 1.2.1. The auditory oddball paradigm and deviant responses in A1.
a, Illustration of the basic oddball paradigm. A sequence of low frequency standard tones (f_1) is commonly presented and randomly interrupted by a rare, high frequency (f_2) deviant tone. After a total of 1000 stimuli, the identity of deviant and standard are swapped. **b,** Left panel: Neural responses to deviants and standards (using the responses to the standard stimulus immediately before a deviant), averaged over all stimulus presentations. Standard stimulation (blue) evokes weaker neural responses as deviant stimulation (red) over the whole course of the stimulus presentation (200 ms, black bar). Right panel: Absolute spiking differences in response to deviant and standard stimulation. The increased response strength to deviant versus standard stimulation is characteristic for the existence of SSA. Neural responses are taken from Ulanovsky et al. 2003.

Aside of measuring absolute deviant-standard differences Ulanovsky et al. also introduced the SSA-index (SI), a normalized measure of deviant-induced response changes. The SI is computed by the difference of the averaged deviant and standard responses to a specific stimulus feature, divided by their sum.

$$\mathrm{SI} = \frac{\mathrm{d}(f) - \mathrm{s}(f)}{\mathrm{d}(f) + \mathrm{s}(f)} \tag{1}$$

In this formula, deviant d(*f*) and standard responses s(*f*) represent the mean spiking response to a respective stimulus feature *f*. The SI is normalized between -1 and 1, with negative values indicating a stronger response to standard and positive values to deviant stimuli. The main advantage of using the SI over absolute deviant-standard differences is that it represents a relative measure of deviant-induced response changes that is less sensitive to the general responsiveness of a given neuron. Without this correction, most SSA results are dominated by deviant-standard differences in neurons with generally high-firing rates (Ulanovsky et al. 2003). An extension of this approach is the common SI (CSI) which combines relative deviant-standard response difference for multiple stimulus features and thus provides a more generalized measure of SSA.

$$\mathrm{CSI} = \frac{(\mathrm{d}(f_1) + \mathrm{d}(f_2)) - (\mathrm{s}(f_1) + \mathrm{s}(f_2))}{\mathrm{d}(f_1) + \mathrm{d}(f_2) + \mathrm{s}(f_1) + \mathrm{s}(f_2)} \tag{2}$$

For the CSI, d(f_i) and s(f_i) represent the mean spiking response to the two stimulus features (f_1 and f_2) that are usually presented in the oddball paradigm. Most recent studies have adopted this approach and used a combination of the oddball paradigm and SI analysis to quantify SSA. However, although the SI and CSI are currently in common use it is important to note that the integration of outgoing signals from sensory cortices to other brain areas is not well understood. Whether absolute (i.e. the overall amount of generated spikes) or relative changes in deviant-induced responses are ultimately more important for stimulus perception is therefore widely unknown.

1.2.3. Functional anatomy of SSA

The functional anatomy of SSA has been studied most extensively studied in the auditory system. Here, various studies used a pure tone oddball paradigm with different tone frequencies to test SSA of neurons at different stations of the auditory pathway up to the secondary auditory cortex. While no consistent SSA was found in the cochlear nucleus of the brainstem (Ayala et al. 2012), it appears to be widespread in other subcortical areas (**Fig. 1.2.2**). Several studies demonstrated SSA in the rat inferior colliculus (IC) (Malmierca et al. 2009; Duque et al. 2012), thalamic reticular nucleus (Yu et al. 2009) and the medial geniculate body (MGB) (Antunes et al. 2010; Bäuerle et al. 2011). Within these areas, SSA is not evenly distributed but only apparent in the non-lemniscal pathway which is associated with the processing of complex sound features (Nelken 2014). SSA is mostly found in the dorsal area of the IC and the medial and dorsal subdivisions of the MGB (Antunes et al. 2010), both of which are part of the non-lemniscal pathway. In contrast, recordings in the lemniscal parts of this subcortical areas yielded very weak SSA (Anderson et al. 2009; Malmierca et al. 2009; Bäuerle et al. 2011) and a recent study in the lemniscal part of MGB showed that deviant responses can be abolished by pharmacological inactivation of cortex (Bäuerle et al. 2011). Hence, weak subcortical SSA in the lemniscal auditory thalamus might be due to corticofugal back projections from cortex which appears to be the first lemniscal station that shows genuine SSA.

The distribution of SSA in other sensory pathways is not as well understood. In the visual pathway SSA has been mainly reported in the primary visual cortex (Movshon and Lennie 1979; Müller et al. 1999; Reches et al. 2010; Dhruv and Carandini 2014) but also the higher visual area MT (Patterson et al. 2014), while no evidence for SSA was found in the lateral geniculate nucleus in thalamus (Dhruv and Carandini 2014). In the somatosensory system reports on SSA are scarce and have only been reported in the somatosensory cortex (Katz et al. 2006). Although the specificity of somatosensory adaptation is less clear, it is reasonable to assume that SSA is equally observed in different sensory areas and may be generated by the same physiological mechanism.

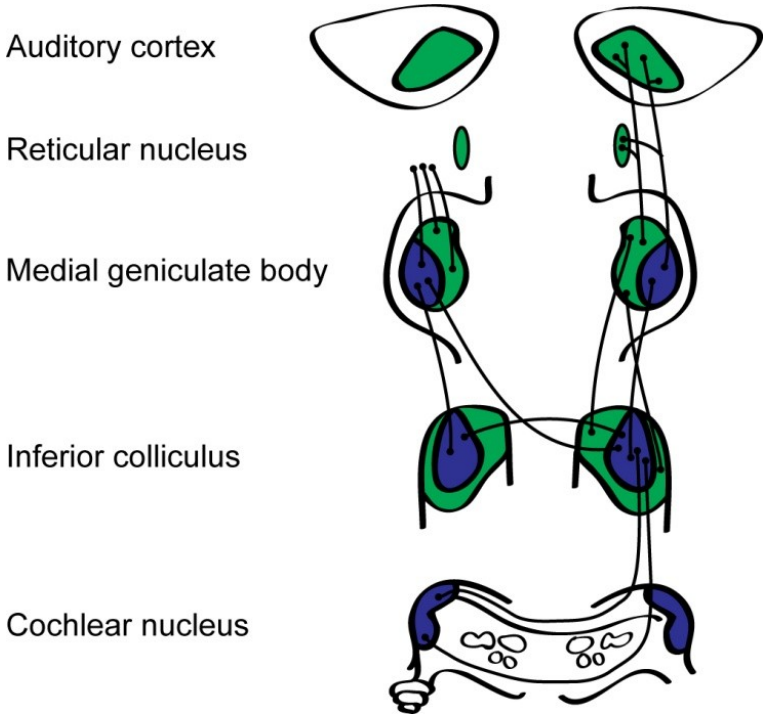

Figure 1.2.2. SSA in the auditory pathway.
Illustration of SSA in different areas of the auditory pathway. Blue areas show very weak or no SSA. Areas that show robust SSA are marked in green. SSA is found in the non-lemniscal parts of the IC and MGB, the thalamic reticular nucles and the auditory cortex. No SSA was found in the cochlear nucleus. Figure modified after Nelken 2014.

1.2.4. Potential mechanisms of SSA

As stated in section 1.2.1, SSA cannot be accounted for by a generalized reduction in neural excitability as sensory neurons are still responsive to deviant stimulus presentation. Several models have been proposed to account for sensory SSA and it may also be that the observed neural responses are due to the combination of several distinct mechanisms. A general methodological issue is in the exclusive usage of the CSI for SSA analysis. Here, overly strong neural tuning towards one stimulus feature can result in a robust deviant-standard response difference for the preferred feature but no response to either standard or deviant of the non-preferred feature. As the non-preferred response difference is zero, the CSI will be dominated by responses to the preferred stimulus and thus lead to the assumption of true SSA although responses could also be explained by general adaptation. Some past studies did not control for this possibility by also analyzing SIs to different stimulus features separately, which may have led to a false-positive report of SSA in the recorded areas (Duque et al. 2012; Nelken 2014). A second mechanism that contributes to SSA is the relation between synaptic inputs to a sensory neuron and its respective spiking threshold. While both stand-

ard and deviant stimulation may evoke corresponding changes in the membrane potential, the spiking threshold can increase their relative difference if deviant stimulation evokes a robust spiking response while standard stimulation remains mainly below threshold. Although this mechanism, called the 'Iceberg effect' only applies if SSA already exists in the neuronal inputs, it may generate increases in SSA, for example in the neocortex (Katz et al. 2006; Dhruv and Carandini 2014; Hershenhoren et al. 2014).

The most commonly assumed mechanism for *de novo* generation of SSA is based on the frequency-dependent adaptation of stimulus-specific inputs on a single sensory neuron. As mentioned earlier, cortical adaptation is mainly due to depression of thalamocortical synapses, leading to an attenuation of thalamocortical signal transmission with repeated stimulation (Chung et al. 2002; Khatri et al. 2004b; Katz et al. 2006; Castro-Alamancos 2002). Adaptation in the receiving sensory neuron is therefore not a neuronal fatigue that prevents the generation of a stimulus-evoked spiking response but a reduction in synaptic input strength. In this case, stimulus-specificity can be achieved if different synaptic inputs transmit stimulus-specific information that converges on the same sensory neuron. The adaptation of one of these sensory channels will selectively reduce the neurons responses to the corresponding stimulus while remaining responsive to other synaptic inputs that convey differential stimulus features. In the auditory system this model is also known as the adaptation of narrowly tuned modules (ANTM) model (Nelken 2014). Although the ANTM model accounts for several important aspects of SSA, it does not accurately predict the strength of deviant responses that are observed in sensory cortex (Taaseh et al. 2011). This was also demonstrated at the level of membrane potentials of cortical neurons, thus excluding that stronger cortical SSA might be explained by a combination of input depression and the iceberg effect (Hershenhoren et al. 2014). It is therefore likely that SSA in cortex is amplified by intracortical stimulus processing, although the exact mechanism is still not understood.

1.2.5. True deviance detection and experimental controls

SSA in auditory cortex has also been shown to exhibit 'true' deviance detection; a selective increase in neural response strength when a deviant interrupts the regularity of a standard sequence (Ulanovsky et al. 2003; Taaseh et al. 2011; Hershenhoren et al. 2014). Importantly,

this is different from the main assumption of the ANTM model that explains difference between deviant and standard stimuli by the selective adaptation of standard responses. Because this additional feature of SSA cannot be explained by input adaptation, it has been stated that the term stimulus-specific adaptation might be misleading and should be replaced by single-cell habituation (Nelken 2007, 2014).

Testing for true deviance detection requires additional experimental controls because the standard flip-flop design allows no general differentiation whether deviant-standard differences are due to reduced standard or increased deviant responses. The first control that can be applied is the usage of a deviant-alone setting where deviant stimuli are presented as in the basic oddball paradigm but standard stimulation is omitted (**Fig. 1.2.3a)**. Deviant-alone stimulation therefore allows to measure deviant responses in the absence of standard stimulation which can then be compared to deviant responses in the basic oddball paradigm. This comparison allows an assessment of whether deviant-standard differences can be explained by an adaptation model, which predicts that a deviant-alone should be stronger or at least equally strong as in the flip-flop design. In contrast, true deviance detection would predict that a deviant in the flip-flop design represents a rule violation from the standard sequence and should thus evoke a larger response as the deviant-alone. Several SSA studies that used this approach found that a deviant in the flip-flop design evokes weaker response as with deviant alone stimulation (Eriksson and Villa 2005; Umbricht et al. 2005; Todd et al. 2013), arguing against deviant responses as a prediction error signal.

However, the main strength of the deviant-alone control, i.e. that it predicts opposing results when assuming either input adaptation or a prediction error, is also its main disadvantage. If both mechanisms are affecting standard and deviant responses simultaneously, the deviant-alone control may be too conservative because a prediction error can only be recognized if it overcomes lower deviant responses due to the standard-evoked adaptation load (Nelken 2007; Todd et al. 2013). To circumvent this problem, a better control should induce a comparable degree of adaptation without the regularity that is established in the flip-flop design. Hence, a second control has been established where a wide range of different standard stimuli are randomly presented in one sequence. In this ‘many-standards’ de-

sign, every presented stimulus has the same probability as the deviant in the flip-flop design but because of the random stimulation pattern a deviant stimulus does not represent a rule violation from a fixed stimulus sequence (**Fig. 1.2.3b)**. Using this control, several studies showed that deviant responses may indeed encode true deviance detection because deviant stimuli evoke stronger responses in the flip-flop design as in the many-standards control, which is not explained by the ANTM model (Ulanovsky et al. 2003; Taaseh et al. 2011; Hershenhoren et al. 2014; Imada et al. 2012). Furthermore, a recent study by Yaron et al. (Yaron et al. 2012) showed that absolute deviant responses are stronger in a random than a periodic oddball sequence (**Fig. 1.2.3c)**, demonstrating that neural responses are sensitive to specific patterns in stimulus history that go beyond changes in stimulus presentation probability.

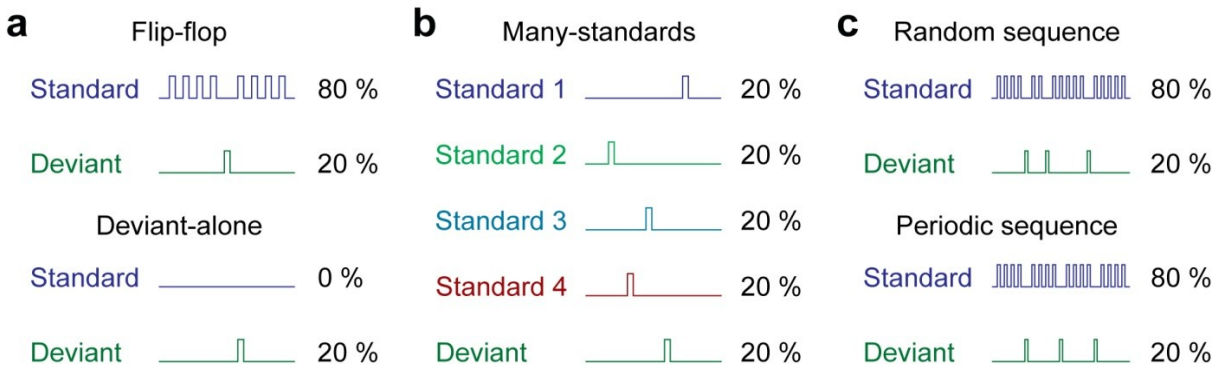

Figure 1.2.3. Overview of different experimental paradigms
a, Comparison of the classic flip-flop and the deviant-alone paradigm. Numbers to the right indicate the probability of standard and deviant stimulus presentation in percent. During deviant-alone stimulation, the deviant sequence is conserved but standard stimuli are omitted. **b**, Illustration of the many-standards paradigm. A sequence is composed of a randomized combination of different standards and the deviant stimulus. While the deviant sequence is the same as in the flip-flop design, there is no fixed background sequence against which a deviant stimulus could evoke a rule violation signal. **c**, Comparison of a fully randomized and a sequential oddball sequence. In both cases, the standard and deviant stimulation probability is equal but the periodic sequence contains a repetitive motive of standard and deviant stimulus presentation.

The underlying mechanism for true deviance detection is unknown and could result from a combination of stimulus-specific input depression and intracortical stimulus processing. Intracortical deviance detection may involve differential deviant processing in different cortical layers (Mill et al. 2012) or the generation of cortical population spikes whose generation depends on the specific stimulus history (Loebel et al. 2007). However, none of these

proposed models can so far account for the effect size of cortical SSA or its sensitivity to sequence periodicity.

1.2.6. SSA and mismatch negativity

A similar effect as with SSA is also seen in MMN, an additional deflection in human EEG recordings occurring roughly 150-250 ms after onset of a deviant stimulus (**Fig. 1.2.4)**. Aside of stronger deviant responses, MMN shows a number of specific response features that are equally observed in SSA, such as the 1-trial effect in 50-50% blocks (Sams et al. 1984) and an increased deviant response in the many-standards paradigm (Jacobsen and Schröger 2001a). Even more as in SSA, MMN is considered to be a specific rule violation signal that is based on the existence of a sensory-memory trace and results from higher-order sensory processing (Näätänen et al. 2005; May and Tiitinen 2010). MMN is observed under a large variety of brain states, including coma patients where it is used as a potential tool to assess higher cognitive function and chance of coma awakening (Morlet and Fischer 2013). Because it is observed during coma, anesthesia (Yppärilä et al. 2002), sleep (Atienza and Cantero 2001) or in newborns (May and Tiitinen 2010), MM is interpreted as the result of an automatic, subconscious cortical change detection-process (May and Tiitinen 2010; Näätänen et al. 2007). However, there are several important differences between SSA and MMN and the role of SSA in the generation of MMN it is still under intensive debate. First, SSA usually occurs on the level of individual neurons whereas MMN in EEG recordings is by definition a population signal. Second, SSA and MMN have vastly different response timings where SSA occurs concomitantly with early sensory evoked responses while MMN is delayed by at least 150 ms after stimulus onset. Lastly, MMN has been shown to occur in more abstract settings, such as omitted stimuli or by a conjunction of different stimulus properties (Tervaniemi et al. 1994; Näätänen et al. 2005). Although such complex deviant signals have not been tested in the animal model thus far, it is likely that they arise from complex information processing that occurs in higher-order cortex instead of early sensory areas. Accordingly, a recent study showed that MMN in auditory cortex of cats is most pronounced in the downstream, secondary area A2 (Pincze et al. 2001).

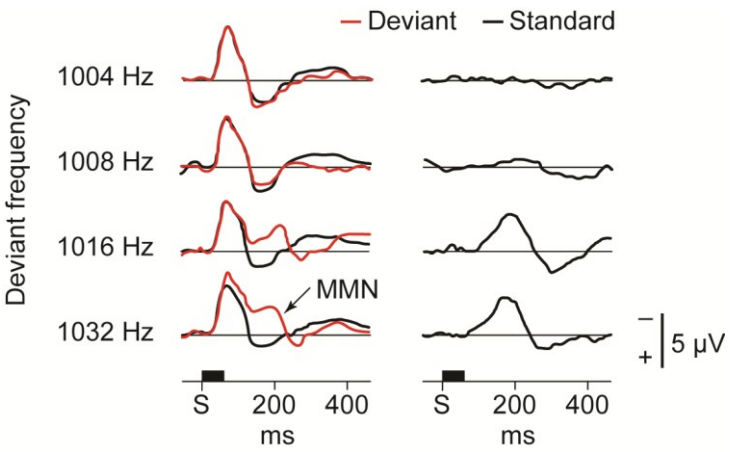

Figure 1.2.4. MMN in human EEG recordings
The left panel shows averaged EEG responses over frontal cortex to either standard (1000 Hz) or deviant tones. As the frequency of deviant tones diverges from the standard (top to bottom), deviant responses show an increasing, secondary response component from 150-250 ms that is characteristic for MMN. Right panel show deviant-standard differences. Figure after Näätänen et al. 2005.

In summary, the physiological source of MMN is currently widely unknown and a prominent opinion in the MMN field is that SSA is merely due to input depression and not directly involved in the generation of this complex phenomenon. Given the non-trivial properties of SSA, this seems to be overstated but shows that a direct relation between SSA and MMN has not yet been established. Probably, MMN reflects network activity in higher-order cortical areas but is generated by the same mechanism of SSA in early sensory cortices. Future studies may thus resolve the perceived difference between SSA and MMN by explaining the exact mechanism of SSA, which may then be transferred from early sensory cortex to stimulus processing in other brain areas.

1.3. Experimental approach and specific aims of the doctoral thesis

The main objective of the doctoral thesis was to provide a direct relation between adaptation in somatosensory cortex and stimulus perception. To achieve this goal, we defined a set of specific questions that could be conclusively answered by using different experimental approaches in both anesthetized and awake rats. The questions in 1.3.1 – 1.3.3 were addressed in the first study of the thesis that is presented in chapter 2. The questions in 1.3.4 – 1.3.6 were addressed in the second study that is presented in chapter 3.

1.3.1. How does adaptation affect frequency discrimination in the rodent?

Behavioral studies on adaptation mostly focus on how the perception of a single or a pair of sensory stimuli is affected by pre-exposure to an adaptive stimulus sequence (Ollerenshaw et al. 2014; Tannan et al. 2006; Goble and Hollins 1993; Tannan et al. 2007). However, when rodents sweep their whiskers over a rough surface the whisker is constantly deflected, resulting in a continuous stimulus sequence rather than a single-pulse deflection. Such stimulus sequences convey a rich set of texture-related information, e.g. the whisker deflection frequency. Whether rodents use such frequency information for texture discrimination is not well understood, because a higher deflection frequency results in more whisker deflections but also a higher degree of frequency-dependent adaptation. Repeated whisker deflections may therefore have a much lower perceptual intensity (Ollerenshaw et al. 2014) and it is unclear whether this would reduce the animal's ability to extract frequency information.

To address this question, I helped to develop and modify an advanced 2-AFC paradigm for head-fixed rodents (Mayrhofer, Skreb, Behrens, et al. 2013). In this paradigm, rats were trained to discriminate two stimulus sequences, presented to a single whisker on each side of the animal's snout simultaneously, based on stimulus frequency. Using chronically implanted 16-contact electrode arrays, I then performed extracellular recording of neurons in somatosensory cortex of awake, stimulus-engaged animals. Based on the acquired data I created a theoretical model that predicted animal performance based on cortical activity patterns.

1.3.2. Does cortical adaptation causally affect stimulus perception?

Although a combination of psychophysics and electrophysiological measurements allows inferring the relation between neural activity and stimulus perception, a causal relation can only be established by direct manipulation of neural activity in somatosensory cortex and measuring corresponding changes in animal behavior (Carandini and Churchland 2013).

To do so, I used optogenetic stimulation to directly modulate the activity of cortical neurons without whisker stimulation (Zhang et al. 2006). Here, the blue light-sensitive ion

channel channelrhodopsin-2 (ChR2) was virally delivered into neurons of a single barrel in each hemisphere. Transfected cells could later be stimulated by blue light illumination of the cortex and we measured behavioral detection and discrimination performance when neurons were driven in either an adaptive or non-adaptive manner.

1.3.3. Does cortical adaptation enhance discrimination of stimulus amplitude?

While human psychophysical studies showed that adaptation enhances stimulus discrimination in various stimulus features (Tannan et al. 2006; Goble and Hollins 1993; Tannan et al. 2007), enhanced stimulus discrimination in rodents has been shown only for stimulus location (Tannan et al. 2006). We sought to extend this knowledge by testing whether adaptation also enhances stimulus discrimination based on amplitude.

I therefore modified our behavioral paradigm by presenting two simultaneous stimulus sequences on each side of the animal. The target sequence contained a deviant stimulus of higher amplitude that had to be detected while the non-target side contained a distractor stimulus of equal amplitude as the preceding stimulus sequence. Aside of testing the behavioral implications of this paradigm, we also used optogenetic stimulation to relate behaviorally advantageous effects of adaptation directly to neural adaptation in somatosensory cortex.

1.3.4. What are the behavioral implications of SSA?

While the behavioral advantages of general adaptation have been well established (Ollerenshaw et al. 2014; Tannan et al. 2006; Goble and Hollins 1993; Tannan et al. 2007), it is unclear to which extent this effect depends on the adaptation with regard to specific stimulus features. To address this question, I modified the paradigm described in 1.3.3 so that deviant stimuli were not only of different amplitude but were modified additionally with respect to other stimulus features, such as deflection direction and whisker identity.

1.3.5. Is cortical SSA fully explained by input depression?

The main theory behind SSA is the ANTM model, assuming the depression of different sensory input channels (Nelken 2014). In cortex, these channels are thought to be implemented

by stimulus specific thalamocortical projections onto individual cortical neurons. However, whether this mechanism fully explains cortical SSA is still under debate (Nelken 2014) and has not been experimentally tested in the somatosensory cortex.

Using a somatosensory oddball paradigm, I tested whether single neurons in somatosensory cortex show SSA to various stimulus features that were also tested behaviorally. I then created a theoretical model that predicted stimulus response amplitude in the oddball paradigm based on the assumptions of the ANTM model. Lastly, I analyzed extracellular recordings in different cortical depths to assess whether deviant-induced response amplitudes vary across different layers in somatosensory cortex.

1.3.6. Could cortical SSA contribute to the generation of MMN?

Although SSA and MMN share many important features, it is still under debate whether they represent separate phenomena or if SSA contributes to the generation of MMN (Näätänen 1992; Nelken 2007). By combining layer-specific deviant-response analysis with a deviant-alone control condition, I sought to identify specific neural response patterns in somatosensory cortex that may resolve the mismatch in temporal and predictive response properties between SSA and MMN.

Chapter 2 : Tactile frequency discrimination is enhanced by circumventing adaptation

S. Musall, W. von der Behrens, J.M. Mayrhofer, B. Weber, F. Helmchen and F. Haiss

Nature Neuroscience, published 21 September2014.
See also accompanying News & Views article by Yang and O'Connor

My contributions to this study were the following: I was involved in the conceptual and experimental design of the study and performed electrophysiological recordings and optical stimulation in awake and anesthetized rats. I also did the behavioral training and psychophysical testing of rats and strongly contributed to the data analysis and writing of the manuscript.

Neocortical responses typically adapt to repeated sensory stimulation, improving sensitivity to stimulus changes but possibly also imposing limitations on perception. For example, it is unclear whether information about stimulus frequency is perturbed by adaptation or rather encoded by precise response timing. Here, we addressed this question in rat barrel cortex by comparing performance in behavioral tasks with either whisker stimulation, causing frequency-dependent adaptation, or optical activation of cortically-expressed ChR2, eliciting non-adapting neural responses. Circumventing adaption by optical activation substantially improved cross-hemispheric discrimination of stimulus frequency. This improvement persisted when temporal precision of optically-evoked spikes was reduced. We could replicate whisker-driven behavior only by applying adaptation rules mimicking sensory-evoked responses to optical stimuli. Conversely, in a change-detection task, animals performed better with whisker compared to optical stimulation. Our results directly demonstrate that sensory adaptation critically governs the perception of stimulus patterns, decreasing fidelity under steady-state conditions in favor of change detection.

2.1. Introduction

How sensory information is transformed into a cognitive percept remains a major question in neuroscience. Numerous studies quantified how cortical activity relates to perception, either following sensory stimuli (Salinas et al. 2000; Stüttgen and Schwarz 2010; Adibi and Arabzadeh 2011; Mayrhofer, Skreb, Behrens, et al. 2013) or upon direct cortical stimulation (Romo et al. 1998; Huber et al. 2008; Sachidhanandam et al. 2013). However, neural response properties are dynamic and modulated by contextual factors such as behavioral state, explorative movements or stimulus history (Fanselow and Nicolelis 1999; Castro-Alamancos 2004b; Hentschke et al. 2006). A prominent and omnipresent feature in sensory systems is the rapid attenuation of responses with repeated stimulation (Ohzawa et al. 1982; Wilson 1998; Khatri et al. 2004b; Ulanovsky et al. 2004). Such adaptation can occur at different stages along the sensory pathway, including biophysical effects at sensory receptors (Fraser et al. 2006) as well as adaptive discharge behavior of neurons in subcortical structures like the brainstem (Minnery and Simons 2003) and thalamus (Chung et al. 2002; Khatri et al. 2004b). Buildup of inhibition at various stages also contributes to adaptive re-

sponse behavior (Hartings and Simons 2000; Hirata et al. 2009). However, adaptation is particularly strong in neocortex (Hawken et al. 1996; Chung et al. 2002; Ulanovsky et al. 2003; Katz et al. 2006), mainly due to short-term depression of thalamocortical synapses (Chung et al. 2002; Khatri et al. 2004b; Katz et al. 2006). The main advantage of adaptation is believed to be increased coding efficiency by adjusting sensitivity of neural responses in accordance to prevailing conditions of the outside world (Dean et al. 2005; Maravall et al. 2007; von der Behrens et al. 2009; Adibi et al. 2013). Consistent with this notion, psychophysical studies have shown that presentation of an adapting stimulus sequence enhances discrimination of subtle differences between stimuli that are subsequently presented (Goble and Hollins 1993; Tannan et al. 2007). However, as neural responses are attenuated in relation to the amplitude of the adapting sequence (Garcia-Lazaro et al. 2007; Adibi et al. 2013) the perceived intensity of subsequent stimuli is reduced accordingly (Laskin and Spencer 1979; Gescheider et al. 1995).

How does sensory adaptation affect perception when temporal information, such as stimulus frequency, needs to be extracted from a uniform stimulus sequence? If frequency is defined by inter-pulse intervals of otherwise uniform stimuli ('repetition frequency'), increasing frequency might directly translate to increasing intensity because a sequence conveys more stimuli in a given amount of time (Gerdjikov et al. 2010; Waiblinger et al. 2013). However, adaptation also increases with shorter inter-pulse intervals (Khatri et al. 2004b; von der Behrens et al. 2009); high-frequency sequences therefore elicit stronger adaptation as lower frequencies. If frequency information is encoded by firing rates of cortical neurons (Luna et al. 2005; Gerdjikov et al. 2010), adaptation might therefore obstruct perception of frequency differences. Alternatively, repetition frequency might be conveyed by precise response timing regardless of changes in response amplitude (Ewert et al. 2008; Harvey et al. 2013).

We addressed this question in the rat barrel cortex (BC), the whisker-related region in primary somatosensory cortex (S1) known to show strong and rapid adaptation that is specific for stimulus frequency and whisker identity (Khatri et al. 2004b; Katz et al. 2006; Stüttgen and Schwarz 2010). For rats trained to perform in a two-alternative forced choice

(2-AFC) task with bilateral single-whisker stimulation (Mayrhofer, Skreb, Behrens, et al. 2013), we show that discrimination performance of stimulus sequences with different repetition frequencies is explained by adaptation of neurons in BC. Optogenetic direct activation of BC neurons allowed us to circumvent sensory adaptation, which resulted in profound differences in animal behavior. Specifically, stimulus detection as well as discrimination of repetition frequency was strongly enhanced. Conversely, whisker-driven behavior could be replicated when optical stimulus trains were modified to mimic sensory-evoked adaptation, while reducing temporal precision had minor effects. In a change-detection task, with deviants embedded in the stimulus trains, animal performance was higher with whisker rather than optical stimulation. Taken together, our results show that adaption enhances perception of salient stimuli at the cost of reducing fidelity under steady-state conditions.

2.2. Results

We first characterized sensory adaptation by performing extracellular recordings of S1 neurons in the C1-barrel column of awake rats (10 single-units, 23 multi-units; 2 animals), in response to controlled deflections of the principal whisker. Stimulation with 1-s long trains of pulsatile stimuli evoked a strong initial response followed by responses with progressively reduced response amplitude for the second and all subsequent pulses (**Fig. 2.1a**). The degree of adaptation was frequency-dependent, showing stronger response attenuation with increasing frequency (**Fig. 2.1b**). To quantify this effect, we computed the adaptation index (AI) as the mean neural response to all stimuli except the first divided by the first stimulus response (spike counts within 25 ms after each pulse onset). AI strongly decreased with frequency (AI_{5Hz} = 0.88 ± 0.02, AI_{10Hz} = 0.75 ± 0.02, AI_{20Hz} = 0.54 ± 0.02, AI_{30Hz} = 0.36 ± 0.02, AI_{40Hz} = 0.25 ± 0.02; mean ± s.e.m.; n = 33), in agreement with previous studies on adaptation of BC neurons (Castro-Alamancos 2004b; Khatri et al. 2004b; Stüttgen and Schwarz 2010). We did not observe any systematic dependence of adaptation on cortical layer (**Supplementary Fig. 2.1**)

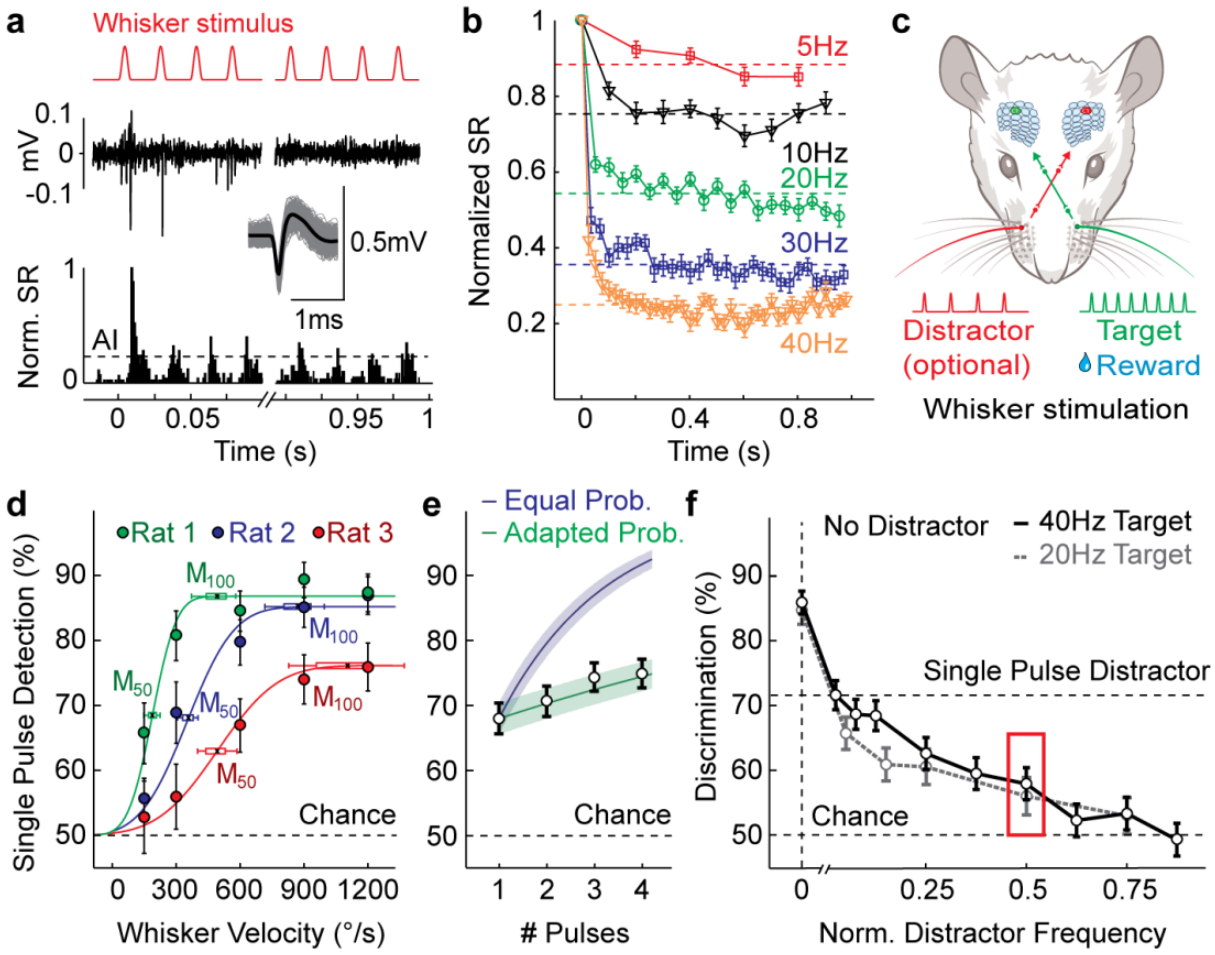

Figure 2.1. Whisker-evoked cortical responses show frequency-dependent adaption that affects performance in detection and discrimination tasks.

a, Extracellular recording in L2/3 BC upon 40-Hz stimulation of the principal whisker. The initial and last four responses are shown. Inset: Single-spike (gray) and mean (black) waveforms. Bottom: PSTH with spike rates (SR) normalized to the initial response. Dashed line shows the AI. **b,** Normalized SR per whisker pulse at different frequencies for all recorded neurons. Dashed lines show AI levels. **c,** Schematic of behavior, using C1-whisker deflections. **d,** Velocity-response curves for detection of single-pulse whisker deflections. **e,** Detection of stimulus trains with variable number of pulses at M_{50} velocity. Circles denote animal performance. Blue and green lines show either equal or adapted detection probability model, respectively. **f,** Repetition frequency discrimination for 20 and 40-Hz target sequences (black and gray), plotted against normalized distractor frequencies (distractor divided by target frequency). Red square highlights equal performance when 20-Hz was either target or distractor frequency. Error bars, s.e.m (**b**), 95% CIs (**d**,**e**,**f**), *n* = 33 cells

2.2.1. Adaptation in S1 barrel cortex governs whisker-mediated behavior

To test the perceptual impact of adaptation, three rats were trained to perform a 2-AFC task for detection and discrimination of repetitive, pulsatile whisker stimulation (**Fig. 2.1c**; see Methods). In the detection task, the stimulus was applied to either the left or the right C1

whisker. A reward was given if the animal responded correctly by licking on the stimulus (target) side at one of two water spouts (**Fig. 2.1c**, green). Detection curves for individual pulses showed a sigmoidal shape with inflection points at half-optimal detection velocities (M_{50}) ranging from 188 to 495°/s (**Fig. 2.1d**). We then presented increasing numbers of pulses at M_{50} velocity with an inter-pulse interval of 25 ms (40 Hz). While single-pulse detection rate was 17.9% above chance level, it only increased by an average of 2.3 ± 0.93% for every extra pulse that was added to the sequence (**Fig. 2.1e**). Thus, detection performance with repeated stimulation was markedly lower than expected if every pulse would have an equal perceptual weight (Stüttgen and Schwarz 2010). However, when adaptation was considered by reducing the detection probability of subsequent pulses according to the observed AI_{40Hz} (see Methods, Eq. 2), the predicted curve matched the measured detection performance (**Fig. 2.1e**, green trace). We could exclude that adaptation is strongly modulated during task-engagement by performing additional recordings of S1 neurons in two rats that were actively engaged in detection of 40-Hz sequences. Here, no significant difference to adaptation in non-engaged animals was observed (**Supplementary Fig. 2.2**). These results imply that the animal's ability to detect uniform stimulus trains is indeed influenced by adaptation of cortical neurons.

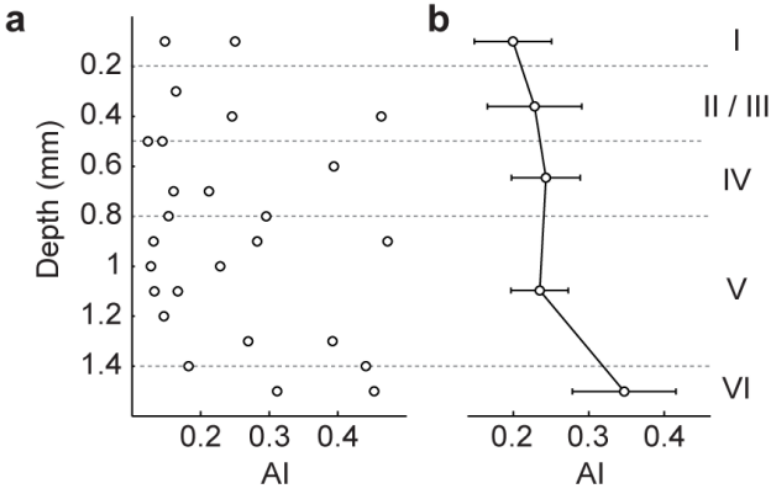

Supplementary Figure 2.1. Distribution of neural adaptation versus recording depth.
a, Adaptation index of all recording sites against their respective depth in cortex during 40Hz whisker stimulation. **b,** Mean adaptation index of every cortical layer. No systematic differences were observed between different cortical layers. Error bars show s.e.m.

Nonetheless, adaptation may still have little effect on discrimination of repetition frequency if such information would be encoded by spike timing. We therefore examined how well animals could perform bilateral discrimination of 1-s long repetitive whisker stimulus trains presented at different repetition frequency. For each animal, the M_{100} whisker velocity was chosen to match its respective optimal single-pulse detection performance (**Fig. 2.1d**). Again, animals had to lick on the side where a target stimulus was presented (randomly switching trial-by-trial between 20 Hz and 40 Hz as a target). Concurrent with the target on one side, another stimulus train with variable repetition frequency was presented on the opposite side as a distractor (1-35 Hz; always lower than the target repetition frequency, **Fig. 2.1c**). Animals robustly detected target stimuli in the absence of any distractor (84.4 ± 1.9% and 86.1 ± 1.7% for 20 and 40-Hz target, respectively; mean ± 95% CI; n = 1500) but a single pulse distractor was sufficient to significantly reduce behavioral performance to 65.6 ± 2.4% (20-Hz target) and 71.7 ± 2.3% (40-Hz; $p < 0.001$). Discrimination performance further decreased with increasing distractor frequency, reaching levels not significantly different from chance level for repetition frequencies close to the target. 20-Hz sequences were presented either as a target or distractor (against 40-Hz) and animals could readily exchange target and distractor sequences depending on whether they were presented against a sequence of higher or lower repetition frequency (**Fig. 2.1f**, red square).

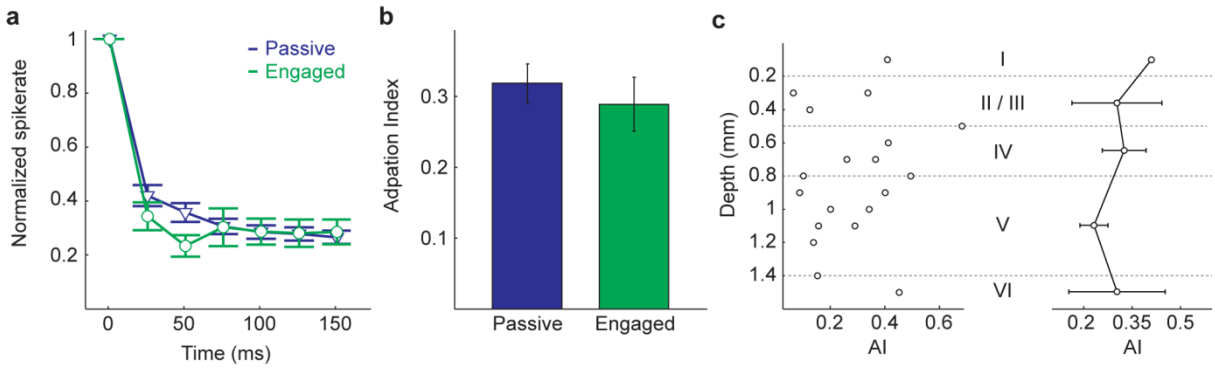

Supplementary Figure 2.2. Adaptation of cortical neurons in task-engaged animals.
a, Normalized SR per whisker pulse at 40-Hz stimulation for all recorded neurons. Blue triangles show recordings from two passive animals (*n*=33, same as in **Fig. 2.1b**), green squares show recordings in two task-engaged animals (*n*=19). Dashed lines show AI levels. **b,** Comparison of mean adaptation in the first 175 ms after stimulus onset. **c,** Adaptation index of all recording sites against their respective recording depth in cortex during 40-Hz whisker stimulation in task-engaged animals. **d,** Mean adaptation index for every cortical layer. Error bars show s.e.m.

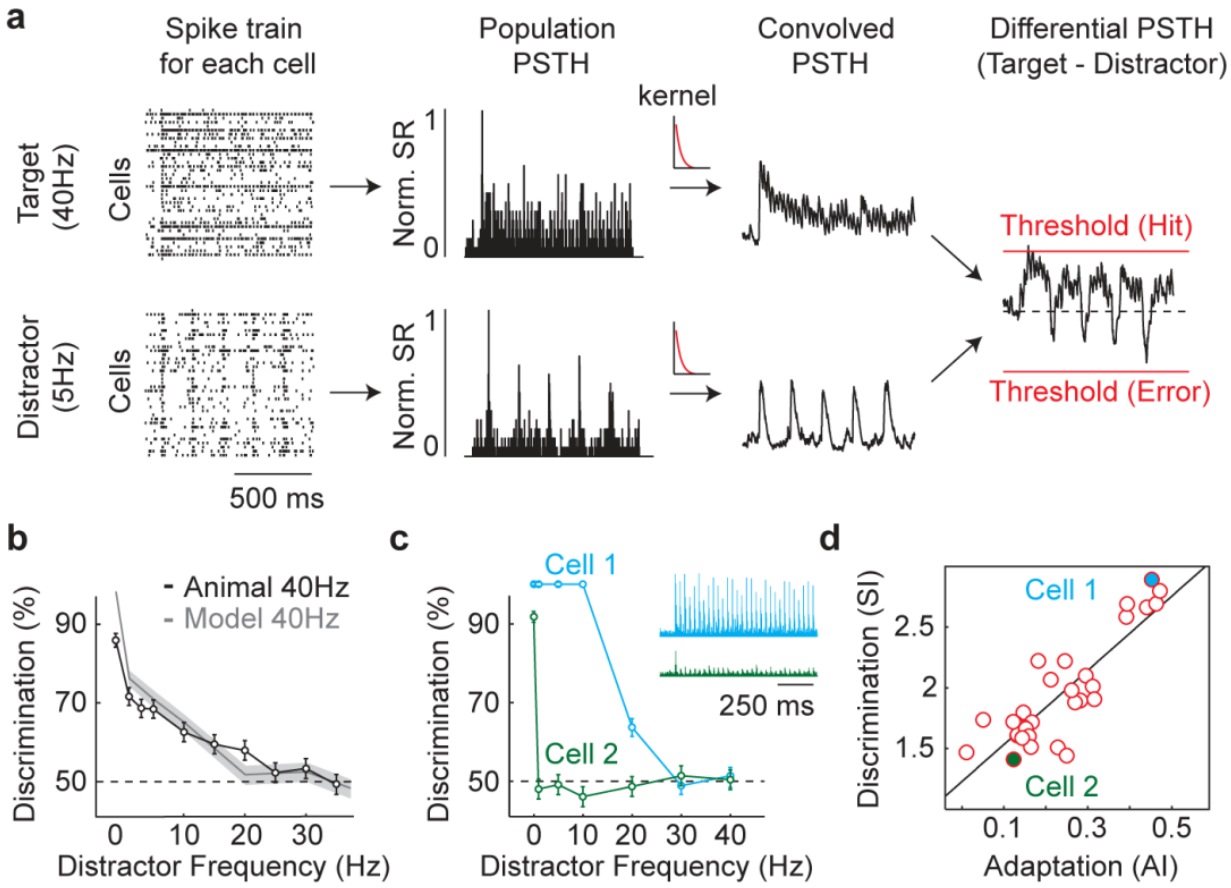

Figure 2.2. A model for repetition frequency discrimination based on neural response probabilities.
a, Illustration of our model for discrimination of a 40-Hz target versus a 5-Hz distractor sequence. For target and distractor, a single spike train was generated for each cell and summed into a population PSTH. PSTHs were normalized and convolved with an exponential decay kernel. Model responses were generated by subtracting the distractor from target PSTH and applying a threshold to the resulting differential PSTH. For each distractor, this approach was repeated for 1500 trials **b,** Repetition frequency discrimination for 40-Hz target sequences (black), plotted against normalized distractor frequencies. Gray shading shows model discrimination performance. Error bars, 95% CIs **c,** Discrimination performance of two example cells. Cell 1 (blue trace and PSTH) shows low adaptation and high discrimination performance. This is reversed in Cell 2 (green trace and PSTH). Error bars, 95% CIs. **d,** Correlation between the AI_{40Hz} of individual cells and their respective similarity index (SI) to optimal discrimination performance. Marked in green and blue are cells in panel **c**.

The disproportionally large impact of a single pulse distractor can be explained by the rapid adaptation that follows the first pulse; the distractor would mask the simultaneously presented first pulse of the target sequence while subsequent pulses are already adapted and insufficient for robust target identification. To test this hypothesis, we used a probabilistic model for stimulus detection and discrimination. Model performance was based on the integration of stimulus-evoked activity, derived from electrophysiological recordings of BC neurons (**Fig. 2.2a**). More specifically, we constructed peristimulus time histograms (PSTHs)

of the response probabilities of the population of recorded neurons for a target and distractor sequence, respectively. Both PSTHs were convolved with an exponential decay function and the distractor PSTH was subsequently subtracted from the target PSTH. A trial was counted as a hit when the peak spike-count of the resulting differential PSTH exceeded a given threshold α (**Supplementary Fig. 2.3**; see Methods) and an error occurred if the differential PSTH fell below –α. If the threshold was not crossed, a trial was counted as either a hit or error at 50% probability. The model could replicate the impact of single- and multi-pulse distractors on discrimination performance at varying repetition frequency and achieved performance levels that were highly comparable to trained animals (**Fig. 2.2b**).

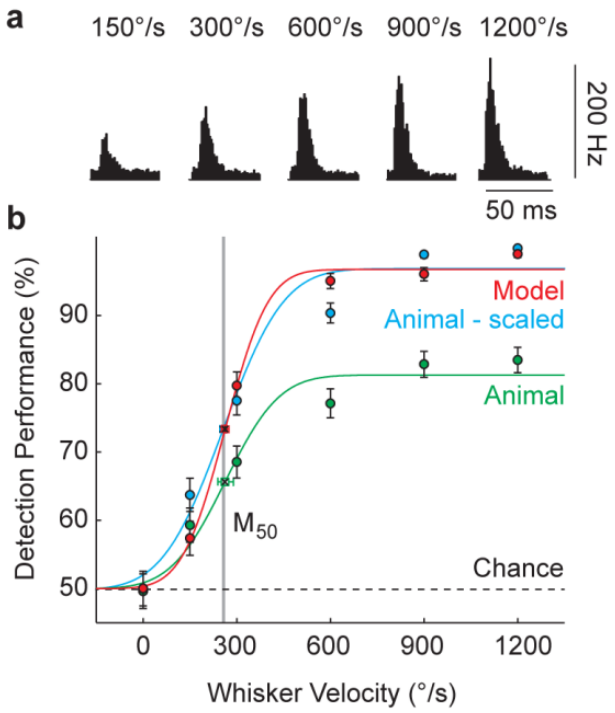

Supplementary Figure 2.3. Model threshold calibration.
a, Detection threshold α was determined by tuning the model with neural responses to single whisker deflections. **b,** The threshold that achieved the highest similarity index between modeled (red) and scaled animal (blue) single pulse detection performance was used for further analysis. As a result model achieved higher absolute detection performance as the animals (green) but sensitivity to single deflections, defined by the inflection curve of the tuning curves (M_{50}), was highly comparable.

Interestingly, when PSTHs were based on single-cell responses model discrimination performance varied between individual cells but strongly correlated with their degree of adaptation: Neurons that adapted weakly displayed the strongest discrimination performance (r = 0.87, $p < 0.001$; n = 33; **Fig. 2.2c,d**). Taken together, these results suggest that frequency-dependent adaptation not only determines the sensitivity of stimulus detection but also markedly affects the animal's ability to discriminate sequences of different repetition frequency.

2.2.2. Optogenetic stimulation of cortical neurons improves behavioral performance

We next asked how sensory perception and task performance might be altered when adaptation is reduced. To circumvent sensory adaptation we decided to stimulate BC neurons directly by expressing channelrhodopsin-2 (ChR2) in order to optically drive spiking activity with blue light stimulation (Boyden et al. 2005). ChR2 was virally delivered into the C1 barrel columns in both hemispheres of the trained animals and induced robust ChR2 expression, spanning all layers and extending 2.1 ± 0.3 mm horizontally (mean ± s.d.; n = 8 injection sites in four trained rats; see also **Supplementary Fig. 2.4**). Short glass fiber tips (400 µm diameter, connectorized to fiber optics and illumination system) were then implanted over the injection site (**Fig. 2.3c**; see Methods). Separate in vivo experiments confirmed that trains of blue light pulses induced high-fidelity spiking activity in individual neurons for frequencies up to 40 Hz (15 single units in 7 rats) (**Fig. 2.3a** and **Supplementary Fig. 2.5**). This was also confirmed by additional recordings in an awake rat (**Supplementary Fig. 2.6**). As optical stimulation caused negligible adaptation of BC neurons (AI > 0.9 for all frequencies), application of 1-ms light pulses instead of whisker stimuli allowed us to test behavioral performance under essentially adaptation-free conditions (**Fig. 2.3b**). All three animals (same as in **Fig. 2.1**) were able to detect light-induced target stimuli with high reliability, after three to five sessions with light stimulation (~150 -300 trials). To normalize perceived intensity of whisker and light stimuli, we measured psychometric curves with single light pulses of varying intensities for each hemisphere (**Fig. 2.3d**). Required light intensities for pulse detection were very low ($M50_{min}$: 1.22 mW/mm^2, $M50_{max}$: 2.92 mW/mm^2), suggesting that only neurons that were close (< 0.35 mm) to the tip of the glass-fiber implant were activated by light (**Supplementary Fig. 2.4d,e**). We then repeated the target detection task with increasing numbers of light pulses using M_{50} light intensities. In contrast to whisker stimulation, detection rates with direct cortical stimulation were well explained by equal detection probability of individual pulses (**Fig. 2.3e**), in accordance with earlier experiments using intracortical microstimulation (Butovas and Schwarz 2007).

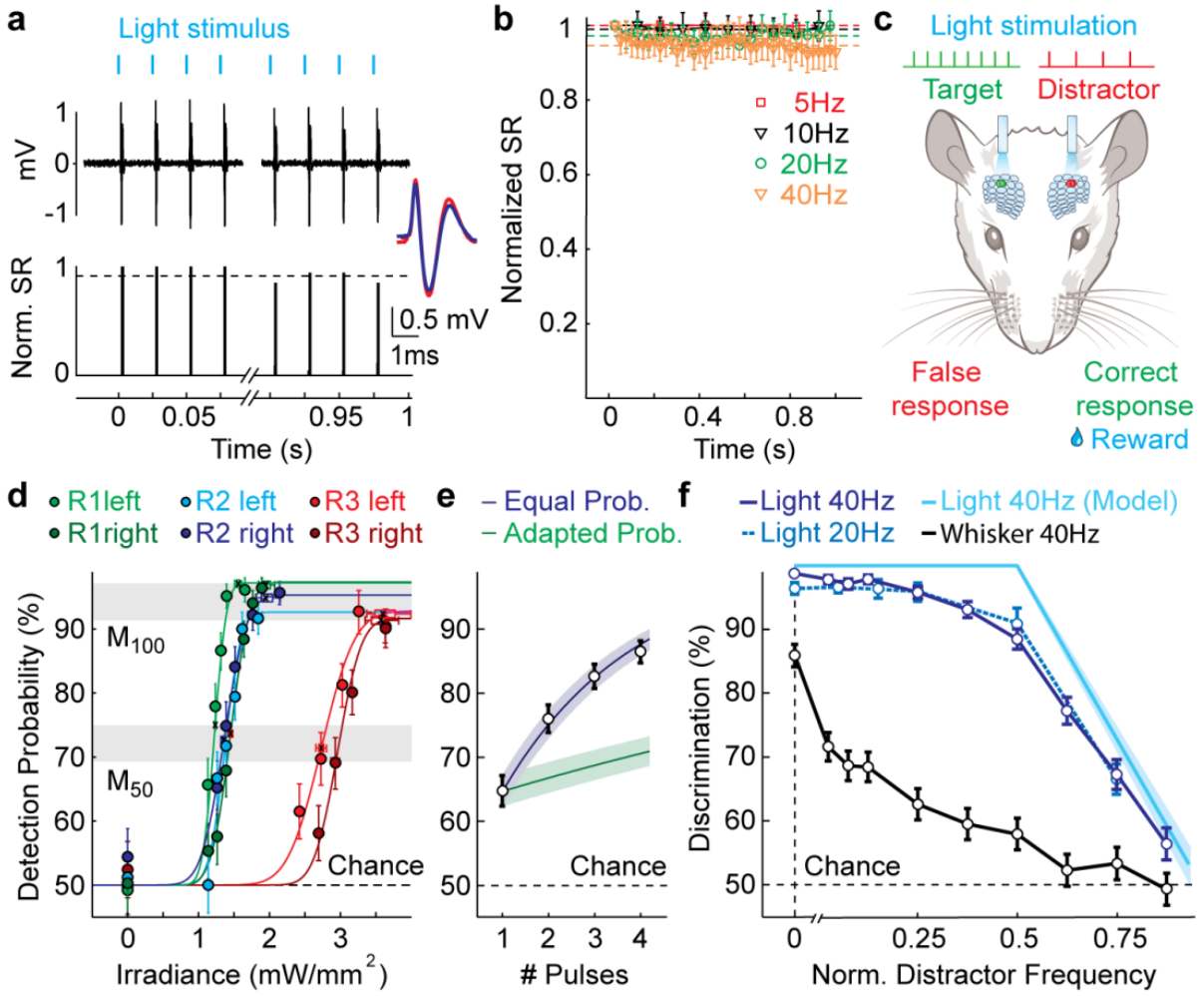

Figure 2.3. Optogenetic stimulation induces adaptation-free responses that result in increased detection and discrimination performance.

a, Extracellular recording of BC neuron expressing ChR2. 1-ms blue light pulses induced spiking up to 40 Hz. Bottom: Normalized PSTH over 50 trials. Inset: Comparison of light-induced (red) and spontaneous (blue) waveforms. Dashed line denotes the AI. **b,** Normalized SR per light pulse at different frequencies for all recorded neurons. Dashed lines show AI levels. **c,** Schematic of behavior with optical stimulation of identified C1 barrels in both hemispheres. **d,** Irradiance-response curves for single light pulse detection. Gray bars mark minimal-to-maximal ranges for M_{50} and M_{100} values. **e,** Detection of stimulus trains with variable number of light pulses. Conventions as in Fig. 2.1E. **f,** Repetition frequency discrimination for 20- and 40-Hz target sequences, using optical (dark/light blue) or whisker (black) stimulation. Performance plotted against normalized distractor frequencies (distractor divided by target frequency). Light blue trace shows model performance. Error bars, s.e.m (**b**), 95% CIs (**d**,**e**,**f**), *n* = 15 cells

This indicates that non-adaptive neural activation results in uniform perceptual weight of individual pulses within a sequence. Subsequently, we applied bilateral optical BC stimulation (M_{100} light intensities) using either 20 or 40 Hz as target repetition frequency combined with various lower-frequency distractors. Remarkably, discrimination performance based on

light stimuli was significantly better compared to whisker stimulation (40-Hz targets: 25.8% root-mean-square error RMSE, $p < 0.01$; **Fig. 2.3f**). Presentation of a single pulse distractor did not result in any significant decrease in discrimination performance (No distractor: 97.3 ± 0.8% and 98.9 ± 0.5%, single pulse distractor 97.5 ± 0.7% and 98.3 ± 0.73% for 20 and 40-Hz target, respectively; mean ± 95% CI, p = 0.43 and 0.11), suggesting that the initial pulse in

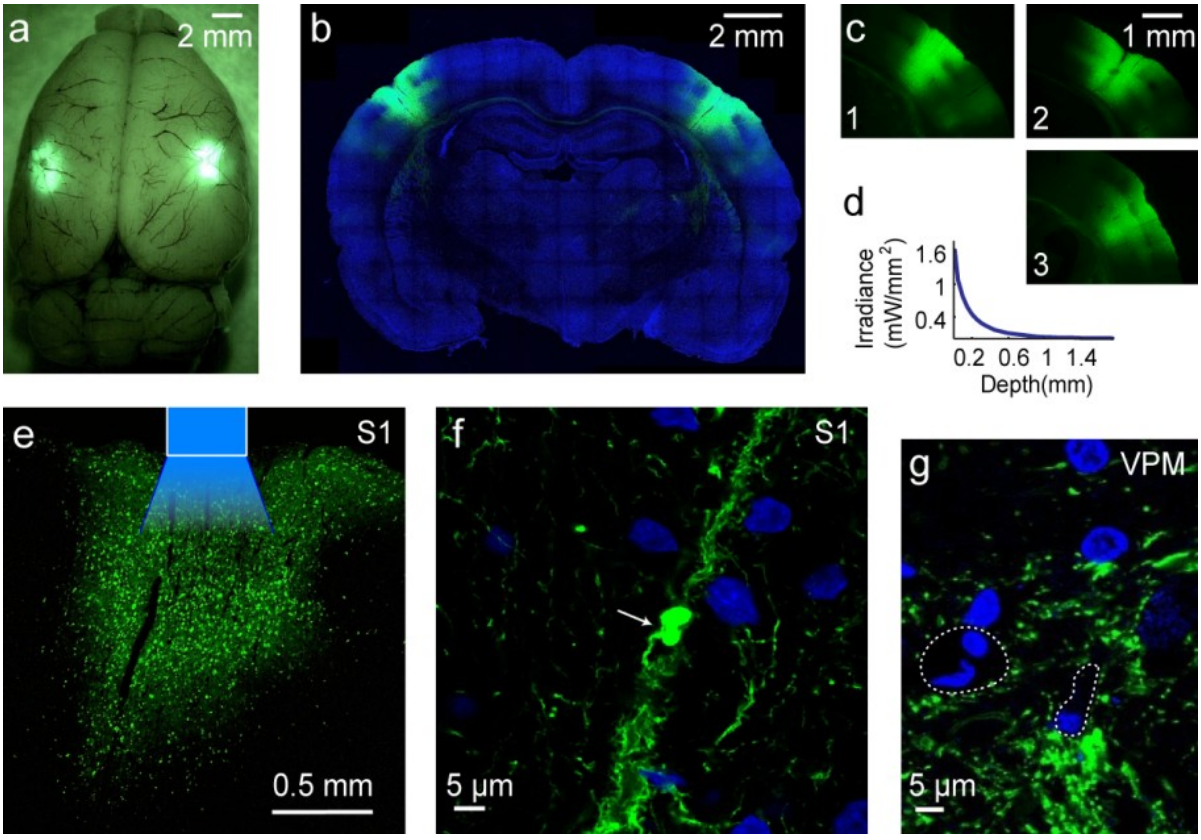

Supplementary Figure 2.4. Histological analyses of ChR2 expression.

a, Macroscopic image of ChR2-YFP fluorescence (green) of a bilaterally injected rat brain with equal expression in BC of both hemispheres. **b**, Coronal brain section, stained with DAPI (blue) showing the middle of the injection site. **c,** Examples of ChR2 expression in all three animals that were used for behavioral assessment with light stimulation. The spatial profile of ChR2 expression was highly comparable across animals and injection sites. **d**, Theoretical estimates for changes in light irradiance with distance from the fiber tip. **e**, Overview of ChR2 expression site in the right BC. The illustration shows the glass fiber (blue square) on the brain surface and a rough estimation of the cortical area that is affected by blue light stimulation (blue cone). **f**, Magnified view on local projections of $ChR2^+$ neurons in cortex. White arrow denotes a localized accumulation of ChR2-YFP, indicating occurrence of a local axonal swelling. These local changes in morphology were observed repeatedly in all animals and might be due to long-term expression of ChR2 (Miyashita et al. 2013). No other signs of cellular damage from ChR2 expression were observed. **g**, ChR2-YFP labeled projections from cortex to the ventral posteromedial nucleus (VPM) in thalamus. Nuclei of thalamic cells (identified by DAPI staining in blue) showed no overlap with ChR2-YFP fluorescence and were surrounded by non-fluorescent areas (dotted white circles) that are presumably cell bodies. This indicates that thalamic neurons were not retrogradely labeled with ChR2-YFP. Similar results were also seen in cortical area S2 (not shown).

the target sequence did not carry disproportionally more perceptual weight than subsequent pulses. Due to the previous perceptual calibration with whisker and optical stimulation, these behavioral differences cannot be explained by a general difference in perceived stimulus intensity (see also **Supplementary Fig. 2.7**). Based on the electrical recordings for different stimulation frequencies (**Fig. 2.3b**) we again modeled single-cell discrimination performance. Consistent with the experimental data, modeled discrimination performance was strongly enhanced compared to whisker stimulation over the range of distractor frequencies (**Fig. 2.3f**; cf. **Fig. 2.1f**).

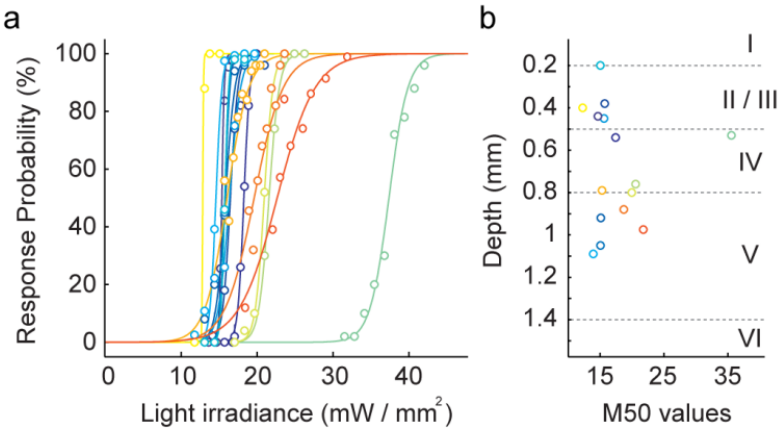

Supplementary Figure 2.5. Light-sensitivity, cortical distribution and adaptation of individual ChR2-expressing neurons.
a, Neurometric tuning curves of all single neurons, recorded under anesthesia. Circles denote firing probability after stimulating with 50 pulses at 10 Hz repetition rate. **b**, Recording depth of all recorded neurons against their respective M_{50} value. We observed no clear relation between recording depth and sensitivity to light.

2.2.3. Whisker-mediated behavior is mimicked by adapting optical stimulus sequences

The profound behavioral differences between whisker and optical stimulation can be explained by the differential degree of adaptation. However, light stimuli not only induce non-adaptive firing but also synchronous, millisecond-precise activation of cortical neurons. Increased stimulus discrimination could therefore be due to changes in adaptation or the sharp temporal profile of light-induced cortical activity. To address the latter possibility, we modified our light stimuli from 1-ms square-wave pulses to short 15-ms long light ramps, which reduced time-locking of neuronal activation and resulted in a spread of stimulus response latencies comparable to whisker stimulation ($\sigma_{Whisker}$ = 2.94 ± 0.34 ms, σ_{Ramp} = 3.09 ± 0.39 ms, p = 0.81; mean ± s.e.m.; n = 15; **Fig. 2.4a** and **Supplementary Fig. 2.8**). Despite this reduction in temporal precision, light ramp stimulation barely reduced discrimination per-

formance, which remained significantly different from whisker stimulation (RMSE 21.56%, $p < 0.05$; **Fig. 2.4b**), indicating that temporal precision alone cannot account for the large difference to whisker stimulation.

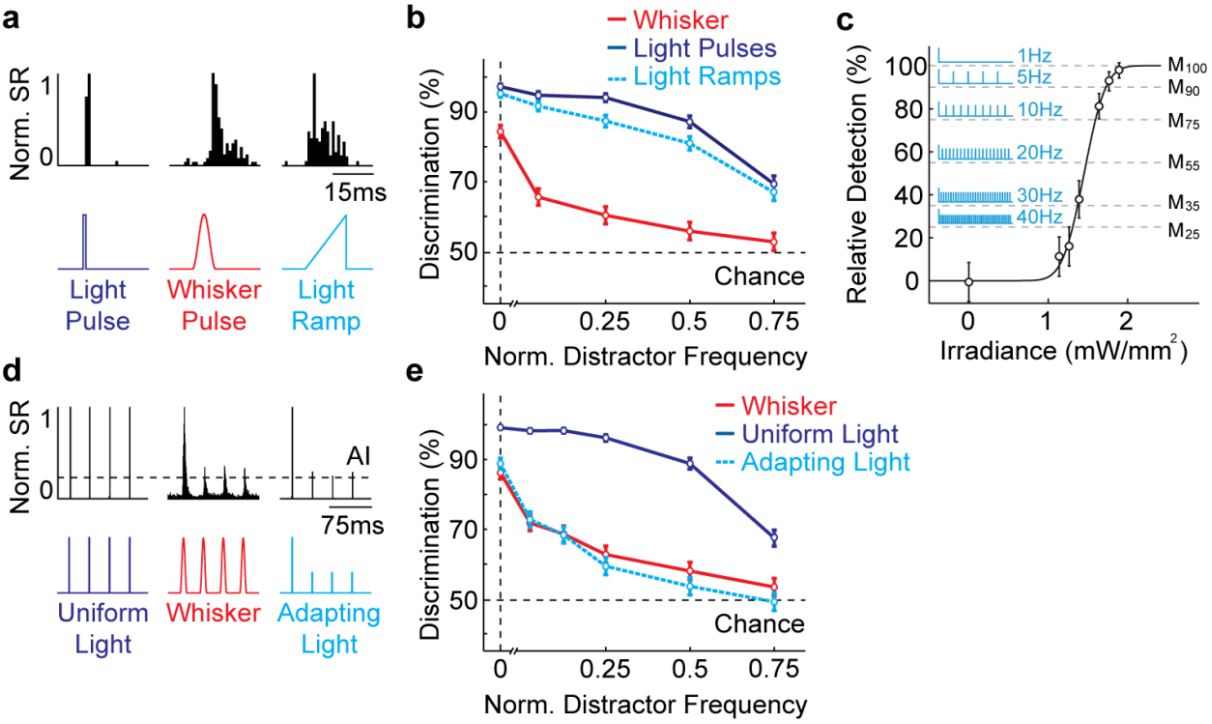

Figure 2.4. Adapting light stimulation reproduces whisker evoked repetition frequency discrimination performance.

a, Normalized PSTHs in response to different stimulus types (shown below traces). **b**, Repetition frequency discrimination with light pulses (dark blue), whisker stimulation (red), and light ramps (light blue). **c**, Example for construction of adapting light stimuli. Based on single light pulse detection, we identified irradiance values that resulted in differential detection performance (M_{25}-M_{100}). Irradiance of the initial pulse was set to M100 amplitude, irradiance of subsequent pulses was set to match single pulse detection performance and the adaptation index for the respective distractor frequency. **d**, Normalized PSTHs in response to different 40-Hz stimulus sequences (shown below traces). **e**, Discrimination performance with uniform light stimulation (dark blue), whisker stimulation (red), and adapting light stimulation (light blue). Error bars, 95% CIs; Performance plotted against normalized distractor frequencies (distractor divided by target frequency) (**b,e**).

To directly test whether sensory adaptation is the main cause of the behavioral differences, we adjusted our light stimuli to mimic sensory-evoked adapting responses. We reduced light irradiance during pulse sequences based on the psychometric curves of individual animals so that for each repetition frequency the corresponding AI value for whisker stimulation was reached (**Fig. 2.4c**). For example, for 40-Hz stimulation light irradiance of the initial pulse was set to optimal (M_{100}) single pulse detection whereas for subsequent pulses irradiance was reduced to 25% detection performance (M_{25}) to match AI_{40Hz} = 0.25 (**Fig. 2.4d**; see

Methods). Application of these adapting light stimuli in the behavioral paradigm reduced the discrimination performance levels to values closely resembling the performance achieved with whisker stimulation (RMSE = 3.1%, p = 0.99; **Fig. 2.4e**). We conclude that detection as well as discrimination of repetitive sensory stimuli is largely governed by adaptation while temporal precision has surprisingly little impact on behavior.

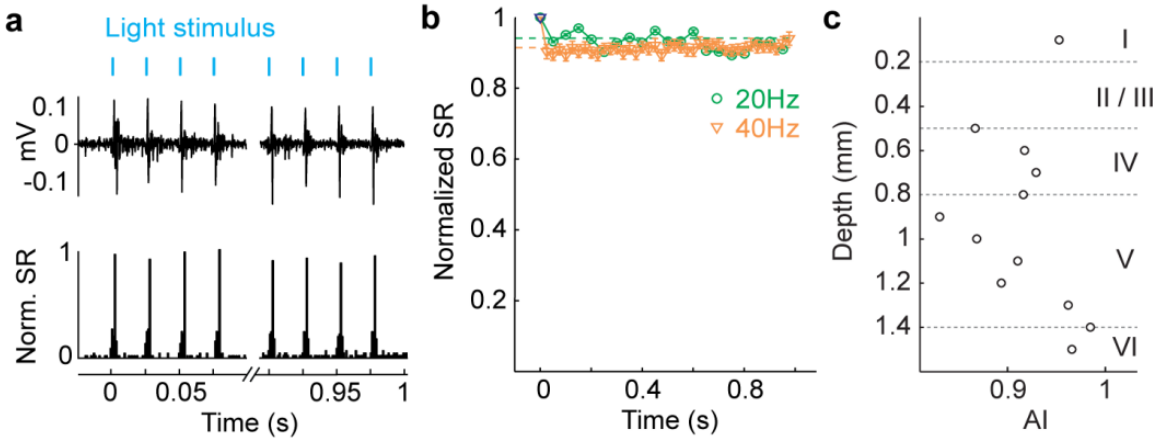

Supplementary Figure 2.6. Neural responses to optical stimulation in the awake, non-engaged animals.
a, Extracellular recording in L5 BC upon 40-Hz stimulation with blue light pulses. Only the initial and last four responses are shown. Bottom panel shows a PSTH with spike rates (SR) normalized to the initial response. **b**, Normalized SR per light pulse at 20- and 40-Hz stimulation over all recorded neurons. Dashed lines show AI levels. **c**, Adaptation index of all recording sites against their respective depth in cortex during 40-Hz light stimulation.

This conclusion is further supported by experiments, in which 40-Hz whisker targets were paired with light distractors of lower repetition frequency (**Fig. 2.5a**). When discriminating whisker from uniform light stimuli, animals were strongly biased towards light distractors with increasing repetition frequency. This bias was especially pronounced for distractor frequencies above 20 Hz, where animals almost exclusively chose light stimuli (**Fig. 2.5b**, dark blue). To test if this bias could be reduced by decreasing light intensity, we also presented light distractors at M_{50} irradiance (**Fig. 2.5b**, light blue). Here, animals performed better compared to whisker distractors for frequencies below 20 Hz but remained biased towards light distractors at higher repetition frequencies. This asymmetric behavior with low light intensity was also observed when we tested animal's stimulus preference by concomitantly presenting whisker and light stimuli of equal repetition frequency (**Fig. 2.5c**). For single pulses, animals favored the whisker stimulus and rarely responded to the side that corresponded to the optical stimulus. However, in case of 40-Hz trains animals mostly preferred optical

over whisker stimulation. Perception of uniform optical stimuli thus differs from whisker stimulation depending on repetition frequency, even when light intensity is reduced. Conversely, animals showed no preference for either whisker or optical stimuli when adapting light stimulation was used. Furthermore, discrimination with 40-Hz whisker targets and adapting light distractors was not significantly different from pure whisker stimulation (RMSE = 5.54%, p = 0.29; **Fig. 2.5d**).

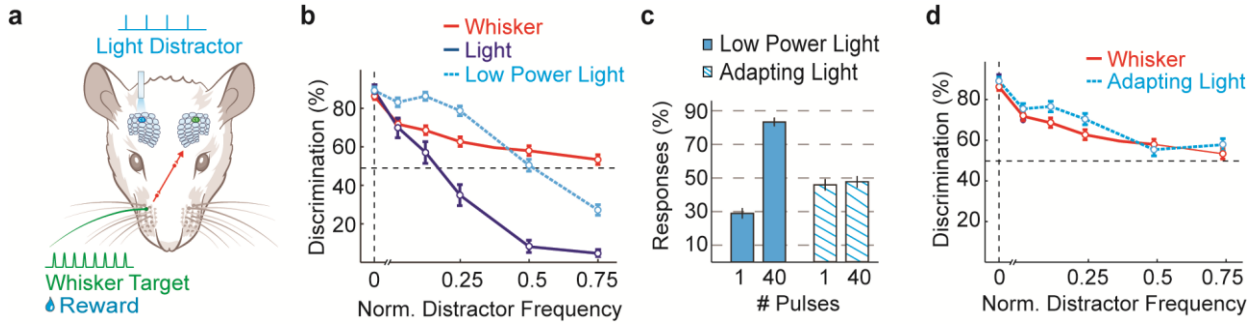

Figure 2.5. Adapting light is comparable to whisker stimulation.
a, Schematic of behavior with combined whisker and light stimulation. **b**, Discrimination performance using whisker distractors (red) or uniform light distractors of either M_{100} (dark blue) or M_{50} (light blue) irradiance. **c,** Animal stimulus preference with presentation of whisker and light stimuli of equal repetition frequency. Shown is the percentage of all trials were animals responded towards light stimuli. 'Low power' and 'Adapting' refers to modality of light stimulus. **d**, Discrimination performance using whisker distractors (red) or adapting light distractors (light blue). Error bars, 95% CIs; Performance plotted against normalized distractor frequencies (distractor divided by target frequency) (**b,c,d**).

2.2.4. Whisker-driven adaptation facilitates detection of deviant stimuli

Given the strong improvement in detection and discrimination behavior when circumventing adaptation, we also sought to address potential beneficial effects of adaptation. If the enhanced ability to discriminate subtle differences between stimuli after exposure to an adapting stimulus sequence is in fact due to the adaptation of cortical neurons, detection of a deviant stimulus in a sequence should be easier with adapting responses to whisker stimulation compared to non-adapting light-evoked responses. We therefore added a single deviant stimulus to 20-Hz whisker stimulus trains. This protocol was verified by recording from BC neurons, with the amplitude of the 20-Hz sequence set according to the mean M_{50} detection performance across all tested animals (350°/s) while the deviant amplitude was set to mean M_{100} (850°/s). Both stimuli induced robust neural responses in cortical neurons with a relative firing rate difference of ~50 spikes/s (**Fig. 2.6a**). Response amplitude strongly

adapted during the M_{50} pulse sequence, while the M_{100} deviant stimulus was less affected (**Fig. 2.6b**). Accordingly, the difference in neural response amplitude to uniform and deviant stimuli increased (non-adapted: 44.1%; adapted: 65.4%). This finding is in agreement with a recent study, showing that adaptation increases the threshold for neural responses to remain above the intensity of an adaptor sequence while response amplitudes to stronger stimuli remain unchanged (Adibi et al. 2013).

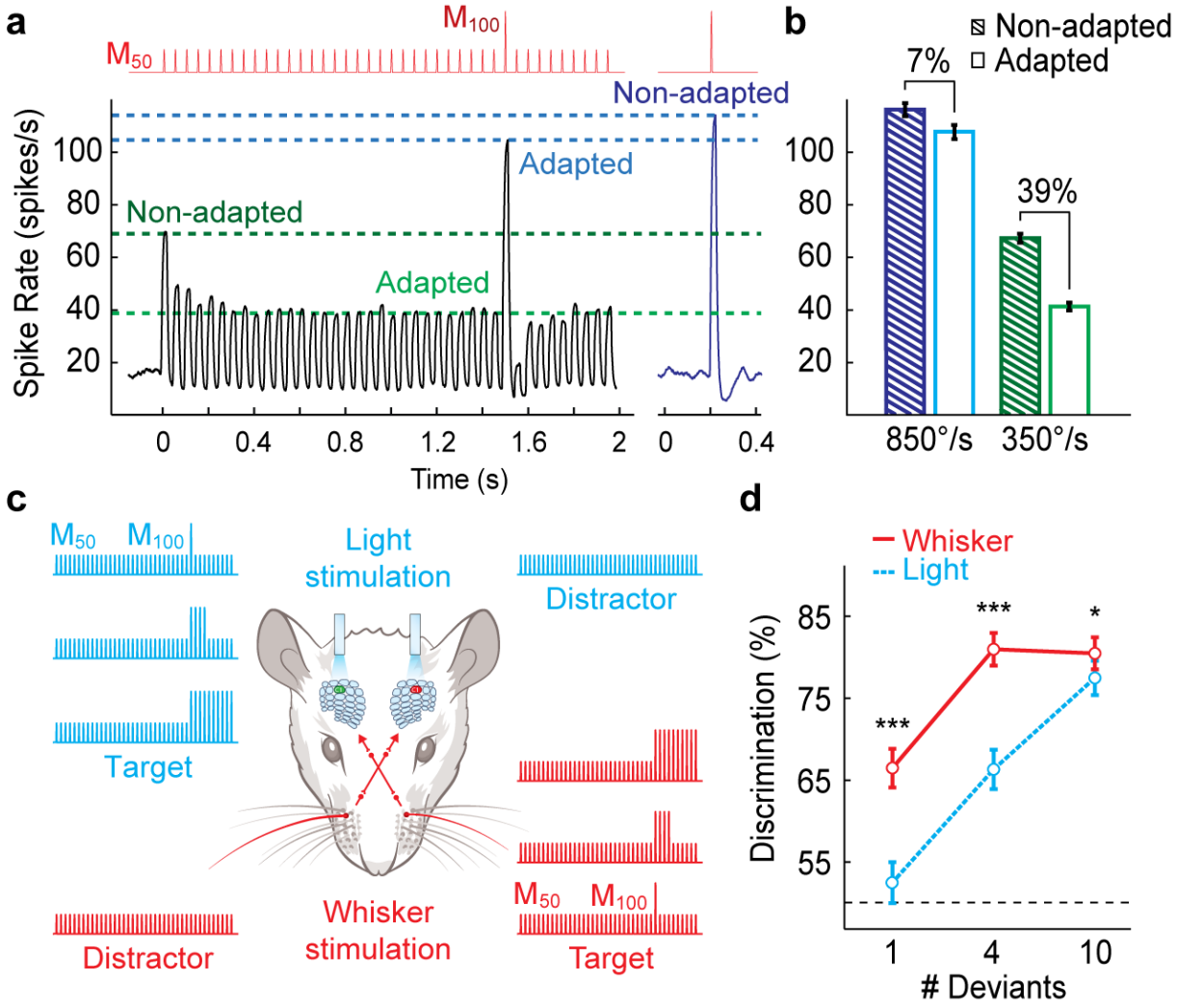

Figure 2.6. Sensory adaptation facilitates deviant detection.
a, Neural response to a 20-Hz whisker stimulation sequence with a single deviant (top). For display only, PSTHs were smoothed with a 25 ms moving average. Response amplitude to subsequent pulses was decreased relative to the initial pulse (green lines) while deviant response amplitude remained close to non-adapted single-pulse responses (blue lines and dark blue trace). **b**, Mean firing rates in response to non-adapted and adapted deviant and base stimuli. **c**, Schematic for behavior with deviant detection. Stimuli were either sequences of whisker deflections (red) or light pulses (blue). **d**, Deviant detection was better with whisker compared to light stimulation. Error bars, s.e.m. (**b**), 95% CIs (**d**). n = 33 cells; *$p < 0.05$,*** $p < 0.001$

To test whether this difference in neural responses would translate into improved perceptibility of deviant stimuli, we changed our behavioral task and bilaterally presented two 20-Hz base sequences of either whisker or light stimuli at M_{50} amplitude to our trained animals. The target sequence (left or right) contained 1, 4 or 10 additional M_{100} deviant pulses after 1.5 s (**Fig. 2.6c**). Animals were rewarded when successfully identifying the deviant-containing target sequence and omitting the uniform 20-Hz distractor sequence. In contrast to light stimulation where detection of single deviants remained at chance levels (52.2 ± 2.5%; $p = 0.10$; mean ± 95% CI), animals could detect the occurrence of a single whisker deviant (67.2 ± 2.4%; $p < 0.001$; **Fig. 2.6d**). The same result was observed in the model, where change detection was enhanced when base and deviant stimuli were adapted (non-adapted: 53.1 ± 2.5%, adapted: 61.3 ± 2.4%, $p < 0.01$). For both whisker and light stimuli, performance further increased when additional deviant pulses were presented. Interestingly, there was no difference in behavioral performance for 4 and 10 whisker deviants (81.7 ± 2.0 vs. 81.2 ± 2.0; $p = 0.53$) whereas performance with light stimulation continuously increased with deviant number. This dependency is to be expected when assuming that single deviants are

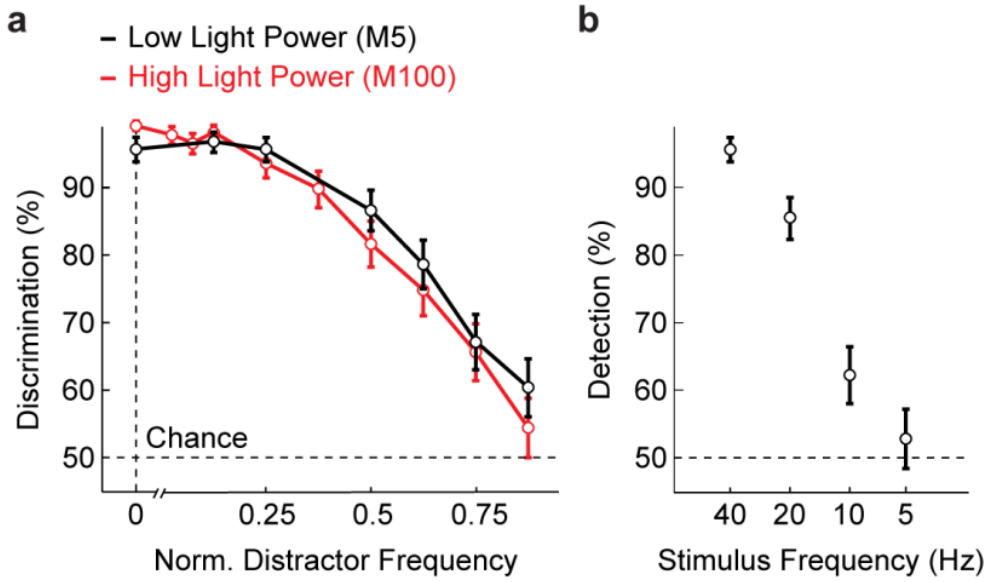

Supplementary Figure 2.7. Behavioral effects of optical stimulation with low light power.
a, Repetition frequency discrimination with 40-Hz target sequences, using optical stimulation with either low (M_5 of single pulse detection, black) or high (M_{100} of single pulse detection, red) light power. Performance is plotted against normalized distractor frequencies (distractor divided by target frequency). **b**, Detection of optical stimulus sequences at low light power with different repetition frequencies. When using low light power, animals were unable to reliably detect sequences at repetition frequencies below 40-Hz. Error bars, 95% CIs

more robustly detected due to their increased perceptual contrast against ambient stimuli, while repeated deviants are also subject to adaptation (**Supplementary Fig. 2.9**). For light stimulation, deviant detection is directly related to the number of deviant presentations – analogous to detection of a pulse sequence (**Fig. 2.3e**). Consequently, the perceptual weight of ambient stimuli increases, obscuring identification of transient signal deviations.

2.3. Discussion

Our results demonstrate that animal behavior is profoundly shaped by sensory adaptation and provide a direct link between neural activity in the primary sensory cortex and stimulus perception. We show that sensory adaptation reduces perceived intensity of uniform whisker deflection patterns, with the attenuation of neural responses directly relating to a reduced detection probability of repeated stimuli. While reduced sensitivity to repeated stimulation has been demonstrated earlier (Stüttgen and Schwarz 2010), our results confirm that this is indeed well explained by adaptive response behavior of cortical neurons (**Fig. 2.1e** and **Fig. 2.3e**). Stimulus discrimination was also markedly affected by adaptation, being worse with whisker stimulation compared to non-adapting optical stimulation (**Fig. 2.3f**). This result might appear to mismatch previous studies showing a beneficial effect of adaptation to stimulus discrimination (Goble and Hollins 1993; Tannan et al. 2007; Wang et al. 2010). However, whereas we studied discrimination of concurrently presented stimulus sequences that were adapting over time, earlier studies focused on discrimination of instantaneous stimulus features (like intensity or location) after presenting an adapting stimulus sequence. In fact, our behavioral results, showing that adaptation enhances perception of change in a uniform stimulus sequence are in good agreement with this earlier work. Notably, we demonstrate that such increased perception of salient stimuli is associated with a diminished representation of uniform stimulus patterns.

The observed differences in behavioral performance indicate that the degree of adaptation has to be finely tuned in order to optimize cortical processing for solving a given task. Indeed, adaptation can dynamically change according to the behavioral state and different brain areas exhibit different degrees of adaptation (Fanselow and Nicolelis 1999; Cas-

tro-Alamancos 2004b; Hentschke et al. 2006). Understanding the balance between change-perception and steady-state fidelity is essential for comprehending neocortical information flow and has also clinical implications because impaired adaptation has been associated with neuropsychiatric disorders, such as autism (Pellicano et al. 2007; Tannan et al. 2008) and schizophrenia (Umbricht and Krljes 2005). Combining optogenetic manipulation of neural response patterns and psychophysical assessment of the perceptual consequences is a promising path to achieve this goal.

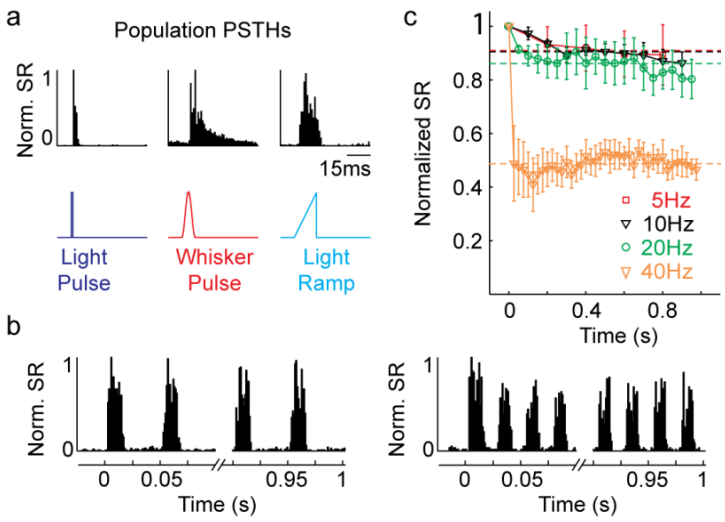

Supplementary Figure 2.8. Neural responses to light ramp stimulation.
a, Normalized PSTHs in response to different stimulus types. PSTHs were constructed after combining spike data from all recorded neurons into one dataset, thus showing differences in response behavior over the whole neural population. **b,** Normalized population PSTHs for 20- (left panel) and 40-Hz (right panel) light ramp stimulation. Shown are the first and last 100 ms of the stimulus sequence. **c**, Normalized SR per light ramp stimulation at different repetition frequencies over all recorded neurons. Dashed lines show AI levels.

While several recent studies have utilized a combination of behavior and cortical stimulation to achieve a deeper understanding of the transfer from local-circuit activity to sensory perception (Sachidhanandam et al. 2013; Huber et al. 2008; O'Connor et al. 2013), the possibility to control neural adaptation had not been exploited up to now. With the presentation of light pulses in a 40 Hz sequence, we observed that the detection probability for each pulse remained constant and independent from the amount of presented pulses in a train (**Fig. 2.3e**). This corresponds to the observation that the number of stimulated sensory neurons can be traded off against the number of generated action potentials per neuron to produce the same perceptual intensity within a timeframe of up to 250 ms (Huber et al. 2008). This activity has to be read out by higher order cortical areas, integrating the overall amount of action potentials in a given period of time. The fact that higher-order networks, receiving S1 activity, appear to be able to optimally integrate all stimulus-evoked information (Brunton

et al. 2013) is surprising, especially in comparison to the strong modulation of perception by adaptation in S1 itself. Furthermore, it is important to note that intracortical synapses have also been shown to display adaptive response behavior (Abbott et al. 1997). While it is probable that light stimulation drives a sufficient amount of neurons in S1 non-adaptively to provide a corresponding output to other areas, the implications of intracortical adaptation for signal integration in higher cortical areas remains unclear. A possible interpretation could be that synaptic transmission to higher-order networks shows less depression (Gil et al. 1999) and integration of synaptic inputs operates over longer time scales as in S1, which would also explain why we observed only minor behavioral effects when changing temporal precision of light-induced cortical activity. In contrast, neural synchrony in thalamus has been shown to be crucial to drive activity in cortex, suggesting a transformation from temporal to rate coding at the thalamocortical synapse (Bruno and Sakmann 2006; Temereanca et al. 2008; Wang et al. 2010). A future experiment would thus be expression of ChR2 in thalamus and subsequent activation of axonal arbors within cortex to test whether reduced temporal precision would result in according changes in cortical firing and eventually animal behavior.

The finding that rats show relatively low frequency discrimination performance is in good agreement with a recent study by Waiblinger et al, demonstrating that rats perform poorly in detecting changes in frequency of an ongoing stimulus sequence (Waiblinger et al. 2013). To understand the underlying mechanism we used a theoretical model, based on integration of firing rates in each hemisphere and detection of their relative difference (**Fig. 2.2a**). The fact that our psychometric data could be replicated by this simple approach (**Fig. 2.1f**) suggests that repetition frequency is mainly encoded by firing rates rather than inter-spike intervals. Consequently, this rate code also explains how adaptation interferes with discrimination of stimulus sequences as it reduces firing rates in a frequency-dependent manner (Khatri et al. 2004b). In the context of texture discrimination, our findings support the hypothesis of texture coding by transient kinematic events, rather than frequency information (von Heimendahl et al. 2007; Ritt et al. 2008; Wolfe et al. 2008; Jadhav et al. 2009; Waiblinger et al. 2013). When animals sweep their whiskers over a surface they are deflected transiently due to discrete, high-velocity ‘slip-stick’ events (von Heimendahl et al.

2007; Ritt et al. 2008; Wolfe et al. 2008; Jadhav et al. 2009). The occurrence of such events is closely related to texture roughness, creating a detailed 'kinetic signature' of different surfaces (von Heimendahl et al. 2007). A contact sequence containing slip-stick events can be compared to a pulse sequences containing velocity deviants, as used in the present study (**Fig. 2.6**). The occurrence of tactile deviants evoked an increase in cortical activity that was close to non-adapted stimulus response amplitude while the remaining sequence was strongly adapted. As a consequence, the contrast between uniform and deviant pulses was increased and deviant perceptibility increased. This suggests that the main cue for texture discrimination might not be steady whisker vibration but changes in firing rate that are due to slip-stick events. In other words, firing rates of BC neurons would largely reflect the overall degree of stimulus diversity in a deflection pattern, rather than just the intensity of surface-induced whisker deflections. The encoding of such a 'diversity signal' due to adaptation is supported by the notion that BC firing is increased with stimulus variance (Maravall et al. 2007) and the enhanced perception of stimulus intensity when presented as irregular sequences in humans (Lak et al. 2010).

The profound perceptual differences that we observe between sensory-evoked adapting and optically-induced non-adapting S1 activity have also implications for experimental approaches to induce synthetic sensory stimuli based on neural stimulation. We and others observed that artificial S1 stimulation can drive learned behavior that was based on previous sensory stimulation (Romo et al. 1998; O'Connor et al. 2013; Sachidhanandam et al. 2013), suggesting that peripheral sensory input can be substituted by direct stimulation of cortical neurons. Moreover, animals that were trained to respond to S1 stimulation could readily transfer this behavior to whisker stimulation in a simple detection task (Sachidhanandam et al. 2013). In the 2-AFC setting used in the present study, however, animals did require a certain amount of trials with light stimulation before reaching stable behavioral performance. In fact, it is not surprising that the perception of synthetic stimuli appears to largely differ from peripheral stimulation (**Fig. 2.3f; 2.4b; 2.5b**). As we show in the present study, synthetic stimuli induced perceptions comparable to whisker stimulation when imposed with adapting time courses (**Fig. 2.5d**) up to the point where animals showed no preference for either optical or whisker stimulation when repetition frequency was equal

(**Fig. 2.5c**). We therefore argue that synthetic stimulation approaches have to consider adaptation rules in order to induce more naturalistic sensory perception. The emulation of adaptive response behavior could also serve as a basis to implement effective cortical stimulation strategies for brain-machine interfaces or neuroprosthetics. Further optogenetic application could address the importance of different cell types and their functional connectivity, ultimately leading to optimized stimulation patterns that are naturally interpreted by neocortical circuits.

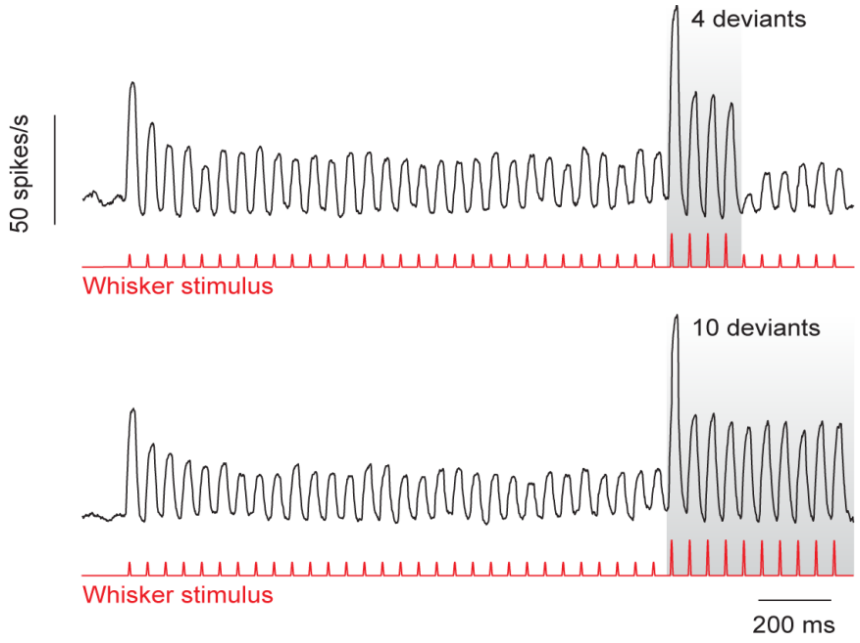

Supplementary Figure 2.9. Adaptation of deviant stimuli with repeated stimulation.
PSTHs of BC neurons in response to a 2-s long whisker sequence with either four or ten deviant pulses after 1.5 s. To remain comparability to **Fig. 2.6a**, PSTHs were smoothed with a 25-ms moving average.

2.4. Methods

2.4.1. Animals and surgical procedures

All experimental and surgical procedures were approved by the local veterinary authorities (Veterinary Office, Canton Zürich). They conform to the guidelines of the Swiss Animal Protection Law, Veterinary Office, Canton Zurich (Act of Animal Protection 16 December 2005 and Animal Protection Ordinance 23 April 2008). Behavioral data with tactile and optogenetic stimulation were obtained from three female adult Sprague-Dawley rats (250-350 g). Additional electrophysiological data were obtained from two adult, female Sprague-Dawley rats under wakefulness and from seven female adult Sprague-Dawley rats under isoflurane anesthesia (see below). Rats were housed in groups of two with food ad libitum

and were subjected to water deprivation for 5 days/week during behavioral testing. Body weight was monitored prior to each of the two daily testing sessions, during which water acted as reward. To ensure that animals' weight between training sessions remained above 90% of their initial weight, additional water was given if it dropped below this threshold. The animals were housed in groups of two under an inverted 12:12 h light-dark regime and trained during their active dark cycle.

In a first surgery, a head post was implanted as described previously (Mayrhofer, Skreb, Behrens, et al. 2013). In brief, animals were anesthetized with 2% isoflurane in oxygen and nine titanium screws (Modus 1.5, 3-mm length; Medartis, Basel, Switzerland) were inserted into the skull, acting as anchors for the headcap. The headcap was formed by layers of transparent light-curing dental cement (Tetric EvoFlow; Ivoclar Vivadent, Schaan, Liechtenstein) on top of a bonding layer (Gluma Comfort Bond; Heraeus Kulzer, Hauna, Germany) that was applied to the cleaned skull. All animals were 12-15 weeks old on day of headpost implantation. In a second surgery, a viral construct that contained the ChR2 gene was injected into the C1-barrel in S1 under isoflurane anesthesia (1–2%). The head was fixed in a stereotaxic frame (David Kopf Instruments, Tujunga, CA), the skull over the barrel cortex was thinned and a cortical response map was created using intrinsic optical imaging at 630 nm illumination (Grinvald et al. 1986). Subsequently, a small craniotomy (~1 mm^2) was made to allow injection of the viral construct AAV1.hSyn.hChR2-EFYP.WPRE.hGH (Titer = $5.7x10^{-13}$ GC/ml; Penn Vector Core, Philadelphia, PA). For better diffusion in tissue, 1 µl of 30% Mannitol was added to 1.5 µl aliquots of virus solution. To prevent dimpling of the brain the dura was incised at the injection site. For each hemisphere, a total amount of 1 µl was injected using a microinjection pump (WPI Inc., Sarasota, FL) and pulled glass pipettes. Injection depth was 500 µm and the flow rate 50 nl/min. After virus injection, a multimode glass fiber (length ~6 mm, diameter = 400 µm, NA = 0.48, Thorlabs Inc., Newton, NJ), glued into a short stainless steel ferrule (length ~5 mm) was positioned above the injected barrel. The ferrule was then fixed to the headcap using light-curing dental cement. After surgery animals were provided with analgesics (110 mg/kg body weight, Novaminsulfon; Sintetica, Mendrisio, Switzerland) and antibiotics (100 mg/kg body weight, Ceftriaxon; Rocephin,

Roche Pharma, Switzerland). For each animal we waited at least 4 weeks for expression of ChR2 before starting behavioral testing with blue light stimulation.

2.4.2. Histology and estimate of light transmission in cortex

The mean extent of ChR2 expression for all injections was 2.1 ± 0.3 mm (mean ± standard deviation) and highly consistent across all behaving animals and injection sites. To estimate the size of the illuminated area in cortical tissue, we used a theoretical model based on measurement of light transmission through brain slices (**Supplementary Fig. 2.4d**) (Aravanis et al. 2007). To generate model estimates, we used the brain tissue light transmission calculator (under http://www.stanford.edu/ group/dlab/optogenetics /calc), provided by the Deisseroth lab. The lowest required intensity for robust single pulse detection was 1.6 mW/mm^2 at the brain surface. At a distance of 0.18 mm light irradiance was 0.5 mW/mm^2, which, to the best of our knowledge, is the lowest intensity that was shown to induce spiking in awake animals (Guo et al. 2014). Assuming that light might also affect neurons slightly below this value, we therefore estimate that light stimulation should only drive neural activity within a distance of about ~0.35 mm from the fiber tip (until irradiance was below half of 0.5 mW/mm^2). Also, when applying the simplified assumption that light spreads equally in all directions from the fiber tip, it is also possible that adjacent barrels were affected by light stimulation.

2.4.3. Behavioral setup and paradigms

Three female adult rats were trained to perform in a 2-AFC paradigm for detection and discrimination of whisker stimuli. The behavioral setup has been described in detail previously (Mayrhofer, Skreb, Behrens, et al. 2013). In brief, animals were placed in a head fixation box and the C1-whiskers were stimulated with a set of piezo bending actuators (Piezo Systems, Woburn, MA). Whisker stimuli consisted of individual or uniform sequences of prototype pulses (single-period 120-Hz cosine wave). Whisker deflection velocity was changed by modifying prototype peak amplitude (maximal deflection amplitude = 300 μm) whereas frequency was changed by varying inter-pulse time intervals (**Supplementary Fig. 2.10**).

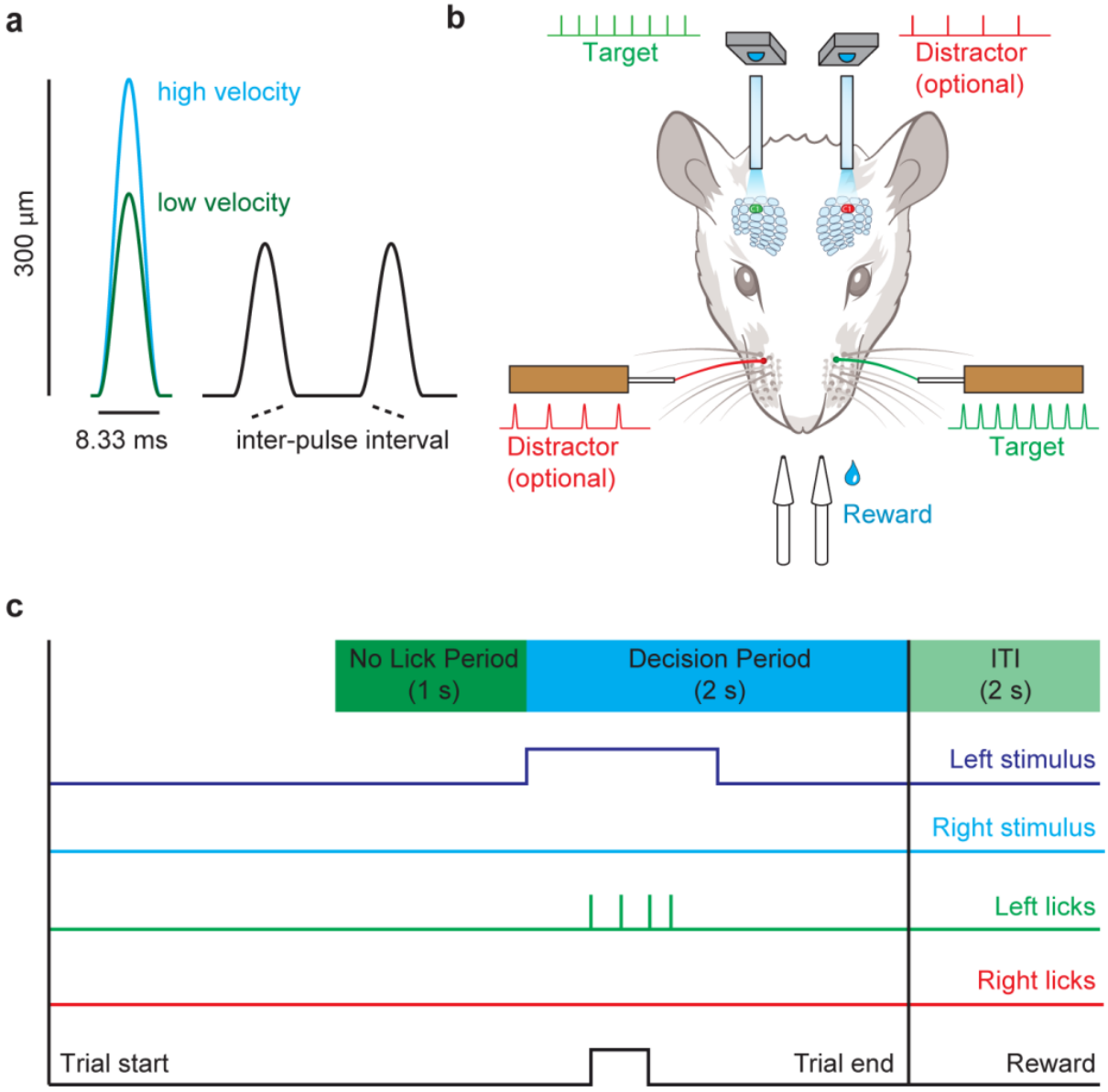

Supplementary Figure 2.10. Illustration of whisker stimuli and single trial timing.
a, To change whisker stimulus velocity, we adjusted the amplitude of the 120 Hz cosine prototype pulse (left). To change repetition frequency, the interval between two prototype pulses was varied (right). **b**, Illustration of the behavioral setup, showing the piezo bending actuators used for whisker stimulation and LEDs that were connected via glass fibers for optical stimulation. Animals received a water reward when licking on the water spout that corresponded to the target side. **c,** Temporal organization of a single trial during behavioral testing.

Animals performed three different tasks: Detection of single stimuli or stimulus trains, discrimination of stimulus trains at different repetition frequency and detection of deviant pulses of higher deflection velocity. During stimulus detection, stimuli were presented to

either the left or the right C1 whisker and animals received a water reward when correctly responding to the respective stimulus side by touching one of two water spouts (positioned to the left and right in front of the animals head) with their tongue. Initially, head-fixed animals had to detect single pulsatile stimuli of differing velocities. The resulting detection performance of every animal was then used to adjust whisker deflection velocities during subsequent behavioral testing (see also 'Behavioral data analysis' and **Fig. 2.1d**). To test detection performance with increasing pulse counts, deflection velocities were adjusted to M_{50} detection performance and short trains of pulsatile stimuli of differing lengths (1-4 pulses with an inter-pulse interval of 25 ms) were presented to the animal. During repetition frequency discrimination, animals had to compare pairs of vibrotactile stimuli that were presented simultaneously at both whiskers. Deflection velocities were set to M_{100} detection performance. High repetition frequency stimuli (20/40 Hz) were always considered as the target, which had to be chosen over a distractor stimulus of lower repetition frequency (1/3/5/10/15/20/25/30/35 Hz). Trials of different target and distractor repetition frequency were randomly intermixed within each session. 20 Hz sequences could occur as either target or distractor stimuli, thus ensuring that animals had to rely on repetition frequency to discriminate sequences instead of identifying a constant target percept. See also **Supplementary Fig. 2.10b** for an illustration of the behavioral setup. For deviant detection, a 2-s long, vibrotactile stimulus at 20 Hz and M_{50} deflection velocity was presented at both whiskers. After 1.5 s a deviant at M_{100} deflection velocity was embedded in the target stimulus. The deviant sequence was 1, 4 or 10 pulses long and animal's response after deviant occurrence was measured to compute deviant detection performance.

The trial structure was as follows: After trial start, stimuli were presented after 2.5 s with a temporal jitter of up to 30% to avoid animal's prediction of stimulus occurrence. A no-lick period of 1 s prior to stimulus onset was used. Licks that occurred within this period resulted in a shift of the stimulus onset by 1 s (**Supplementary Fig. 2.10c**). Stimulus duration was 1 s for stimulus detection and discrimination and 2 s for deviant detection. Stimuli were presented to either the left or the right C1 whisker and animals received a water reward when correctly responding to the stimulus side by licking the respective water spout. The decision period at which the animal's response was measured was 2 s after stimulus onset

or occurrence of the deviant in case of deviant detection. Two additional rats were trained on detection of 40-Hz sequences at M_{100} velocity to obtain electrophysiological recordings of BC neurons in task-engaged animals.

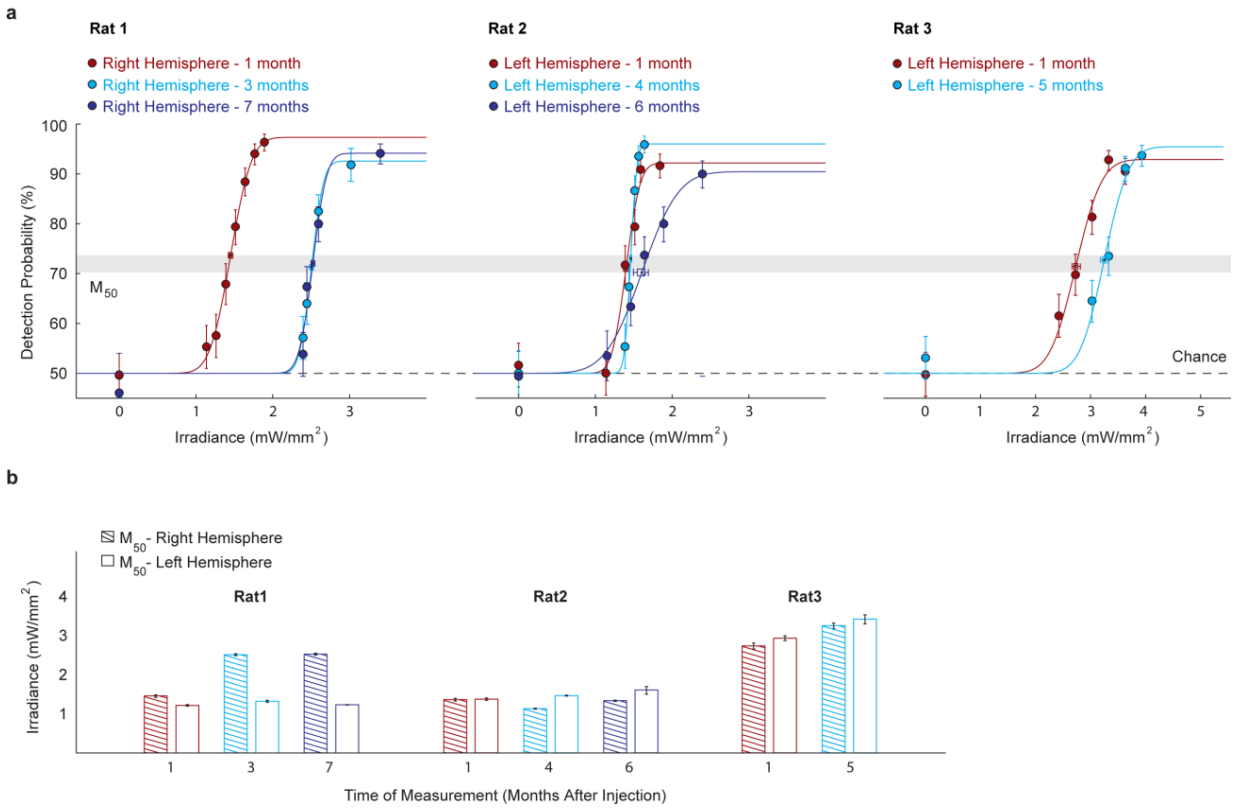

Supplementary Figure 2.11. Long-term stability of optical stimulation.
a Psychometric curves for detection of single light pulses at different time points after ChR2 expression. **b,** M_{50} values for all animals and hemispheres over the course of up to seven months after initial ChR2 expression. Although we observed some changes in required irradiance over time M_{50} values where mostly stable, indicating that our approach for cortical stimulation was suited for stable long-term application.

2.4.4. Optogenetic stimulation

For light stimulation, we connected the glass fiber implants with ~1 m long glass fibers (diameter = 1000 µm, NA = 0.48, Thorlabs Inc., Newton, NJ) that were attached to high-power LED light sources (λ = 470 nm, Nichia Corp., Tokushima, Japan). Light stimuli consisted of pulse trains with equal frequencies as during whisker stimulation. Each pulse consisted of a 1-ms long square wave. Again, single light pulse detection performance was used to assess the required light intensities for subsequent behavioral testing (intensity was measured for each hemisphere individually). In each animal we tested responsiveness to light pulses repeatedly over the course of behavioral testing and adjusted light intensity accordingly (**Sup-**

plementary Fig. 2.11). This was usually done between different behavioral paradigms, for rat 1 the second test was performed earlier after we noticed an imbalance in stimulus perception between left and right hemisphere (**Supplementary Fig. 2.11a**). Behavioral paradigms for stimulus detection, discrimination and deviant detection were the same for both whisker and light stimulation. To reduce temporal precision of neural excitation, 1-ms pulses were subsequently modified to 15-ms light ramps of monotonically increasing intensity (**Fig. 2.4a**). Here, stimulus discrimination was tested only with frequencies up to 20 Hz because we observed unreliable response behavior of stimulated neurons with 40-Hz light ramp sequences (**Supplementary Fig. 2.8**). This change in reliability is most likely due to the 15-ms duration of light ramps, reducing the duration of the break between two ramps to 10 ms (instead of 24 ms with 1-ms pulses), which is too short to ensure sustained ChR2 stimulation (Boyden et al. 2005).To recover adaptive neural behavior during light stimulation, light amplitude of non-initial pulses was modified according to adaptation indices derived from electrophysiological recordings: The initial pulse in a sequence was set to M_{100} amplitude, following pulses were reduced depending on stimulus frequency and single pulse detection performance (for more details, see also 'Behavioral data analysis'). For all paradigms we used 500 trials per animal and condition, resulting in 1500 trials in total. Only when combining whisker targets with uniform light distractors (**Fig. 2.5b**, dark blue) less trials were acquired at higher distractor frequencies, due to the strongly biased animal behavior (at least 150 - 200 trials per animal). For an exemplary overview of the complete training schedule for different behavioral paradigms see **Supplementary Fig. 2.12**. In case of stimulus discrimination with low light power (**Supplementary Fig. 2.7**), only one animal was tested (Rat 3). Data presented in this figure therefore consists of 500 trials per data point.

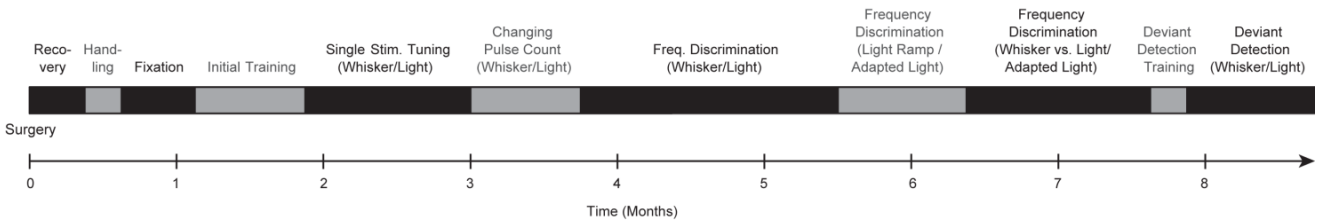

Supplementary Figure 2.12. Overview of behavioral paradigms.
Schematic overview of the time course for training and data acquisition, using different behavioral paradigms. Time point zero remarks the surgery for injection of the viral construct.

To ensure that animals would not be able to use visual cues from light stimulation, fibers and connectors were shielded with black rubber tubing. In addition, a blue LED was positioned ~10 cm above the animals head. This masking LED produced light flashes (irradiance = 150 mW/mm^2) of equal length as every light pulse presented on the brain surface, thus preventing the animal from associating potential visual cues with target or distractor side. To keep conditions constant over all behavioral sessions, the masking LED was also active during whisker stimulation (producing 1-ms light pulses for every whisker deflection). Whisker movements during optogenetic stimulation (**Supplementary Fig. 2.13**) were monitored with a laser curtain and a linear CCD array (3.5 µm resolution at 2.5 kHz sampling rate; RX 03; Metralight, San Mateo, CA). To ensure robust tracking of whisker motions, a light polyimide tube (weight = 0.7 mg, diameter = 250 µm) was put on the C1 whisker All components of the setup were controlled and monitored with millisecond temporal precision by a custom-written program (LabVIEW 2010, National Instruments, Austin, TX) running on personal computers using multifunctional data acquisition cards (PCI-6259; National Instruments).

2.4.5. Electrophysiological recordings

For electrophysiological recordings in awake animals two adult, female Sprague-Dawley rats were chronically implanted with single shank, 16-contact electrode arrays with 100 µm contact spacing (NeuroNexus, Ann Arbor, MI). Surgical procedures were the same as for implantation of glass fibers (see above). We implanted two probes in rat 1 (one on each hemisphere) and a single probe in rat 2, resulting in 48 recording sites in total. 10 sites were removed from the analysis as they showed no visible spiking activity; from the remaining we recorded 10 single-units and 23 multi unit clusters over all cortical layers. Adaptation of individual recording sites and layers are shown in **Supplementary Fig. 2.1**. Recordings were made with a commercially available system (Multi Channel Systems MCS, Reutlingen, Germany), consisting of two 8-channel pre-amplifiers (2x gain), a 64-channel amplifier (600x gain) and a 64-channel PCI-bus data acquisition card. Data were digitized with a bandwidth of 0.1 Hz – 15 kHz at 32 kHz and 12 bit. For stimulation we used piezo bending actuators (Piezo Systems, Woburn, MA) that were driven by a 3-channel piezo controller (Thorlabs,

Newton, NJ). Movement of the stimulator was calibrated with a laser displacement sensor (Micro-Epsilon, Ortenburg, Germany) and strain gauge sensors mounted directly on the piezo element. Single whiskers were plugged into a glass capillary that was glued on the element. The distance between capillary tip and whisker base was ~5 mm and we always stimulated the whisker that corresponded to the recorded barrel (either C1 or D1). Each trial consisted of a 1-s baseline and 1–2 s stimulus presentation. Inter-trial duration was 2 s. Different stimuli were presented in randomized order. We recorded neural responses to three sets of stimuli: First, single whisker pulses at differing velocities (150, 300, 600, 900, and 1200°/s). Second, 1-s long pulse trains with a whisker velocity of 850°/s and different frequencies (1, 5, 10, 20, 30, and 40 Hz). Third, 2-s long pulse trains with a velocity of 350°/s and repetition frequency of 20 Hz with and without deviant pulses (1, 4 or 10 pulses with a velocity of 850°/s) after 1.5 s. In the same set, we also presented single pulses with a velocity of 350°/s or 850°/s. To acquire a sufficiently high amount of trials in response to all presented stimuli, different stimulus sets were presented in separate recording sessions. In each session, animals were recorded for a total duration of up to 40 minutes. All three recording sessions were always performed within 24 hours. Visual data inspection showed no observable difference in recording quality or spontaneous activity of neurons. For recordings in task-engaged animals, two trained, female Sprague-Dawley rats were implanted with 16-contact electrode arrays in the left hemisphere. Surgical procedures were the same as described above. Animals were trained to detect 40-Hz whisker stimulus sequences, applied to the principal whisker and we recorded responses from 19 recording sites across all cortical layers (**Supplementary Fig. 2.2c**).

To record neural responses to light stimulation, we acquired electrophysiological data under isoflurane anesthesia from seven female adult Sprague-Dawley rats. Animal temperature was monitored with a rectal temperature probe and maintained at 37°C by a feedback-controlled heating pad (Harvard Apparatus, Holliston, MA). The head was fixed in a stereotaxic frame (David Kopf Instruments, Tujunga, CA). After exposing the skull, the bone over the left barrel cortex was thinned and the corresponding whisker representation was identified using intrinsic optical imaging. A small (~2 mm^2) craniotomy was made and the dura was incised at the point of penetration. Lastly, a small acrylic dam was built around the

skull opening and filled with saline. To record neural activity from individual neurons, pulled borosilicate glass pipettes with an impedance of 7-10 MΩ were used. Pipettes were filled with 0.9% NaCl solution and connected to a silver wire that was used for recording. To identify ChR2-expressing neurons, we used a light pulse at low repetition rate (1 ms; 0.5 Hz) while moving through cortex and only recorded cells that showed consistent responses to light stimulation. We recorded well isolated single units (*n* = 15) and performed additional control recordings to ensure that glass pipette recordings were not contaminated by any potential light induced artifacts (Cardin et al. 2010) (data not shown). For illumination we used ~1-m long glass fibers (diameter = 400 µm) that were connected to a blue diode laser (λ = 473 nm, Omicron-Laserage, Offenbach, Germany) and positioned directly above the recording site. For each recorded neuron we presented 1-s long stimulus trains (peak irradiance = 100 mW/mm^2) of differing frequencies (1, 5, 10, 20, and 40 Hz) and pulse durations (either 1-ms long square-wave pulses or continuously increasing 15-ms long ramps). Different frequencies and single pulse profiles were presented in the same recording session in pseudo-randomized order. Electrophysiological data were 1000-fold amplified and digitized at 32 kHz and 16 bit with a bandwidth of 1 Hz – 5 kHz, using a commercially available USB recording system (Multi Channel Systems, Reutlingen, Germany).

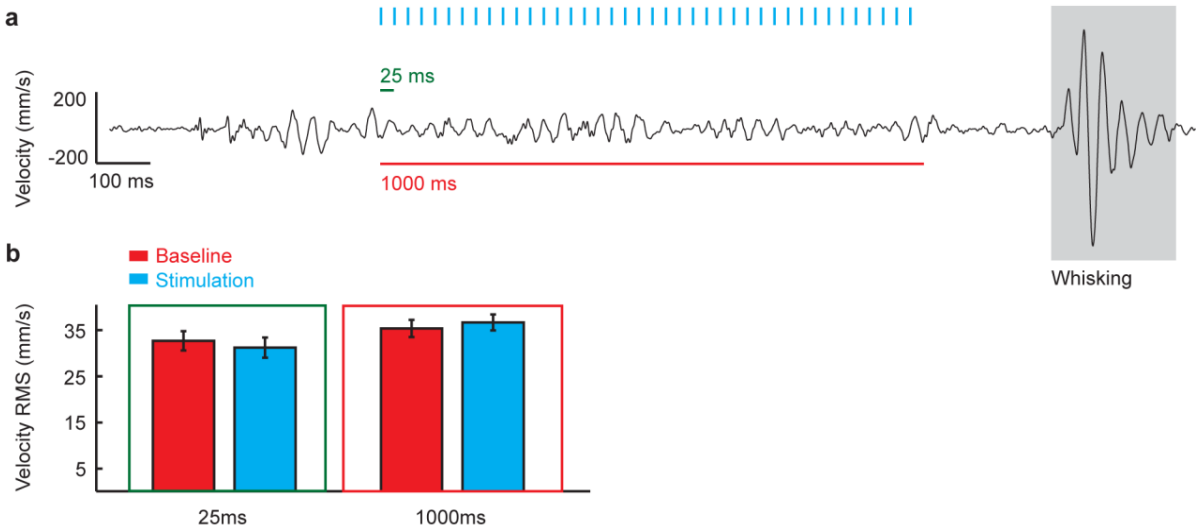

Supplementary Figure 2.13. Whisker movements during optical stimulation.
a, Single trial example for velocity of the C1 whisker during 40 Hz stimulation of its corresponding barrel in S1. Gray square indicates changes in velocity due to whisking activity. **b,** Root-mean-squared (RMS) whisker velocity, either 25 or 1000 ms before (baseline) and after (stimulation) light pulse presentation. In both cases, we did not observe any significant difference between the two conditions.

The same system was also used for recording neural responses to light stimulation in one female Sprague-Dawley rat that was awake but not engaged in a behavioral task. Here, a 400-µm diameter glass fiber was connected to a 16-contact electrode array (same as described above) using dental cement. The array was implanted in BC of the left hemisphere and we recorded neural responses from 12 recording sites in response to optical stimulation at 20- and 40-Hz (**Supplementary Fig. 2.6**). Optical stimuli were delivered as described for behaving animals, peak irradiance was set to 100 mW/mm^2.

2.4.6. Behavioral data analysis

All data analysis procedures were implemented using MATLAB (2010b, The Mathworks, Inc., Natick, MA). The data set consisted of behavioral recordings from three rats in three conditions (stimulus detection, repetition frequency discrimination and deviant detection) with whisker, light or combined stimulation. A trial was counted as correct (hit) when the animal's initial response was on the target side or as a false (error) in the opposing case. A no-lick response within the 2-s time window after the start of the decision period was classified as a missed trial. Performance was computed as #hits/(#hits + #errors). To test for significant differences between behavioral conditions we used a binomial test. To avoid any multiple comparison bias, we additionally applied Bonferroni correction for the required p-value to reach significance. Statistical comparison of discrimination curves was done by using a two-sample Kolmogorov-Smirnov test. The RMSE was computed as the root-mean-square of the difference between two curves. To analyze psychometric single-pulse detection curves, we used a Matlab toolbox for psychophysical data analysis (version 2.5.6; see http://bootstrap-software.org/psignifit/). To adjust fit parameters and obtain statistical significance the toolbox implements the maximum-likelihood method described by Wichman and Hill (Wichmann and Hill 2001). We fitted a cumulative Gauss function to detection performance of individual animals and computed the turning point and asymptote (corresponding to M_{50} and M_{100}, respectively). In case of single light pulse stimulation, we additionally computed different values on the curve that corresponded to AIs of different frequencies (40Hz – M_{25}, 30Hz – M_{35}, 20Hz – M_{55}, 10Hz – M_{75}, 5Hz – M_{90}). The resulting light intensities

of each individual hemisphere were later used to determine the degree of attenuation of repeated pulses in 'adapting light' stimulus sequences (**Fig. 2.4c**).

For detection of stimulus sequences at varying pulse counts, the estimation of equal detection probability was based on the assumption of combinatorial probability of detecting at least one pulse in a sequence of *n* pulses:

$$P_{Sequence} = 1 - (1 - P_{Pulse})^{n} \quad (1)$$

To explain reduced detection probability of subsequent pulses by attenuation of neural response amplitude, the AI for 40Hz was added to the second and further pulse detection probability.

$$P_{AdaptedSequence} = 1 - (1 - P_{Pulse}) * (1 - P_{Pulse} * AI_{40Hz})^{n-1} \quad (2)$$

To apply both approaches to the 2AFC configuration, the minimum detection probability P_{Chance} was fixed at 50%. To correct for chance detection probability, P_{Pulse} was therefore computed as

$$P_{cPulse} = (P_{Pulse} - P_{Chance}) / (1 - P_{Chance}) \quad (3)$$

Finally, to maintain comparability to the measured behavioral data, chance performance was again added to $P_{cSequence}$.

$$P_{cSequence} = P_{cSequence} * (1 - P_{Chance}) + P_{Chance} \quad (4)$$

To estimate animal reaction times, we also computed median response times during whisker and light stimulation. Response time was calculated as the time difference between stimulus onset and the first lick response that was detected. We analyzed response times for successful detection of 40-Hz stimulus trains (7,000 trials per animal, 21,000 trials in total) for each whisker and light stimulation (**Supplementary Fig. 2.14**). Significance between reaction times with whisker and light stimulation was computed with a Wilcoxon rank-sum test for equal medians.

2.4.7. Electrophysiological data analysis

Raw-data was high-pass filtered at 600 Hz and thresholded to identify spike occurrence. For multi-unit activity (MUA) a threshold of 4 standard deviation units (SDU) was used. For single unit activity (SUA), the threshold was set to 15 SDUs. Resulting spike times were then downsampled to 1 kHz. In all subsequent analysis, we only used one individual session per stimulation paradigm and recording site. In awake recordings, trials that contained transients due to animal movement could be reliably identified by scanning for instantaneous occurrence of spiking in all 16 recording channels. Trials that met this criterion were removed from the analysis (~12% of all trials, remaining trial count per stimulus type and session varied from 71 to 103). In case of task-engaged recordings, we only analyzed trials,in which animals produced a behavioral response (hit or error). In this case, we also analyzed only the first 175 ms after stimulus-onset to avoid data contamination by movement artifacts that were due to licking responses of the animal. We used the Glass's Δ for single-pulse spike probabilities as a measure for the signal-to-noise-ratio (SNR) of each recording. Glass's Δ was computed as

$$\Delta = (\mathrm{mean}_{\mathrm{Signal}} - \mathrm{mean}_{\mathrm{Baseline}}) \,/\, \mathrm{SD}_{\mathrm{Baseline}} \tag{5}$$

where $\mathrm{mean}_{\mathrm{Signal}}$ is the mean neural response within 25 ms after the onset of the first pulse in a stimulus sequence and $\mathrm{mean}_{\mathrm{Baseline}}$ the mean spontaneous activity 25 ms prior to stimulus onset. $\mathrm{SD}_{\mathrm{Baseline}}$ is the respective standard deviation. To extract firing probabilities, we computed the PSTH for every recording, repetition frequency and stimulus type (bin size = 1 ms).

For adaptation indices (AIs), we computed the mean firing within 25 ms after each whisker/light pulse for stimulus sequences of varying repetition frequency. Subsequently, we subtracted the mean baseline activity (500 ms before stimulus onset) and normalized all values relative to the initial pulse response amplitude (**Fig. 2.1b**). AIs were defined as the mean response strength of all pulses except the first one in each stimulus sequence. To ensure that AIs were not spuriously high due to low SNR, only recordings with a Glass's $\Delta > 0.5$ were used for this analysis (33 out of 38 units). To test for differences in the spread of

stimulus response latencies between whisker and 15-ms light ramp stimuli, we fitted each PSTH for single stimulus presentation with a Gauss distribution and used the standard deviation σ as a measure of the distribution width. Significance was obtained using an unpaired *t*-test.

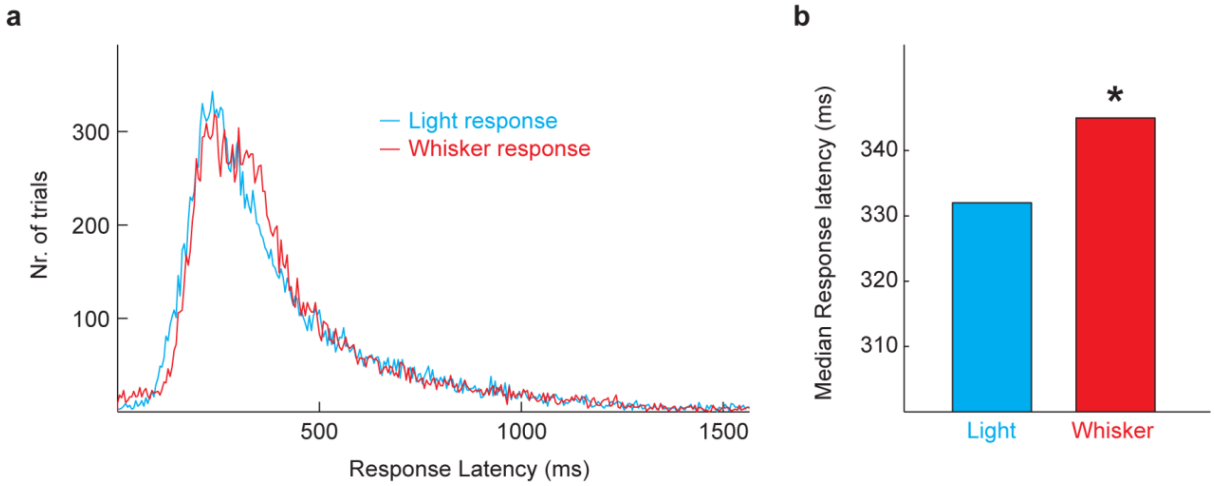

Supplementary Figure 2.14. Differences in response latency between whisker and optical stimulation. **a,** Distribution of response latencies for 21000 trials of either whisker or optical stimulation. Bin size is 5 ms. For visual purposes only, distributions were cut after 1550 ms. **b,** Median response latencies were significantly different ($p < 0.001$) with 332 ms during light and 345 ms during whisker stimulation.

During deviant presentation, we computed the mean response strength within 25 ms after presentation of single pulses at mean M_{50} (350°/s) and M_{100} (850°/s) amplitude (non-adapted response). For adapted responses, we computed the mean response strength to either an M_{100} deviant or a standard M_{50} pulse in 20 Hz sequences at M_{50} amplitude after 1.5 s. To test for significant differences between adapted and non-adapted responses, we used a paired *t*-test. Before *t*-testing, we performed a Lilliefors test on each condition to confirm they followed a normal distribution ($p<0.05$ for all tested cases).

2.4.8. Modeling of behavioral performance

Based on a previous study (Stüttgen and Schwarz 2010), we constructed a theoretical model to relate behavioral performance to neural activation patterns during different conditions. For each cell (n = 33) we used its respective PSTH to construct a single Monte-Carlo sampled spike train. Spike trains of all cells, were then summed together to compute a population PSTH in response to a single stimulus presentation. To include temporal integration, the population PSTH was convolved with an exponential decay function of the form $\exp(-t/\tau)$

(normalized to have an integral of 1, where *t* is time in milliseconds). To approximate membrane time constants of pyramidal cells in adult animals, the time constant τ was set to 20 ms (Trevelyan and Jack 2002). The same procedure was repeated to compute two convolved population PSTHs, mimicking the two respective hemispheres in a 2-AFC condition. As in our behavioral paradigm, one PSTH was computed using a higher repetition frequency as a target, the other with lower repetition frequency as a distractor. Subsequently, the distractor PSTH was subtracted from the target PSTH. If the peak spike-count of the resulting differential PSTH exceeded a threshold α, the trial was counted as a hit. Conversely, if spike counts went below a negative threshold –α, the model produced an error. The first threshold crossing after stimulus onset was always used to determine model behavior. In trials were the threshold was not crossed model performance was fixed at chance levels and therefore trials were either counted as hit or error with 50% probability. In each condition, the above procedure was repeated for 1500 trials. An illustration of the model is given in **Fig. 2.2a**. The same approach was also used for adapting and non-adapting single pulse discrimination. Here, recordings of 20-Hz base sequences with and without occurrence of a single deviant were used to obtain target and distractor PSTHs and perform 'adapting pulse' discrimination. Only threshold crossings after deviant occurrence were taken into account. 'Non-adapting' pulse discrimination was achieved by using neural responses to single pulses of deviant (target) and base (distractor) amplitude.

To determine the detection threshold α, we tuned the model by detecting single whisker deflections of varying amplitude (150, 300, 600, 900, and 1200°/s) against stimulus-free spontaneous activity. We tested different thresholds between 0.05 and 1 with a step size of 0.01 and each resulting model was compared to animal's mean single pulse detection performance. Animal performance was normalized by dividing with its maximum, thus allowing the model to obtain optimal detection performance while still resembling the same psychophysical dynamics. Similarity index *S* between animal and model performance was

$$S = log(1/RMSE) \tag{6}$$

where RMSE is the root-mean-squared error between real and modeled detection performance. The highest similarity was achieved by using a threshold of α = 0.64. As shown in

Supplementary Fig. 2.1, the model exceeded animal's detection performance while both single pulse detection curves were well described by a cumulative Gaussian function and had almost identical inflection points. This indicates that our theoretical approach was fit to resemble animal behavior in a 2AFC condition while achieving strong signal detection performance. The same threshold was used during all behavioral conditions, i.e. repetition frequency discrimination and deviant detection. In addition, we used the same approach as described above but created spike traces solely based on firing probabilities of individual cells (the amount of produced traces was kept equal to the population model) to assess their repetition frequency discrimination performance (**Fig. 2.2d**).

Chapter 3 : Processing of sensory deviations in the primary somatosensory cortex

S. Musall, M. Durmaz, F. Haiss, B. Weber, W. von der Behrens

Cerebral Cortex, in review 5 June 2015.

My contributions to this study were the following: I was involved in the experimental design of the study and performed a part of the electrophysiological recordings in anesthetized rats. I also did part of the behavioral training and psychophysical testing of rats. I also performed the data analysis and was involved in writing the manuscript.

Background: Stimulus-specific adaptation (SSA) to repetitive stimulation has been proposed as a potential mechanism to separate behaviorally relevant features from a stream of continuous sensory information. SSA in the neocortex is believed to be due to short-term depression of stimulus-specific inputs onto sensory neurons. However, whether this mechanism fully accounts for cortical SSA and how it affects sensory perception is unknown. To address these issues, we tested the behavioral implications of SSA in a deviance detection paradigm and characterized neural responses to deviant stimuli in rat somatosensory cortex.

Results: We trained rats to detect single-whisker deviant stimuli and found that detection performance was strongly enhanced when deviants differed in multiple features from background stimulation. Likewise, changes in different stimulus features also evoked robust SSA in single neurons in somatosensory cortex. Notably, SSA was weakest in the granular input layer and significantly stronger in the supra- and infragranular layers, implying that a major part of SSA is generated within the cortex. This was corroborated by a deviant-specific late sensory response, occurring in a subpopulation of layer IV neurons roughly 200 ms after stimulus offset.

Conclusion: Our study provides the first behavioral evidence for enhanced perception of rare deviant stimuli, characterized by a set of specific stimulus features. Moreover, we found that deviant responses are actively amplified within cortex, especially in the supragranular layers. These results demonstrate the functional importance of cortical SSA and strongly implicate deviance detection as a feature of intracortical stimulus processing.

3.1. Introduction

The sensory environment is usually composed of many different sources, forming a complex scene that has to be structured by the nervous system in order to achieve efficient stimulus processing. A first step to reduce sensory input diversity is the reduction of neural responses to highly repetitive stimuli (Wark et al. 2007). Such adaptation of neural responses is an omnipresent feature in sensory systems and occurs at virtually all stages of the sensory pathway (Ohzawa et al. 1982; Khatri et al. 2004b; Ganmor et al. 2010b). A special case of adaptation that is mainly observed in the neocortex is stimulus-specific adaptation (SSA) without a

generalization towards other stimulus features (Ulanovsky et al. 2003; Katz et al. 2006; Hershenhoren et al. 2014). Here, sensory neurons selectively adapt to highly repetitive stimuli but retain their responsiveness to deviant stimulus features. Importantly, such deviant stimuli are not required to be of higher physical intensity to increase neural responses; as might be expected with general adaptation (Dudai 2004; Nelken 2007). SSA is thus a potential single cell correlate of habituation (Netser et al. 2011; Gutfreund 2012). A similar effect is also seen in electroencephalographic (EEG) recordings in humans, showing an additional negative response to deviant stimulation, called mismatch-negativity (MMN) (Näätänen 2009; Todd et al. 2013). Whether SSA is a potential source of MMN is still under intensive debate (Nelken 2007; Sussman and Shafer 2014; Stefanics et al. 2014) and has been subject of numerous studies (Ulanovsky et al. 2003; Fishman and Steinschneider 2012; Harms et al. 2014).

Recent studies also showed that adaptation in somatosensory cortex improves detection of deviating whisker stimuli (Musall, von der Behrens, et al. 2014) and discrimination of neighboring whiskers (Ollerenshaw et al. 2014). Although these behavioral effects could be explained by general firing-rate adaptation, it is likely that enhanced deviant perception critically depends on the stimulus-specific separation of repetitive and deviating stimuli that is the hallmark of SSA. SSA has been observed in the auditory (Hershenhoren et al. 2014; von der Behrens et al. 2009; Farley et al. 2010; Mill et al. 2011; Taaseh et al. 2011) and visual system (Movshon and Lennie 1979; Müller et al. 1999; Reches et al. 2010) as well as the somatosensory cortex (Katz et al. 2006). A common explanation for SSA is the conversion of stimulus-specific inputs onto a single sensory neuron (Katz et al. 2006; Nelken 2014). Repeated stimulation of one of these sensory channels will reduce its transmission efficacy due to short-term synaptic depression (Chung et al. 2002; Khatri et al. 2004b; Katz et al. 2006) while the neuron still remains responsive to other synaptic inputs. Although this input depression model accounts for many aspects of SSA, deviant responses in cortex are stronger as theoretically predicted (Taaseh et al. 2011) which might be due to intracortical response modulation (Szymanski et al. 2009).

In the present study, we sought to address the behavioral implications of SSA and whether it is enhanced by intracortical stimulus processing. We trained rats in a deviant detection paradigm and presented deviant stimuli that differed in several stimulus features from a simultaneously presented background sequence. In agreement with the presumption of SSA, we found that changing stimulus features strongly enhanced perception of deviant stimuli. We then performed electrophysiological recordings of single neurons and local field potentials (LFP) in somatosensory cortex and used an oddball paradigm (Squires et al. 1975b) to identify deviant-specific neural response patterns. We found robust SSA to several stimulus features that could be accurately predicted by a simple model using a small set of parameters. To study intracortical deviant processing, we applied spike and current-source density (CSD) analysis and found a distinct laminar response pattern that was specific for deviant stimulation. Furthermore, we observed a second sensory response to deviant stimulation that was restricted to neurons in the granular layer and occurred not until several hundred milliseconds after stimulus onset.

3.2. Results

3.2.1. Somatosensory deviant perception

Our first goal was to address whether SSA has a significant impact on deviant perception. We therefore trained three rats in a behavioral discrimination paradigm where single-whisker deviant stimuli were embedded in a 20-Hz standard stimulation sequence (Musall, von der Behrens, et al. 2014). To determine the amplitudes for standard and deviant stimuli we first presented single pulse whisker deflections to either the left or right side of the animal. Animals responded by licking one of two water spouts and were rewarded when choosing the side that corresponded to the side of stimulus presentation.

Based on animal's detection performance (**Fig. 3.1a**, black trace) we used the amplitude that induced the half-optimal single-pulse detection for the standard sequence and optimal detection for deviant stimuli (dashed lines). In the deviant detection paradigm, we presented two 20-Hz whisker stimulus sequences simultaneously to either the C1 or C2 whiskers on both sides of the rat's snout (**Fig. 3.1b**). On the target side, the stimulus se-

quence contained an additional deviant stimulus that occurred after 1.5 s (red trace). Deviant stimuli were always of higher velocity and we wanted to assess whether changing additional stimulus features like deflection direction (blue trace) or whisker identity (green traces) would affect deviant perception. Indeed, we found a profound difference in deviant detection performance between behavioral conditions. Rats detected single velocity deviants in 68.64 % of all trials which was well above 50 % chance performance (**Fig. 3.1c**; binomial test, $P<10^{-5}$, n=1500 trials). Additionally reversing deviant direction strongly increased detection performance to 75.19 % (χ^2 test, $\chi^2(1) = 15.931$, $P < 10^{-5}$). Deviant presentation on the neighboring whisker resulted in an even higher detection performance of 80.61 % ($\chi^2(1) = 109.813$, $P < 10^{-5}$) which was close to optimal single pulse detection performance (84.81%).

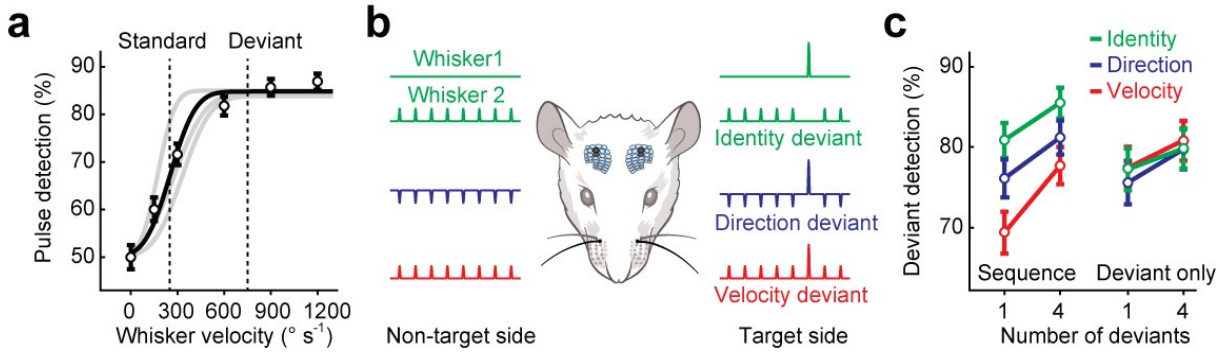

Figure 3.1. Behavioral implications of somatosensory SSA.
a, Single-pulse detection performance against whisker deflection velocity. Circles show mean performance over three animals (n = 1500 trials) and the trace a sigmoidal fit. Gray traces show fits for performance of individual animals. Dashed lines indicate the chosen amplitudes for standard sequences and deviant stimuli.
b, Schematic of the behavioral paradigm for single deviant detection. Two 20-Hz sequences were concomitantly presented on both sides of the animal. The target sequence additionally contained a deviant stimulus, occurring 1.5 s after sequence onset. Velocity deviants (red) were of higher deflection amplitude than standards. Direction deviants (blue) were also of higher amplitude but additionally differed from standards in their deflection direction. Identity deviants (green) were presented on a different whisker as the standard sequence.
c, Deviant detection performance for velocity, direction and identity deviants. When presented in a standard sequence, direction and identity deviants were detected more robustly than velocity deviants ('Sequence'). In the deviant only condition all deviant stimuli were detected equally. Error bars indicate 95% CIs.

This improvement in deviant detection demonstrates the importance of SSA for stimulus perception. Changing the context between deviant and standard stimulation alone increased detection performance by up to 12 % although the physical properties of deviant stimuli were identical in all three conditions. Presenting four uniform deviant pulses in the

target sequence did not further increase the difference between behavioral conditions. This suggests that the observed improvement relies on the increased perceptual contrast of deviants against standard stimuli and is not further modulated by additional deviant presentation (Musall, von der Behrens, et al. 2014). Consequently, no differences between modalities could be observed when deviants were presented without 20-Hz sequences ('Deviant only', **Fig. 3.1c** right, see also **Supplementary Fig. 3.1**).

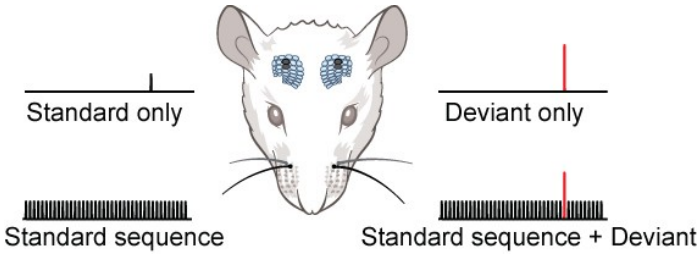

Supplementary Figure 3.1. Comparison of the deviant and deviant only detection paradigm.
In the standard case, a 20-Hz whisker sequence was presented on both sides of the animal (bottom traces) and an additional deviant was embedded in the target set (right trace, red pulse). In the deviant only condition, the standard sequence was omitted and only a single stimulus was presented on both sides. The target stimulus had the same amplitude as the deviant, the non-target the same as the standard.

3.2.2. SSA in rat somatosensory cortex

To assess whether enhanced deviant perception is based on increased neural responses in somatosensory cortex, we simultaneously recorded single-unit (SU) and LFP responses in the rat barrel cortex under isoflurane anesthesia (**Fig. 3.2a**). All recordings were performed, using 16 contact multi-electrode arrays within single barrels that were identified with intrinsic optical imaging and SUs were isolated based on spike waveform (**Supplementary Fig. 3.2**). The oddball paradigm was based on a 1-Hz sequence of pulsatile whisker deflections that were applied to either the contralateral, principal whisker (PW) or an adjacent whisker (AW). In 10% of all stimuli, the high-probability standard sequence (**Fig. 3.2a**, black traces) was interrupted by a deviant stimulus, applied to the other whisker (red traces). After 1000 stimulus presentations, the whisker identity of standard and deviant were swapped and a second block of 1000 stimuli was presented, thus correcting for asymmetric responses to standard and deviant stimulation.

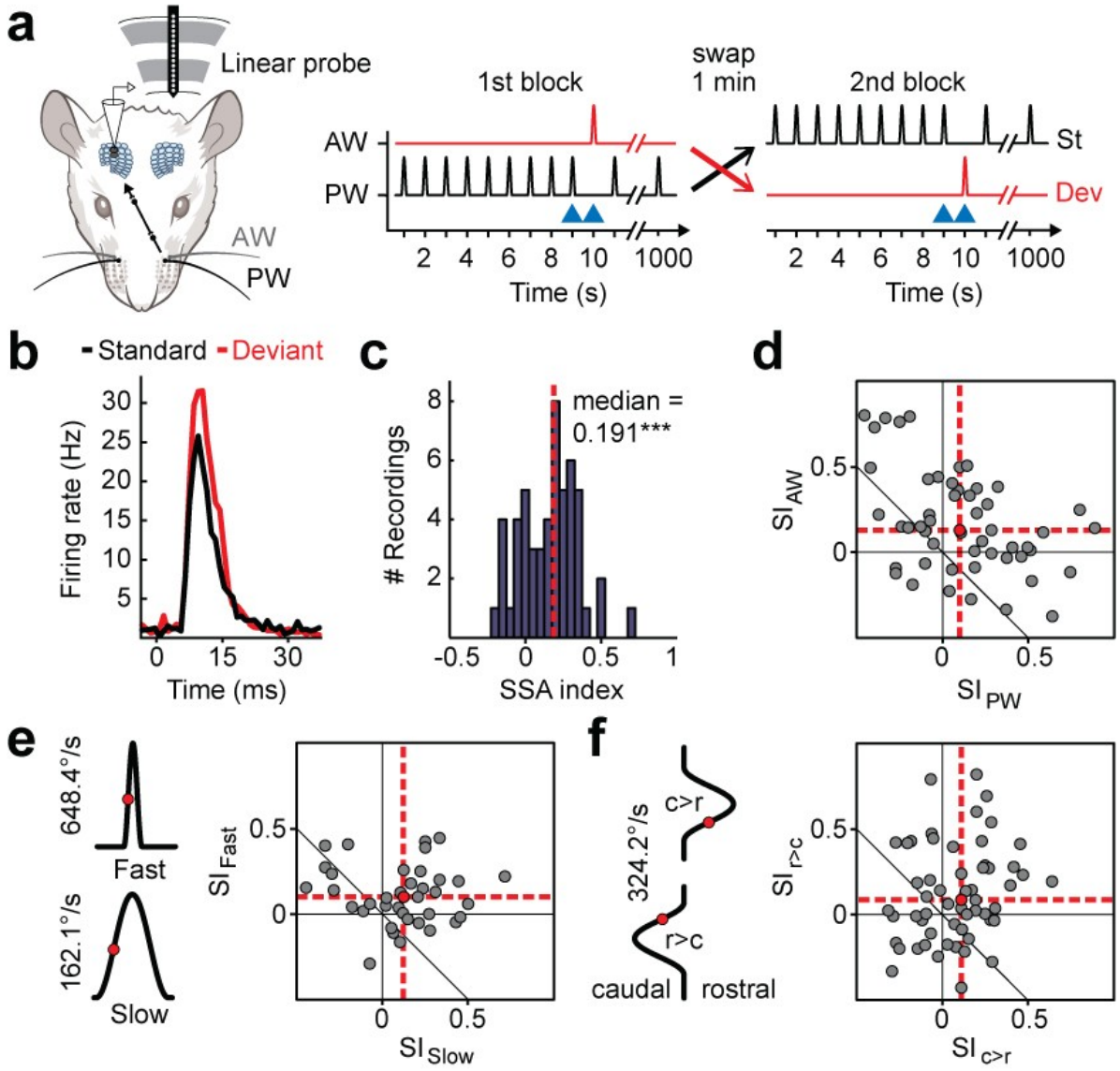

Figure 3.2. SSA to whisker identity, deflection velocity and direction.

a, Illustration of the linear electrode array in barrel cortex and the basic oddball stimulation paradigm. The standard stimulation was first applied to the principal whisker (PW) and in 10% of all stimuli a single deviant stimulus was applied to the adjacent whisker (AW). After 1000 stimulus presentations and a 1 min break the whiskers were swapped (2nd block). Blue arrowheads indicate stimuli that were used for the analysis. **b,** Averaged spiking response over all recorded neurons for either standard (black) or deviant stimulation (red). **c,** Distribution of SI values from all neurons and median SI (*** indicate P < 0.001). **d,** SIs computed separately for standard and deviant stimulation of either the PW (x-axis) or AW (y-axis). Each circle denotes SIs of a single neuron, the red lines and dot indicate median values. **e,** Modified pulses for either fast (upper left) or slow (lower left) whisker stimulation applied to the principal whisker. Red circles denote the point of highest deflection velocity. The scatter plot shows SIs for each stimulus separately (same as in D). **f,** Modified pulses for either caudo-rostral (upper left) or rostro-caudal (lower left) whisker stimulation applied to the principal whisker. Red circles denote the point of highest deflection velocity. The scatter plot shows SIs for each stimulus separately (same as in D).

Fig. 3.2b shows the mean stimulus-evoked spiking response over all recorded neurons. Clearly visible is an increase in response amplitude with deviant presentation that was most pronounced immediately after stimulus presentation when neural responses were highest (peak response difference: 9.86 ± 3.66 Hz, peak response latency: 10.19 ± 0.33 ms, mean ± s.e.m., n = 53 SUs). To quantify changes in response amplitude with deviant presentation, we computed a normalized SSA-index (SI, Eq. 2). The SI ranges from -1 to 1 and negative values indicate a stronger response to standard and positive values to deviant stimuli. SIs were significantly positive over all neurons (**Fig. 3.2c**; signed-rank test, $P < 10^{-5}$), thus showing robust SSA to whisker identity. To assess whether deviant responsiveness differs for the principal or adjacent whisker, we also analyzed SIs for each whisker separately (**Fig. 3.2d**, Eq. 3 and 4). Here, SIs were computed for combinations of standard and deviant stimuli that were presented only to the adjacent ('AW', Y-axis) or the principal whisker ('PW', X-axis). SIs were significantly positive for both PW and AW stimulation (median SI_{PW}: 0.09, signed-rank test, P = 0.037; SI_{AW}: 0.13, P = 0.0002), demonstrating that SSA is also observed for each whisker individually. This also shows that our results are not explained by overly strong tuning towards PW versus AW stimulation (Nelken 2014).

We then tested if SSA is similarly observed for other stimulus features. Here, stimulus sequences were exclusively applied to the PW and instead of whisker identity we changed the deflection velocity between standard and deviant stimuli (**Fig. 3.2e**). Again, deviant-induced responses were stronger than standard responses ($SI_{Velocity}$: 0.059, P = 0.0002, n = 37 SUs) and SSA was robust for both fast and slow whisker deflections (SI_{slow}: 0.125, P = 0.019; SI_{fast}: 0.1, P = 0.0007). Similar effects were also observed when changing whisker deflection direction from caudal to rostral and vice versa (**Fig. 3.2f**, $SI_{Direction}$: 0.07, P = 0.0013; $SI_{c>r}$: 0.111, P = 0.023, $SI_{r>c}$: 0.084, P = 0.0078, n = 55 SUs). The effect size for all three stimulus features was also in good agreement with comparable studies that used oddball stimulation with pure tones in auditory cortex (von der Behrens et al. 2009; Taaseh et al. 2011).

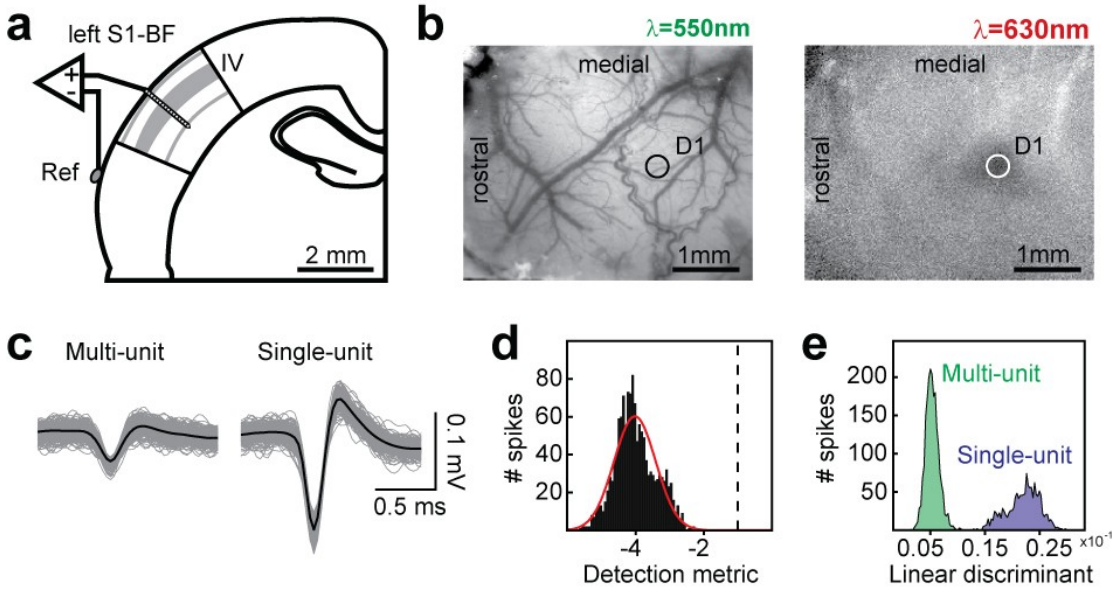

Supplementary Figure 3.2. SSA to whisker identity, deflection velocity and direction.
a, Schematic of the recording electrode (16 linear channels) in the barrel field in primary somatosensory cortex. Recordings were done in the left hemisphere, the reference contact was positioned close to the craniotomy. **b,** Functional mapping of left barrel cortex using intrinsic optical imaging. Left: the vessel picture as seen with green light. Right: the change in red light absorption when the right D1 whisker was stimulated (focused 300 µm below brain surface). **c,** Typical example for spiking activity from a single contact in cortex (depth: 600 µm). The left panel shows low-amplitude multi-unit spiking and the right panel spikes from an isolated single unit. Black traces show mean waveforms, in gray are individual spikes. **d,** Spike amplitudes for the single unit shown in **c**. Amplitudes are normalized by the threshold (dashed line at -1). A Gaussian distribution was fitted to the histogram to estimate the percentage of spikes that remained below threshold. A spike cluster was only counted as a single unit if estimated missing spikes were less than 5%. **e,** Histogram of the Fisher linear discriminate for the multi- and single unit clusters shown in **c**. The linear discriminant is the projection that best separates two multivariate Gaussian distributions. A spike cluster was only counted as a single unit if it was clearly visually separable from other spike clusters on the same electrode.

3.2.3. Importance of repetition rate, deviant probability and channel separation

To determine whether SSA in somatosensory cortex can be explained by stimulus-specific input depression, we first focused on the relation between SSA and stimulus repetition rate. Synaptic depression is frequency-dependent and increases with repetition rate (Chung et al. 2002) which should therefore increase deviant-standard differences accordingly. Such a dependence of SSA on repetition rate has already been implicated by earlier studies in auditory cortex but this relation was weak and only reported for a limited range between 0.5 and 3 Hz (Ulanovsky et al. 2003; Taaseh et al. 2011; Hershenhoren et al. 2014). In contrast, general adaptation in the somatosensory cortex extends over a wide frequency range and is mark-

edly stronger for frequencies above 3 Hz (Khatri et al. 2004b; Katz et al. 2006; Musall, von der Behrens, et al. 2014).

We therefore tested different repetition rates (0.125 to 80 Hz) and measured neural responses to standard and deviant stimuli (**Fig. 3.3a**). Standard responses quickly decreased with frequency and reached a minimum for rates of 40 Hz and higher. The course of this amplitude reduction was well described by a sigmoid fit function (Eq.5) with a neural response range between 14.93 and 0.06 Hz and an inflection point at a rate of 2.05 Hz (red curve). The function also included a parameter *p* to adjust the repetition rate to the probability of standard (*p*St = 0.9) or deviant (*p*Dev = 0.1) stimulation. Changing this parameter thus allowed us to compute expected deviant response amplitudes based on the same fit parameters that were obtained by standard stimulation. Predicted amplitudes matched well with measured deviant responses in the absence of standard stimuli ('Deviant alone', gray squares). However, deviant stimuli that were embedded in a standard sequence consistently evoked weaker neural responses (red circles). Deviant responses are thus reduced by the presence of standard stimuli. In other words, if SSA is due to adaptation of specific sensory channels that convey PW and AW stimuli, these channels are not fully separate and stimulation of one also affects the other. We therefore extended our basic model by an additional term δ to quantify such channel interactions, manifest in the adaptation of deviant responses (Eq. 6). δ is restricted between zero (complete separation) and one (complete overlap) and we determined the optimal δ to match our recorded deviant responses (using otherwise the same fit variables as with standard data). The best fit (red curve) was found for a δ_W of 0.12, indicating that only a low channel interaction has to be assumed to explain cortical response adaptation to different whiskers.

Based on the fitted standard and deviant response curves, we were than able to compute the expected SI values for different repetition rates (Eq. 7) and compare these modeled and measured SIs (**Fig. 3.3b**). We recorded significantly positive SIs even for very low repetition rates of 0.25 Hz ($P = 0.02$) and above ($P < 10^{-5}$). For 0.125 Hz, SIs were only significant for unsorted multi-unit (MU) activity (median SI = 0.044, $P = 0.0048$) but not for single neurons ($P = 0.43$). Effect strength increased with repetition rate and achieved the highest

SIs at 40 Hz. This was also confirmed by our model which predicted increasing SIs for rates above ~0.1 Hz and up to 30.91 Hz (solid green line). For even higher rates SIs were decreasing again (dashed line), suggesting an optimal frequency range where relative differences between standard and deviant responses are highest (**Supplementary Fig. 3.3a**). This was also true for absolute deviant-standard differences although the peak difference was at a lower repetition rate of 4.42 Hz (**Supplementary Fig. 3.3b**).

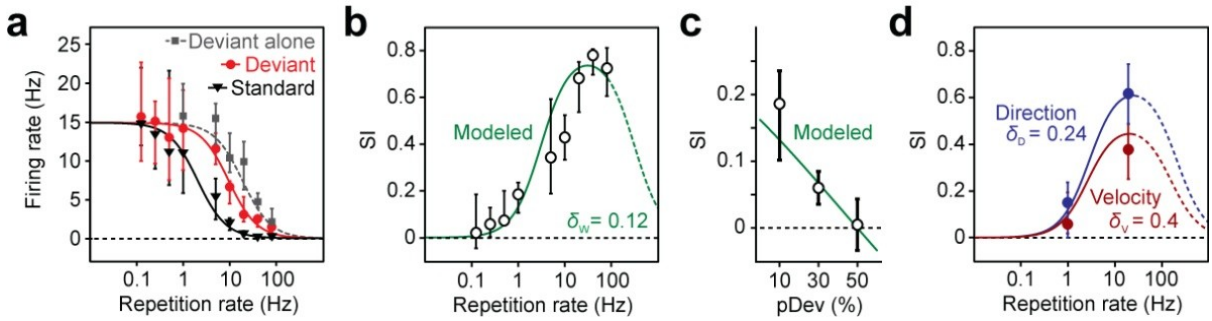

Figure 3.3. Modeling SSA based on oddball repetition rate, deviant probability and response separation.
a, Neural responses to standard, deviant or deviant-alone stimulation. Standard responses were described by a sigmoidal fit function (black curve) that also allowed predicting the course of deviant responses (gray dashed curve). To accurately capture the response amplitudes of deviants embedded in an oddball sequence, the model was modified to quantify the amount of response separation between standard and deviant stimulation (red curve). **b,** Both measured (black circles) and modeled (green curve) SI values showed a steep increase for higher repetition rates. The dashed green curve shows predicted SIs for rates above 80 Hz. The response separation between whiskers given by δW. **c,** Measured and modeled SI values for different deviant probabilities (*p*Dev). **d,** Measured (circles) and modeled (curves) SI values for either direction (blue) or velocity (red) oddballs together with their respective δ_D and δ_V. Dashed lines show predicted SIs for frequencies above 20 Hz. Circles show median values, errorbars 95% CIs (**a-d**).

We then tested whether the model correctly predicts the impact of different deviant probabilities by performing additional experiments with *p*Dev = 0.3 and 0.5. The latter is also a control condition as *p*Dev and *p*St are both 0.5 and SIs are thus expected to be zero. We found an almost linear decrease in SIs as *p*Dev was increasing which was also well predicted by the model (**Fig. 3.3c** and **Supplementary Fig. 3.3**). Lastly, we sought to assess the sensory channel separation when changing deflection velocity (δ_V) or direction (δ_D). As the basic course of adaptation was already known, only a small set of experimental data was required to estimate the difference between deviant and predicted 'deviant alone' responses. We used recordings at 1 and 20 Hz and found higher sensory channel interaction for both veloc-

ity (δ_V = 0.4) and direction (δ_D = 0.24) compared to individual whiskers. For both modalities, the predicted SI curves also matched our measured results (**Fig. 3.3d).**

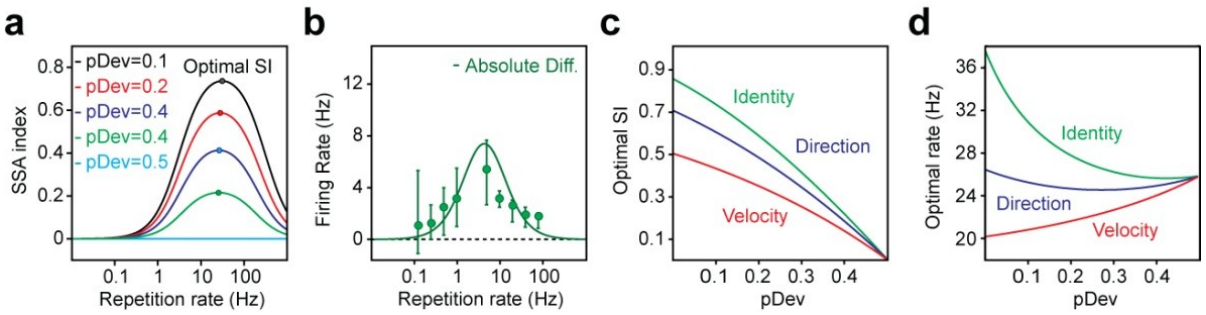

Supplementary Figure 3.3.Measured and predicted oddball responses.
a, Predicted changes in SI values for different deviant probabilities (pDev). As pDev increases, the peak SIs (colored circles) are reduced and also slightly shift towards lower frequencies. SIs remain at zero for pDev = 0.5 (light blue). **b,** Absolute differences between deviant and standard responses against repetition rate. The highest measured deviant-standard differences were found at 5 Hz (green circles). This was in agreement with the model that predicted a peak absolute difference at 4.42 Hz (green curve). **c,** Highest SIs against *p*Dev for different oddball features. **d,** Optimal repetition rate against *p*Dev for different oddball features.

3.2.4. SSA is amplified in supra- and infragranular layers of cortex

The above results show that cortical SSA is generally well explained by stimulus-specific input depression when considering differential degrees of channel interaction for different stimulus features. To assess whether deviant-standard differences are also amplified within the cortical circuitry, we analyzed SSA in different cortical layers. To reveal the spatiotemporal structure of synaptic inputs to the barrel column, we used CSD analysis, based on LFP recordings in all cortical layers. As in earlier studies (Pettersen et al. 2006; Higley and Contreras 2007; Roy et al. 2011), we found a prominent, low-latency current sink between 0.35 and 0.75 mm of cortical depth that was most likely generated by thalamocortical inputs from the ventral posterior medial nucleus (VPM) into layer IV and lower layer III (Meyer et al. 2010). From here onward, we define this input range as the granular layer (**Fig. 3.4**, dashed lines 'G'; see also **Supplementary Fig. 3.4a**) and all recordings above and below as supra- (SG) and infragranular (IG) layers, respectively. The absolute differences between deviant and standard stimulation were most profound in the supragranular layers (**Fig. 3.4b**). CSD-based SIs were lowest in the granular layer (**Fig. 3.4c**, Wilcoxon rank-sum test, $P < 10^{-5}$) and showed two distinct peaks at ~50 µm and between 800 and 1100 µm cortical

depth. Comparable results were also achieved with direction and velocity deviants (**Supplementary Fig. 3.4**).

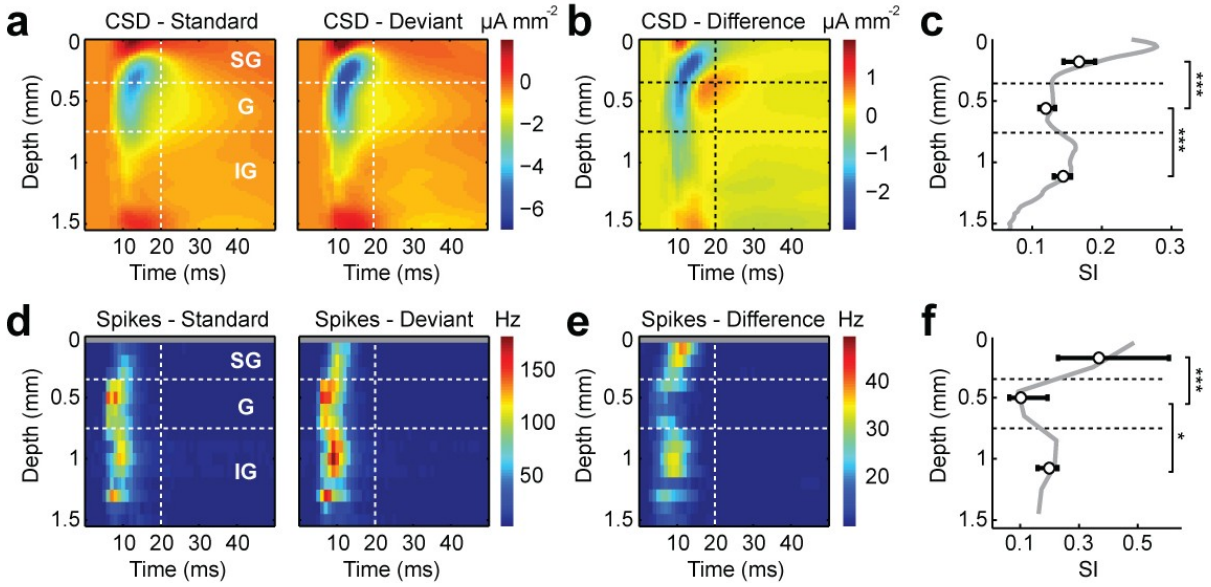

Figure 3.4. Layer-specific modulation of SSA in CSD and spike signals.
a, Averaged CSD responses over all recordings (*n* = 12 experiments) for either standard (left) or deviant stimulation (right). Red colors indicate current sources, blue colors sinks (in µA/mm^2). Dashed horizontal lines show borders of supragranular (SG), granular (G) and infragranular (IG) layers that were determined by depth of the earliest detected current sinks (see also **Supplementary Fig. 3.3a**). Vertical dashed line indicates the end of the time window (starting at zero) that was used for computing SI values. **b,** Absolute CSD differences between deviant and standard stimulation. Blue colors denote stronger current sinks with deviant stimulation. **c,** CSD based SI values against cortical depth. Gray line denotes the median SIs for different depths, black circles show median SIs for SG, G and IG layers (*** indicate P < 0.001, 95% CIs). **d,** Averaged spike responses for all responsive contacts over all recordings (n = 12 experiments, 145 MUs) for either standard (left) or deviant stimulation (right). **e,** Absolute spike differences between deviant and standard stimulation. **f,** Spike based SIs values against cortical depth. Same as in C (* indicate P < 0.05).

To analyze the spatial distribution of spiking activity, we increased the amount of recorded neural signals by including all detected spikes instead of using only single units. Both standard and deviant stimulation evoked the strongest responses in the granular- and infragranular layers (**Fig. 3.4d**). However, absolute response differences were strongest in the supra- and infragranular layers and remained low in the granular layer (**Fig. 3.4e**). A similar distribution was seen in the SI analysis, showing that supra- and infragranular SIs were significantly higher as in the granular layer (**Fig. 3.4f**, $P < 10^{-5}$ and $P = 0.043$, respectively). The spatial profile of SI changes (gray line) also matched our results from the CSD analysis. This selective increase of response differences in the supra- and infragranular layers cannot

be explained by the input depression model and suggests that SSA is actively enhanced within the cortical circuitry.

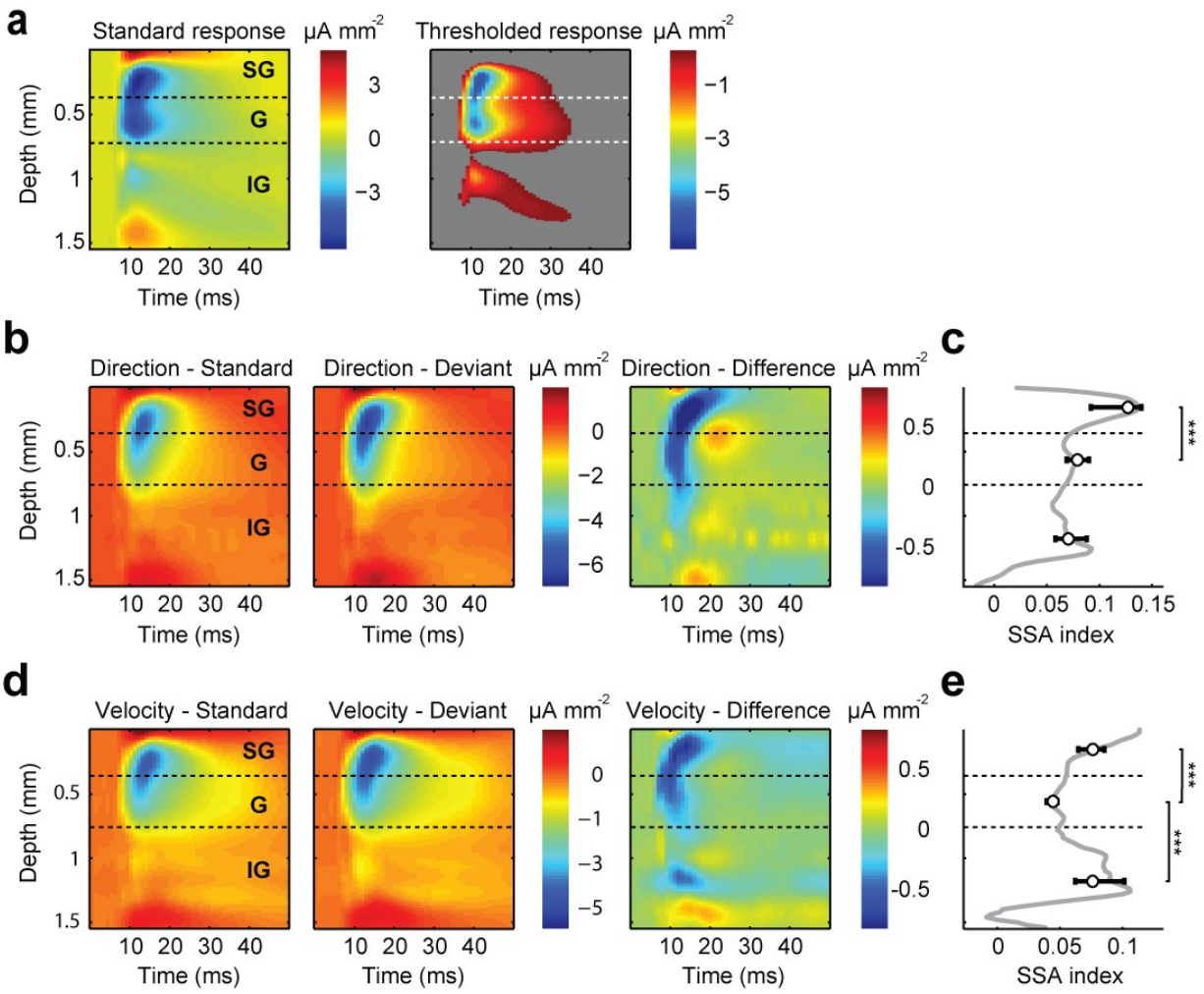

Supplementary Figure 3.4. Single CSD example and results for different stimulus features.
a, Left panel: Example for a mean CSD responses to standard stimulation in an individual recording (*n* = 200 standard presentations). Clearly visible are two current sinks in the granular (G) - and supragranular (SG) and a weaker sink in the infragranular (IG) layer. Right panel: To determine the range of the granular layer, we analyzed data below the 5th percentile and isolated the earliest current sink that was larger than 200 µm and not below 1 mm depth. The average range over all experiments resulted in the approximate range of 350 to 750 µm for the granular layer. **b,** Mean CSD responses to standard and deviant stimulation (left and middle panel) using different stimulus directions. The right panel shows the absolute difference between deviant and standard responses. **c,** CSD based SI values against cortical depth. Gray line denotes the median SIs for different depths; black circles show median SIs for SG, G and IG layers. In contrast to deviants of different whisker identity, SIs for direction were only significantly larger in the SG layers, although a smaller, second peak was still visible in the IG layers. **d,** Same as **b** for velocity deviants. **e,** Same as **c** for velocity deviants. Here, SIs in both SG and IG layers were equally higher as in the G layer. (*** indicate $P < 0.001$, errorbars 95% CIs).

3.2.5. Long-latency sensory responses in the granular layer

Starting roughly 115 ms after stimulus onset we observed a second difference in deviant-standard spiking responses (**Fig. 3.5a**). This later response was only observed in a small subset of recordings (19 of 145 MUs, 5 of 53 SUs) and mostly confined to the granular layer (16 MUs, 4 SUs). An even smaller subset was also seen in deeper layer V (3 MUs, 1 SU). Late responses were oscillatory and showed three to four peaks at intervals of ~70 ms (**Fig. 3.5b**, right). We could exclude that this was due to a stimulation artifact or stimulus-induced whisker movements during this time period by tracking the stimulator and resulting whisker movements (**Supplementary Fig. 3.5**). Interestingly, late responses were highly selective for deviant stimulation and SIs based on neural responses between 150 and 400 ms clearly exceeded SIs to early stimulus responses (**Fig. 3.5b** left, $P < 10^{-5}$). Furthermore, late-responding cells had only very weak deviant selectivity in their early responses, compared to other cells in the granular layer (**Fig. 3.5c**, right panel, $P < 10^{-5}$).

The low early SI and the spatial confinement to layer IV and deeper layer V suggests that these cells receive direct inputs from VPM, driving their early responses without strong deviant-specificity. This also fits to their overall low response latencies (7.32 ± 0.32 ms). However, the source of the deviant-specific late responses is less clear. Probably, later sensory responses are also present in other cortical layers but remain insufficient to induce a spiking response. In this case, the spatial confinement of responsive cells might be because neurons in the granular layer are more excitable than other cortical neurons. To address this, we checked for long-latency deviant-standard differences in the CSDs which mostly reflect changes in the synaptic inputs to a neural population. As with spikes, long latency differences in current sinks were weak but visible and showed a comparable spatiotemporal response profile (**Fig. 3.5d**) as the spiking activity. CSD differences were also strongest at ~200 ms after stimulus onset and mainly confined to the granular layer, thus indicating that the layer specificity of later spiking responses is not due to differential neural excitability but specific synaptic input to layer IV.

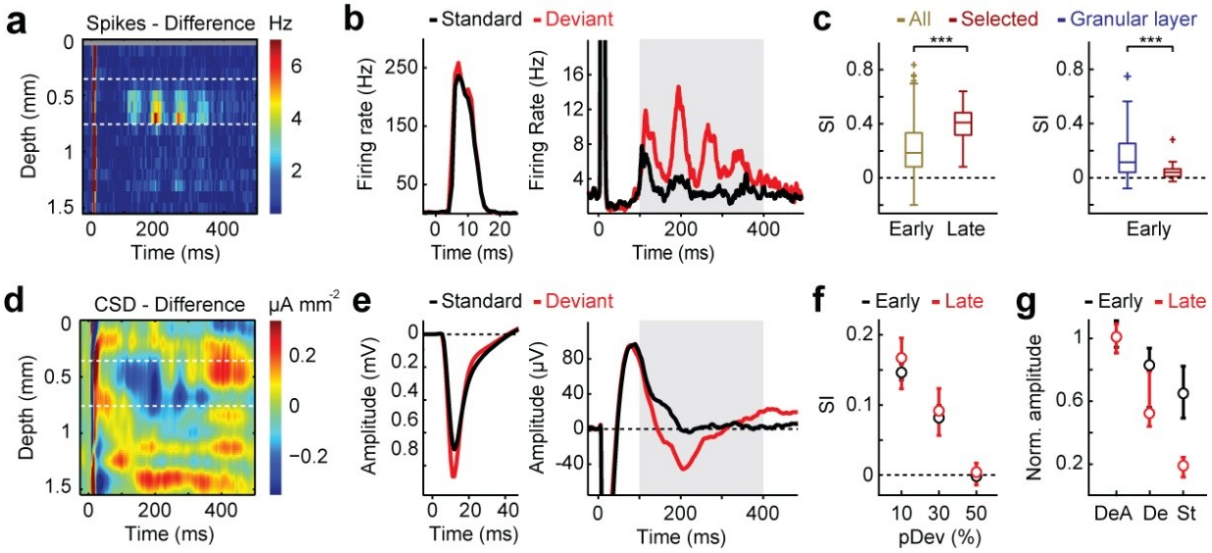

Figure 3.5. Deviant-specific late sensory response in the granular layer.
a, Absolute spike differences between deviant and standard stimulation. **b,** Averaged spiking response over all MUs that exhibited a second, long-latency deviant response (*n* = 19 MUs). The left panel shows the early sensory responses for standard (red) or deviant (black) stimulation. The right panel shows the late sensory response with a clear difference between standard and deviant stimulation 100 ms after stimulus onset. Gray shading indicates the time window that was used for late SI computation**. c,** Left panel: SIs over all MUs (yellow, n = 145 MUs) and late SIs of selected long-latency responsive units (red, same as in **b**). The box shows the first and third quartiles, the inner line is the median. Box whiskers represent minimum and maximum values and crosses are outliers. Right panel: SIs over all MUs in the granular layer (blue, *n* = 56 MUs) and selected long-latency responsive units (red). **d,** Absolute CSD differences between deviant and standard stimulation. Blue colors denote stronger current sinks with deviant stimulation. **e,** Averaged LFP response over all recordings (*n* = 12 experiments). Conventions as in **b**. Differences between standard and deviant stimulation are clearly visible in both early and late sensory responses. **f,** Median SIs based on early (black) and late (red) LFP responses for different deviant probabilities. **g,** Early (black) and late (red) responses to deviant alone (DeA), deviant (De) and standard (St) stimulation. To achieve comparability between early and late responses, all values were normalized to median DeA responses. Error bars show 95% CIs (**f**,**g**)

Both early and late SSA was also found in the spatially less confined LFP signal where the later LFP response was an additional negative component with the same latency as in spiking and CSDs (**Fig. 3.5e**, right). Here, the specificity of early and late responses was equally strong (SI_{Early} = 0.146, SI_{Late} = 0.162, *P* = 0.642, n = 192 contacts). We also observed a similar reduction in effect size when increasing deviant presentation probability (**Fig. 3.5f**), which closely resembled our results from single neurons. Lastly, we compared absolute LFP response amplitudes to standard, deviant or deviant-alone stimulation. This is a control to assess whether differences between deviant and standard responses might represent 'true' deviant detection (as assumed with MMN). If so, deviants should reflect a rule violation

from the background sequence and therefore induce stronger responses as deviants-alone. **Fig. 3.5g** shows the amplitudes of early and late responses, normalized to deviant alone responses ('DeA'). As expected, standard responses ('St') were lower as deviants ('De') but both early and late deviant responses were also significantly lower as deviants alone. Hence, both early and late LFP components do not show a distinct prediction error signal.

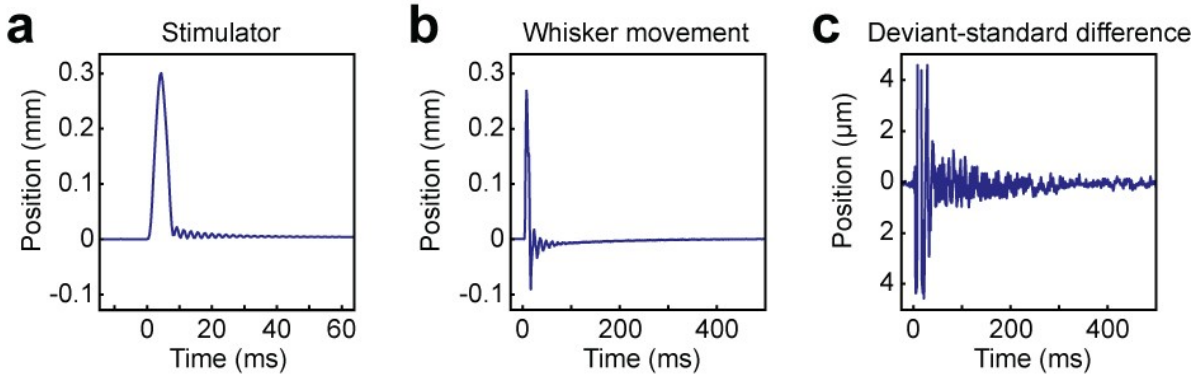

Supplementary Figure 3.5. Measurement of piezo stimulator and whisker movement.
a, Movement of the whisker stimulator measured with laser-shadow tracking. Visible is a 0.3 mm wide deflection, lasting for 8.3 ms. Smaller ripples after return to baseline indicate resonance movements of the piezo element that completely vanish ~50 ms after stimulus onset. **b,** Movement of a stimulated whisker in response to deviant stimulation, measured with laser-shadow tracking. In order to accurately track whisker movements, the stimulator was positioned ~25 mm away from the snout, thus allowing slightly more whisker vibration as under experimental condition. Visible is a positive deflection, corresponding to the stimulator movement and a smaller compensatory movement after stimulation end. No later whisker movements could be observed, indicating that long-latency sensory responses are not due to additional whisker movement with deviant stimulation. **c,** Difference in whisker movement between deviant and standard stimulation. Slight differences of up to 4 µm are visible, probably due to variability in single stimulus whisker movements. As in **b** we observed no later difference in whisker movements that could account for long-latency sensory responses.

3.3. Discussion

In the present study we provide strong behavioral evidence for the importance of SSA for deviance perception. These results were closely related to stimulus-evoked responses of single neurons in somatosensory cortex that increased with presentation of according deviant stimuli. Our simple SSA model showed that cortical responses can be explained by stimulus-specific input depression if different stimulus features are adjusted for the degree of sensory channel interaction. However, layer-specific CSD and spike analysis revealed that deviant responses markedly differ in different cortical layers, strongly implying that incoming deviant signals are further amplified within cortex. This is supported by the deviant-

specific later responses that selectively appeared in neurons that did not show an initial deviant-standard response difference and thus appear to arise from intracortical stimulus processing.

3.3.1. Behavioral implications of SSA

We found that perception of velocity deviants is strongly enhanced when they are presented to an adjacent whisker or in the opposing direction as a standard stimulus sequence. These results relate well to recent behavioral studies on adaptation (Musall, von der Behrens, et al. 2014; Ollerenshaw et al. 2014) and additionally offer evidence for the behavioral relevance of whisker deflection angle. Furthermore, we show that changes in different stimulus features like velocity and whisker identity can be combined to further increase deviant detection performance by up to 12 %. The higher detection performance when changing whisker identity versus deflection direction is consistent with our physiological results that showed that responses to different whisker stimuli are more distinct as for different directions.

3.3.2. SSA in somatosensory cortex

Our physiological recordings revealed robust SSA of neurons in somatosensory cortex for changes in whisker identity, deflection velocity and direction. These results are widely comparable to a large body of literature that used the same experimental methodology in the auditory (Ulanovsky et al. 2003; von der Behrens et al. 2009; Farley et al. 2010; Mill et al. 2011; Taaseh et al. 2011; Hershenhoren et al. 2014) and visual system (Reches et al. 2010), further establishing SSA as a general feature of input processing. Somatosensory SSA had also been reported in an earlier study, showing that cortical responses to single-whisker stimulation are unaffected by prior stimulation of an adjacent whisker (Katz et al. 2006). Based on the input depression model, a complete lack of cross-whisker adaptation suggests that VPM neurons are exclusively tuned to single whiskers and transmit this information in a one to one fashion to their corresponding cortical barrel. Consequently, AW responses have been attributed to intracortical projections between individual barrels (Katz et al. 2006; Armstrong-James et al. 1991; Fox et al. 2003). However, our results show that adaptation to

a neighboring whisker reduces neural responses to single whisker stimulation. In line with other studies in somatosensory cortex (Kwegyir-Afful et al. 2005; Higley and Contreras 2007; Roy et al. 2011), we therefore argue that cortical AW responses are partially mediated by direct multi-whisker inputs from VPM. This notion also holds true for other stimulus features but their lower channel separation suggests that thalamocortical inputs for velocity and direction are less specifically tuned than for individual whiskers. This is in agreement with the rather broad tuning of thalamic neurons for deflection angle (Simons and Carvell 1989) and velocity (Pinto et al. 2000).

3.3.3. Intracortical deviance detection

Whisker stimulation induced robust neural responses throughout cortex and the laminar CSD structure resembled earlier findings in barrel cortex (Pettersen et al. 2006; Higley and Contreras 2007; Roy et al. 2011). Interestingly, deviant stimulation induced layer-specific increases in neural response amplitude that were most pronounced in the supra- and infragranular layers. This was even more evident in the spatial profile of SI values that was highly comparable between spikes and CSDs. SIs were lowest in the granular and very deep (> 1.25 mm) layers and showed a pronounced peak in the supragranular- and a second but weaker peak in the infragranular layers. The layer-specific SI increase in both CSDs and spiking shows that differential responses to standard and deviant stimulation are not just inherited by thalamic projections from VPM but actively amplified in the cortex. This is also indicated by consistent cortical SSA to 1-Hz stimulation while no adaptation at repetition rates below 12 Hz has been observed in either the VPM (Hartings et al. 2003; Khatri et al. 2004a) or the trigeminal ganglion (Ganmor et al. 2010b). Based on the input depression model, layer-specific changes in deviant responses could result from depression of cortical synapses as sensory responses propagate from the granular to the supra- and subsequently infragranular layers (Gilbert and Wiesel 1979; Douglas and Martin 2004). This might have also explained earlier results in auditory cortex where SIs were almost monotonically increasing with cortical depth (Szymanski et al. 2009).

In contrast, we here found that deviant responses are strongest in the supragranular layers (**Fig. 3.4**), which is not explained by corticocortical synapse depression. It thus seems

that enhanced deviant representation is a specific feature of the circuitry implemented in sensory cortices. Interestingly, the laminar profile of highest deviant responses matched well with projection targets from the non-lemniscal somatosensory thalamus (posteromedial nucleus, POm) (Meyer et al. 2010). It is thus possible that interactions between cortex and POm are involved in enhancing cortical deviant responses. This would also relate well to several studies in the auditory system that showed that subcortical SSA appears to be limited to the non-lemniscal pathway (Nelken 2014; Bäuerle et al. 2011; Antunes et al. 2010).

3.3.4. A deviant-specific late sensory response

We also found a second layer- and deviant-specific sensory response about 200 ms after stimulus presentation. Late somatosensory responses have also recently been described in the subthreshold membrane potentials of layer 2/3 neurons (Sachidhanandam et al. 2013). In this study, late responses were only observed in mice that were trained in a stimulus detection task and the size of the late component was indicative for task performance. Here, we show that long-latency spiking responses occur specifically in the granular layer, which may induce subthreshold membrane fluctuations in layer 2/3. Furthermore, the occurrence of late sensory responses under anesthesia shows that they are not exclusively confined to task-engaged animals but seem to at least partially represent a hardwired part of stimulus processing. The long delay and deviant-specificity also indicate that they arise from intracortical network activity. Earlier studies showed that adaptation induces a shift in the balance between excitation and inhibition, resulting in increased neural excitability several hundred milliseconds after stimulus presentation (Ganmor et al. 2010b; Malina et al. 2013). If deviant stimulation has a similar effect on the cortical excitation/inhibition balance, this might open a window of opportunity to evoke late sensory responses that can be modulated by higher cortical areas. However, further studies are needed to elucidate whether late responses originate from the local network activity within S1 or through modulation by other brain regions like the motor cortex (Sachidhanandam et al. 2013).

The existence of late sensory responses has also implications for understanding the physiological origins of MMN. MMN is characterized as a late, deviant specific additional negative wave in EEG recordings and several studies showed that SSA might be related but

is not identical to MMN (Farley et al. 2010; Taaseh et al. 2011; Hershenhoren et al. 2014; Nelken 2014). Only few studies reported to existence of MMN-like stimulus responses in epidural recordings in rodents (Nakamura et al. 2011; Taaseh et al. 2011; Imada et al. 2012; Harms et al. 2014) and a general difference is that stimulus response latencies are much longer than in human MMN (Harms et al. 2014). Our results show that somatosensory stimulation induces an additional late sensory response that has a distinct laminar pattern of neural activity in the granular layer and a higher degree of deviant selectivity as early responses. Late responses are thus likely to be a physiological substrate for MMN and were also visible in the LFP which integrates synchronous synaptic activity from a larger neural population as spike signals and is more comparable to EEG (Musall, von Pföstl, et al. 2014). Indeed, the temporal profile of the late deviant-standard difference in the LFP closely resembles MMN in human somatosensory cortex (Strömmer et al. 2014). However, both early and late deviant responses were lower compared to the deviant-alone condition, which controls for context-independent rarity of the stimulus. This conflicts with the assumption that later responses reflect context-specific deviant detection as in MMN, despite their similar latency and polarity. A probable explanation for this mismatch is the deviant-alone control which might be too conservative because the lack of adaptation with deviant-alone stimulation can overlay context-specific effects with deviant stimulation (Taaseh et al. 2011; Todd et al. 2013; Fishman 2013). Although technically challenging in the somatosensory modality, future studies may use the better suited ‘many standards’ control (Jacobsen and Schröger 2001b) in awake animals to assess whether late responses in barrel cortex also exhibit ‘true’ context-specific deviant detection.

3.3.5. Conclusions

The present study provides comprehensive evidence of deviance detection in primary somatosensory cortex, covering different organizational levels from single cells over intracortical network activity to animal behavior. Our physiological data shows that SSA in cortex goes beyond the framework of the established input depression model and appears to be a feature of intracortical stimulus processing. Moreover, we found a second later response of particularly high deviant specificity that may be a physiological substrate for MMN. Most

importantly, we establish that SSA enhances the perception of deviant stimuli, providing direct behavioral evidence for its functional relevance.

3.4. Experimental procedures

3.4.1. Animal Preparation

All experimental and surgical procedures were approved by the local veterinary authorities of the Canton Zurich. 15 adult female Sprague Dawley rats (233-360 g, Janvier, France) were used for this study. Acute recordings under anesthesia were performed with 12 and behavioral testing with 3 animals. All rats were housed in groups of three under a restricted water-schedule, food ad libitum and an inverted 12:12-h light-dark regime.

The surgical procedure for chronic headpost implantation has been described previously (Schwarz et al. 2010; Mayrhofer, Skreb, von der Behrens, et al. 2013). Briefly, rats were anaesthetized with isoflurane in oxygen and nine titanium screws (Medartis, Switzerland) were inserted into the skull as anchors. The headpost was then attached with dental cement (Vivadent, Liechtenstein). Acute experiments were performed under isoflurane in oxygen anesthesia combined with an analgesic (110 mg/kg Metamizol). Anesthesia levels were kept as low as possible (usually 0.5-1.5 %) and monitored by LFPs and the absence of reflexes. The electrode was a 16 contact linear silicon probe with 100 µm contact spacing (Neuronexus, USA) and positioned in one barrel of the left cortex, identified through intrinsic optical imaging (usually C1 or D1). The electrode was inserted at 100 µm/min until the last contact site reached the cortical surface which was covered with Ringer solution.

3.4.2. Electrophysiological Recordings and Stimulation

Recordings were performed through an extracellular recording system (USB ME16-FAI, Multichannel Systems, Germany). The gain was 1200x, signals were digitized at 32 kHz. The reference electrode was a silver ball ventral to the craniotomy. The experimental control software was custom-written in LabVIEW (National Instruments, USA) and generated an analog stimulation signal at 200 kHz and 16 bit. Single whiskers were placed in a glass capillary glued to a piezo bending actuator (Piezo Systems, USA) that was driven by a controller with

120 V maximum output (Thorlabs, USA). The stimulator and whisker movements were measured with a laser displacement sensor with 0.1 µm resolution (Micro-Epsilon, Germany). Whisker stimuli consisted of a single 120-Hz cosine wave with a deflection of 1.72° (300 µm) and a peak velocity of 648.8 °/s. The distance between the glass capillary tip and the whisker pad was 5 mm. Velocity deviants were either a single 120 Hz cosine wave (648.4 °/s) or a 30 Hz cosine wave (161.1 °/s). Direction deviant stimuli were a 120 Hz cosine wave of 0.86° amplitude and stimulus direction was either from caudal to rostral and back (c>r) or vice versa (r>c).

3.4.3. Experimental Procedures

The electrode was centered in an individual barrel and the principal and an adjacent whisker were stimulated (whiskers were always in the same row). One whisker was randomly assigned as the 'standard', the other as 'deviant'. Subsequently, a stimulus sequence of 1000 pulses was presented to the standard whisker. In 10% of the cases the sequence was interrupted by a single stimulus on the deviant whisker. After the first sequence and a 1 minute break, the whisker identity of the deviant and standard was swapped and a second sequence of 1000 pulses was presented. Oddball effects at different repetition rates were measured by varying the inter-stimulus intervals between 8 s (0.125 Hz) and 0.0125 s (80 Hz). The amount of presented stimuli was adjusted to keep the total protocol duration approximately constant at different rates. Stimulus presentation for different repetition rates (0.125, 0.25, 0.5, 1, 5, 10, 20, 40, 80 Hz) were 500, 1000, 2000, 2000, 4000, 8000, 16000, 32000, 64000 stimuli, respectively. We also measured responses to the deviant-alone stimulation by following the same protocol but omitting presentation of standard stimuli. Deviant-alone recordings were only performed for repetition rates of 1 Hz and higher. For other stimulus features, we used the same oddball paradigm but stimulated only the principal whisker and standard and deviants were stimuli of different deflection velocity or direction.

3.4.4. Electrophysiological Data Analysis

All data analysis was performed in Matlab (Mathworks, USA). For spike detection, the signal was band-pass filtered between 500-5000 Hz and events that crossed a threshold of -6

standard deviations were counted as a spike. SUs were then isolated using the UltraMegaSort 2000 package (Hill et al. 2011). Spike waveforms were aligned, subjected to hierarchical k-means clustering and subsequently aggregated into statistically distinct clusters. Each cluster was then evaluated manually for clear separability in amplitude and principal component space. To consider a cluster as a SU, we required < 0.5 % refractory period violations and < 5 % missed spikes (estimated by a Gaussian-fit of the spike amplitude distribution). To ensure responsiveness to sensory stimulation, we used the Glass's Δ for stimulus-evoked spiking probability as a measure for each neurons signal-to-noise ratio. Glass's Δ was computed as

$$\Delta = (\mathrm{mean}_{\mathrm{Signal}} - \mathrm{mean}_{\mathrm{Baseline}}) \,/\, \mathrm{SD}_{\mathrm{Baseline}} \quad (1)$$

where $\mathrm{mean}_{\mathrm{Signal}}$ is the mean neural response within 20 ms after stimulus onset, $\mathrm{mean}_{\mathrm{Baseline}}$ the mean spontaneous activity 20 ms before the stimulus and $\mathrm{SD}_{\mathrm{Baseline}}$ the respective standard deviation. Firing probabilities were based on the peristimulus time histogram in response to the combined standard and deviant stimulation and we only included SUs with Δ > 2. Glass's Δ was also used to identify neurons that exhibited a late sensory response. Here, we used the same approach with a $\mathrm{mean}_{\mathrm{Signal}}$ between 100-400 ms after stimulus onset.

For LFP and CSD analysis, the continuously recorded signal was resampled to 1 kHz. To compute CSDs we applied the inverse CSD method by Pettersen et al. 2006. We applied the spline iCSD method, which assumes a smoothly varying CSD between electrode contacts based on interpolation of a set of cubic polynomials. We assumed a homogeneous, isotropic conductivity of σ = 0.3 S/m within and directly above cortex (Pettersen et al. 2006). To reduce spatial noise, the estimated CSD was subsequently convolved with a Gaussian spatial filter with a standard deviation of 0.1 mm (Pettersen et al. 2006).

The data analysis was confined to responses elicited by the deviant and the directly preceding standard stimuli (**Figure 1a**). SSA-indices (SIs) were computed based on the averaged responses over all standards/deviants (100 for an oddball sequence of 1000 stimuli). For spikes, the mean response within a window from 0 to 20 ms after stimulus onset was used. For the CSDs, the absolute of the lowest value between 0 and 20 ms after stimulus onset

was used. When computing SIs for late sensory responses we used spiking and CSD responses between 100 and 400 ms. SIs were computed by the following formula:

$$\mathrm{SI} = \frac{\left(\mathrm{d}(f_1)+\mathrm{d}(f_2)\right)-\left(\mathrm{s}(f_1)+\mathrm{s}(f_2)\right)}{\mathrm{d}(f_1)+\mathrm{d}(f_2)+\mathrm{s}(f_1)+\mathrm{s}(f_2)} \tag{2}$$

d(f_i) and s(f_i) are responses to deviant or standard stimulation, respectively. f_i represent the stimulus feature which was changed to induce an oddball effect. To compute SIs for each stimulus feature separately, the above formula was modified to:

$$\mathrm{SI}_1 = \frac{\mathrm{d}(f_1)-\mathrm{s}(f_1)}{\mathrm{d}(f_1)+\mathrm{s}(f_1)} \tag{3}$$

$$\mathrm{SI}_2 = \frac{\mathrm{d}(f_2)-\mathrm{s}(f_2)}{\mathrm{d}(f_2)+\mathrm{s}(f_2)} \tag{4}$$

SI distributions were usually non-normal; we therefore report the median SIs and tested for significance against zero by using a Wilcoxon signed-rank test for zero median. For comparisons between distributions, a Wilcoxon rank-sum test was used. 95% confidence intervals were acquired by computing 1000 bootstraps based on the observed distribution statistics.

3.4.5. SSA Model

To model SSA changes at different repetition rates and deviant probabilities, we used a model based on the adaptation of responses to standard stimuli. Reduced response with increasing repetition rate were well described by a sigmoid fit function of the form

$$S_{\mathrm{St}}(f) = r_{\max} + \frac{\left(r_{\min} - r_{\max}\right)}{1 + e^{\frac{-(\log(f*pSt)-x_{50})}{v}}} \tag{5}$$

with v denoting the sigmoid slope, r_{max} and r_{min} the possible response range in Hz, x_{50} the inflection point, pSt the probability of a standard stimulus (normalized between 0 and 1, usually 0.9) and f the repetition rate in the oddball paradigm. Based on the achieved fit pa-

rameters, we predicted deviant responses by changing the stimulus probability to *p*Dev =1−*p*St (usually 0.1). The resulting curve matched deviant-alone responses but overestimated response amplitude of deviants in the oddball paradigm. This mismatch between deviant and deviant-alone responses was then used to quantify the separation of different sensory channels that convey standard and deviant stimuli by introducing the additional term δ.

$$S_{\mathrm{Dev}}(f) = r_{\max} + \frac{(r_{\min} - r_{\max})}{1 + e^{\frac{-(\log(f*((1-2\,pDev)*\delta + pDev)) - x_{50})}{v}}} \tag{6}$$

Here, δ=1 results in the same responses as with standard stimulation and δ=0 to responses with deviant-alone stimulation. To determine the optimal δ to describe deviant responses we used non-linear least squares regression. Based on the optimal δ we then computed SI values based on the expected deviant and standard responses at each repetition rate or stimulus probability.

$$\mathrm{SI}(f) = \frac{S_{\mathrm{Dev}}(f) - S_{\mathrm{St}}(f)}{S_{\mathrm{Dev}}(f) + S_{\mathrm{St}}(f)} \tag{7}$$

3.4.6. Behavioral Paradigm

The behavioral setup and paradigm has been described in detail previously (Mayrhofer, Skreb, von der Behrens, et al. 2013; Musall, von der Behrens, et al. 2014). Briefly, animals were head-fixed and the C1 and C2 whiskers were stimulated with the same piezo actuators and stimulus parameters as in acute recordings. During single-pulse detection, stimuli were presented to either the left or the right side of the animal which received a water reward when correctly responding to the respective stimulus side. Based on animal's single-pulse detection performance we derived the velocities required for half-optimal (M50) and optimal (M100) stimulus detection. For deviant detection, a 2-s-long, vibrotactile stimulus sequence at 20 Hz and M50 velocity was applied to both whiskers. After 1.5 s, either 1 or 4 deviants at M100 velocity were embedded in the target stimulus. Direction deviants had also an opposing direction as the standard sequence and whisker deviants were presented on the adjacent whisker. All sequences were presented on both whiskers equally and direc-

tion deviants were equally presented from caudal to rostral and vice versa. In case of deviant only controls, the 20-Hz sequence was omitted and only a single stimulus was presented on both sides (**Supplementary Fig. 3.5**).

3.4.7. Behavioral Data Analysis

A trial was counted as correct (hit) when the animal's initial response was on the target side or as a false (error) in the opposing case. A no-lick response in a 2-s time window after single stimulus or deviant presentation was classified as a missed trial. Performance was computed as the fraction of hits from the sum of hits and errors. To test if behavioral performance differed from chance we used a two-sided binomial test and a Pearson's $\chi 2$ test to compare behavioral conditions. In case of multiple comparisons, we additionally applied Bonferroni correction. To analyze psychometric single-pulse detection curves, we used the Psignfit toolbox that obtains fit parameters with the maximum-likelihood method by Wichman and Hill (Wichmann and Hill 2001). We fitted a cumulative Gauss function to detection performance of individual animals and computed the turning point and asymptote (corresponding to M50 and M100, respectively). 95% confidence intervals were computed based on the binomial inverse cumulative distribution function.

Chapter 4 : General discussion

In the present thesis I addressed several questions on adaptation in somatosensory cortex and the resulting stimulus perception. For this last chapter, I will discuss how the results of this work relate to the existing literature on cortical adaptation, their implications for stimulus processing and how future studies might build on the acquired knowledge.

4.1. Cortical adaptation governs stimulus perception

The main objective of the thesis was to establish a direct relation between adaptation of cortical neurons and stimulus perception. There are different results that aid to address this goal, most importantly those that arise from animal behavior. By gradually extending our behavioral paradigm (Mayrhofer, Skreb, von der Behrens, et al. 2013), I could show that sensory adaptation explains behavioral performance when either detecting or discriminating single pulses or short sequences of whisker stimulation. The applied theoretical models were based on sensory adaptation of barrel cortex neurons, suggesting that cortical adaptation is a key determinant of sensory perception. Causal evidence for this hypothesis comes from the optogenetic activation of barrel cortex neurons that allowed inducing either adapting or non-adapting neural responses. Here, the observed behavioral performance with non-adapting stimulation was well explained by the same theoretical models when assuming absence of neural adaptation. Conversely, behavioral performance with adapting stimulation closely resembled whisker-induced behavior. This was even the case when whisker and adapting light stimulation was presented simultaneously. Taken together, these behavioral results demonstrate that adaptation of cortical neurons indeed directly governs stimulus perception.

The fact that non-adapting activity in barrel cortex resulted in equally non-adaptive stimulus perception is interesting because it strongly suggests that higher-order cortical areas integrate sensory information differently as early sensory cortex. If adaptation is not present in sensory cortex, sensory information appears to be integrated in an optimal manner (Brunton et al. 2013). This relates well with the assumption that higher-order areas,

such as the parietal or prefrontal cortex, are mainly involved in accumulation of sensory evidence which requires the integration of sensory information over longer timescales (Kim and Shadlen 1999; Gold and Shadlen 2007; Hanks et al. 2015). Whether neural activity patterns in these areas are subject to adaptation themselves or the importance of adaptation for higher-order information processing is currently unknown. As shown in this thesis, optogenetic stimulation of neurons is a viable tool to investigate the implications of adapting versus non-adapting activity patterns. A future approach for studying the relation between adaptation and cortical information processing would therefore be the optogenetic stimulation of neurons in higher-order cortical areas and to assess the respective behavioral consequences.

4.2. The trade-off between stimulus detection and discrimination

In different behavioral settings, animal performance was either improved or decreased due to adaptation. In accordance with psychophysical studies in humans (Tannan et al. 2006; Goble and Hollins 1993; Tannan et al. 2007), I found that adaptation reduces the perceptual intensity of a stimulus while increasing its discriminability against stimuli of lower amplitude. Hence, adaptation represents a trade-off between stimulus detectability and discriminability which may explain why it is dynamically modulated with behavioral state (Fanselow and Nicolelis 1999; Castro-Alamancos 2004b). During rest, high adaptation might aid to detect unexpected sensory events whereas its reduction during active exploration increases perceptual fidelity (Fanselow and Nicolelis 1999; Chung et al. 2002). Aside of demonstrating that this behavioral effect is equally observed in trained rats, I found that the physiological basis for altered stimulus perception is sensory adaptation of barrel cortex neurons. This relates well to the recent study by Ollerenshaw et al. that found a similar adaptive trade-off for stimulus location. Based on neural recordings in thalamus and cortex, they also suggested that this is due to adaptation in cortex (Ollerenshaw et al. 2014).

My results additionally extent this knowledge by showing that adaptation in single barrel cortex neurons is stimulus specific. The occurrence of cortical SSA has direct implications for stimulus perception and deviant stimuli that differ from background stimulation in

a set of different stimulus features induce a significantly higher perceptual intensity. The same cortical circuitry is therefore sensitive to an array of different stimulus features and enhances change perception in each feature through SSA.

4.3. Variability increases the perceived intensity of stimulus sequences

Most psychophysical studies focus on the perception of a single test stimulus that is presented after an adaptor sequence. Conversely, I simultaneously presented two tactile stimulus sequences to test whether sensory adaptation would prohibit their discrimination based on frequency. Indeed, the low frequency discrimination performance with whisker stimulation shows that rats appear to be unable to avoid the ambiguity in frequency coding that is introduced by frequency-dependent adaptation. This argues in favor of the hypothesis, that the ability for fine texture discrimination relies on the occurrence of slip-stick events, causing high-velocity whisker deflections which increase the perceptual intensity that is induced by a corresponding surface (von Heimendahl et al. 2007; Ritt et al. 2008; Wolfe et al. 2008; Jadhav et al. 2009). However, due to the stimulus-specificity of adaptation there could be an additional mechanism that may contribute to texture discrimination. If sweeping over a texture evokes a high degree of variability in different stimulus features, this would result in decreased adaptation because the incoming sensory input is distributed over a wider range of different synaptic inputs. Preliminary analysis of corresponding recordings in barrel cortex suggests that this is indeed the case (**Fig. 4.1a-c**). Furthermore, SSA may also explain why the activity of barrel cortex neurons is increased when adding noise to a constant single-whisker stimulus sequence (Lak et al. 2010). Consequently, higher feature variability should result in increased perceptual intensity and thus increase both stimulus detection and frequency discrimination. Again, preliminary behavioral data seems to confirm this assumption. Here, presentation of stimulus sequences that alternate between different features, e.g. repeatedly changing deflection velocity or the stimulated whisker increases stimulus detection as well as frequency discrimination performance (**Fig. 4.1d,e**). SSA is therefore not only important for the enhanced perception of low-probability deviant events but also affects the degree of cortical adaptation depending on sequence variability. The encoding of stimulus feature variability might be an important factor to improve texture discrimination

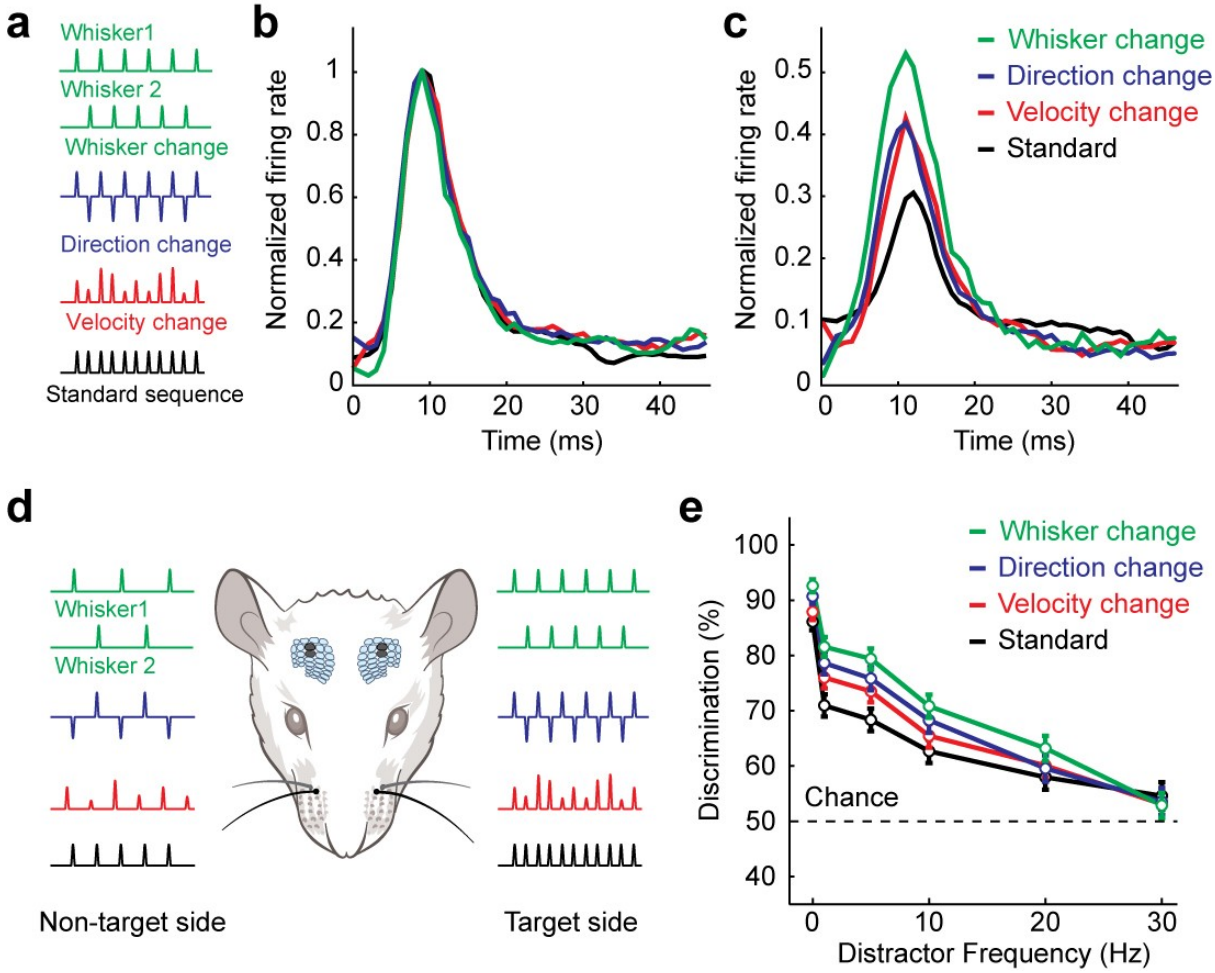

Figure 4.1. Stimulus variability decreases cortical adaptation

a, Different stimulus sequences that alternate in a specific stimulus feature. In contrast to the uniform standard sequence (black), a velocity change sequence has an alternating deflection velocity which each stimulus (red). In the direction change sequence, the deflection direction of each stimulus is the opposite as in the stimulus before (blue). In a whisker change sequence, each stimulus is presented to a different whisker as the stimulus before and the sequence is equally distributed on two neighboring whiskers (green). **b,** Average PSTH over a set of single cortical neurons (n = 50 trials and 23 cells). Shown is the response to the first pulse in different stimulus sequences, normalized by the peak response in the standard sequence. Each condition induces equally strong onset responses. **c,** Same as in **b** but averaged over the first 10 pulses in a 20-Hz stimulus sequence. Neural responses to the uniform standard sequence show stronger adaptation, compared to sequences with higher feature variability. **d**, Illustration of the frequency discrimination paradigm with different stimulus sequences. Animals discriminated concomitantly presented sequences based on frequency. Sequences were either uniform standard sequences or changing in velocity, direction or whisker identity. **e,** Frequency discrimination performance with 40-Hz target stimulation is strongly increased when stimulus sequences have a higher feature variability. As with neural responses, this effect was most pronounced when a sequence was distributed over different whiskers. Differences between conditions were also observed in absence of a distractor stimulus (left data point; '0-Hz' on the x-axis), suggesting that the perceptual intensity of the target sequence was increased by higher feature variability.

but also relates to comparable findings in humans that reported a higher perceptual intensity of stimulus sequences when individual pulses varied in amplitude (Lak et al. 2010). The encoding of feature variability through SSA may therefore be a general property of sensory processing.

4.4. Deviance detection as a feature of intracortical stimulus processing

My results highlight cortical adaptation as an important mechanism to enhance the perception of deviant stimuli. Consequently, deviant detection is reduced with non-adaptive cortical stimulation but enhanced through manipulation of specific stimulus features. However, the exact mechanism that causes cortical adaptation is still unclear. Cortical adaptation appears to be mainly due to depression of thalamocortical synapses onto a single cortical neuron (Chung et al. 2002; Katz et al. 2006) but my extracellular recordings in different cortical depths show that deviant responses are selectively enhanced in the supra- and infragranular layers of cortex. This effect may be explained by intracortical synaptic depression. However, one should expect that in this case deviant responses in the deeper layers V and IV should be strongest because they are generally considered to be the cortical output layers (Gilbert and Wiesel 1979; Douglas and Martin 2004). The fact that deviant responses were highest in the supgragranular layers therefore argues against this possibility. It thus seems that enhanced deviant detection is a specific feature of intracortical sensory processing although its exact mechanism remains unknown. Furthermore, it remains unclear whether intracortical processing merely enhances deviant-standard differences that are already present in the respective cortical inputs or produce increased deviant responses *de novo*, e.g. in response to a specific rule violation as seen with MMN.

Of particular interest for this question is the presence of layer-specific sensory responses of either low or higher response latency. Using a deviant-alone control, I found that both early and late sensory deviant responses are lower compared to deviant-alone stimulation, suggesting that deviant responses are due to stimulus-specific input depression instead of an MMN-like rule violation signal (**Fig. 3.5g)**. However, a more suitable control is the many-standards paradigm which selectively reduces the predictability of a deviant stimulus while leaving the overall amount of cortical adaptation constant (Taaseh et al. 2011; Nelken

2014). Preliminary results with many-standard stimulation of four neighboring whiskers show that early responses are equal for deviants in a flip-flop and many-standards paradigm while late responses are significantly lower in the many-standards control (**Fig. 4.2**). This strongly suggests that late responses are indeed sensitive to a specific-rule violation that is only established in the flip-flop design, whereas early responses can be fully explained by stimulus-specific input depression. Late sensory responses therefore not only resemble the temporal properties of MMN but also show true deviance detection. This relates well to a study by Chen et al. who found that various cell-types in layer II/III of A1 show a deviant specific change in membrane potentials that exhibits an early and late response component (Chen et al. n.d.). Furthermore, they found that the late component of deviant responses of excitatory neurons is significantly lower in the many-standards control and concluded that late deviant responses are a potential substrate for MMN in primary sensory cortex.

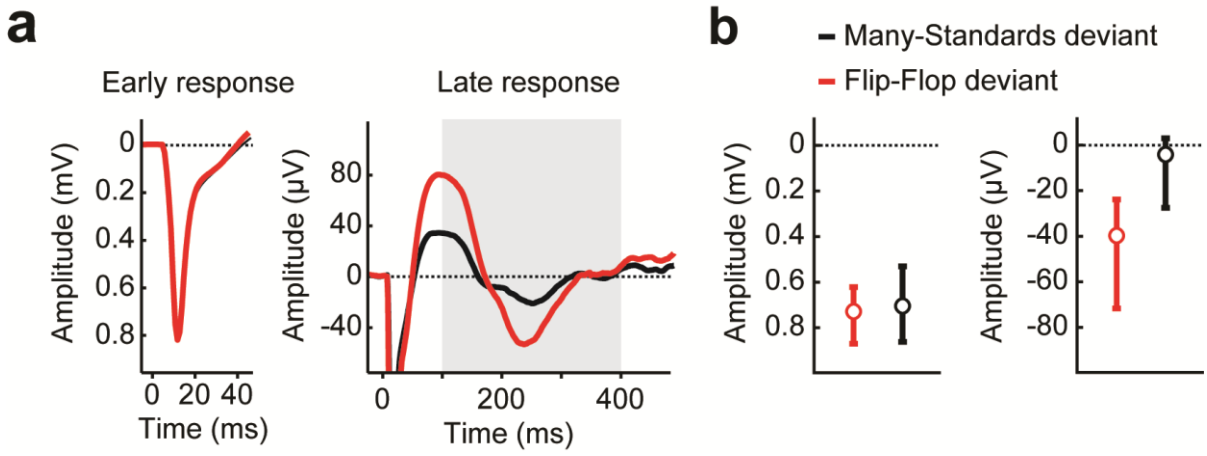

Figure 4.2. Late deviant responses exhibit MMN-like deviance detection
a, Averaged LFP response over 64 recording sites in 2 experiments. The left panel shows the early sensory responses to deviant stimulation in the flip-flop (red) or many-standards (black) paradigm. Both deviants elicited equally strong negative LFP deflections. The right panel shows the late sensory response with a clear difference between both deviant types roughly 200 ms after stimulus onset. Gray shading indicates the time window in which the maximal LFP deflection was detected and used to compute median stimulus responses shown in **b. b,** The left panel shows median response amplitude between 0 and 20 ms after stimulus onset. Deviants in the flip-flop or many-standards paradigm evoked equally strong responses (P = 0.85). The right panel shows median response amplitudes between 100 and 400 ms after stimulus onset. Deviant responses were significantly stronger in the flip-flop compared to the many-standard paradigm (P = 0.000017). This suggests that late deviant responses exhibit true deviance detection as seen with MMN.

In summary, these results demonstrate that a specific subset of neurons in early sensory cortex show two different responses to deviant stimulation. The initial responses occur after short latencies and show SSA that is well explained by input depression and does not seem to reflect a specific rule violation. In contrast, late responses are more deviant-specific as early responses and also reflect true deviance specificity as seen in MMN. The presence of both these responses in specific neurons in the same cortical area may also explain why some studies on SSA reported true deviance detection in A1 neurons (Ulanovsky et al. 2003; Nakamura et al. 2011; Taaseh et al. 2011; Hershenhoren et al. 2014) while others did not (Farley et al. 2010; Eriksson and Villa 2005; Fishman and Steinschneider 2012).

4.5. Outlook

To resolve the transformation from initial SSA towards MMN-like deviance detection in delayed neural responses, it is of crucial importance to better assess the intracortical mechanism that are involved in deviant processing and to identify the origin of the observed late responses. These may be due to reverberating network activity (Chen et al. n.d.), back projections from other cortical areas (Sachidhanandam et al. 2013) as well as thalamocortical feedback loops. A promising path to address these different possibilities might be the application of optical tools, such as optogenetics or calcium imaging, in the rodent cortex to achieve a better understanding of the contribution of different cell-types or signal transformation between cortical layers and different brain areas. Furthermore, one could also use a combination of different opsins that are sensitive to non-overlapping wavelengths of light (Klapoetke et al. 2014). By transfecting and selectively targeting different neuronal populations one could create an oddball paradigm by stimulating different subsets of neurons to produce either standard or deviant responses. This approach would have the major advantage to induce non-adaptive responses in the stimulated area, thus allowing to study how initial spiking responses are modified in upstream projection targets and at which point increased deviant responses occur. To study intracortical processing, one may also specifically stimulate layer IV neurons while recording activity in other cortical layers to study whether enhanced deviant responses can be observed in the absence of thalamocortical input depression.

References

Abbott LF, Varela JA, Sen K, Nelson SB. 1997. Synaptic Depression and Cortical Gain Control. Science. 275:221–224.

Adibi M, Arabzadeh E. 2011. A Comparison of Neuronal and Behavioral Detection and Discrimination Performances in Rat Whisker System. J Neurophysiol. 105:356–365.

Adibi M, McDonald JS, Clifford CWG, Arabzadeh E. 2013. Adaptation Improves Neural Coding Efficiency Despite Increasing Correlations in Variability. J Neurosci. 33:2108–2120.

Adrian ED, Zotterman Y. 1926. The impulses produced by sensory nerve endings. J Physiol. 61:465–483.

Anderson LA, Christianson GB, Linden JF. 2009. Stimulus-specific adaptation occurs in the auditory thalamus. J Neurosci. 29:7359–7363.

Antunes FM, Nelken I, Covey E, Malmierca MS. 2010. Stimulus-Specific Adaptation in the Auditory Thalamus of the Anesthetized Rat. PLoS ONE. 5:e14071.

Aravanis AM, Wang L-P, Zhang F, Meltzer LA, Mogri MZ, Schneider MB, Deisseroth K. 2007. An optical neural interface: in vivo control of rodent motor cortex with integrated fiberoptic and optogenetic technology. J Neural Eng. 4:S143–S156.

Armstrong-James M, Callahan CA, Friedman MA. 1991. Thalamo-cortical processing of vibrissal information in the rat. I. Intracortical origins of surround but not centre-receptive fields of layer IV neurones in the rat S1 barrel field cortex. J Comp Neurol. 303:193–210.

Atienza M, Cantero JL. 2001. Complex sound processing during human REM sleep by recovering information from long-term memory as revealed by the mismatch negativity (MMN). Brain Res. 901:151–160.

Ayala YA, Pérez-González D, Duque D, Nelken I, Malmierca MS. 2012. Frequency discrimination and stimulus deviance in the inferior colliculus and cochlear nucleus. Front Neural Circuits. 6:119.

Bäuerle P, Behrens W von der, Kössl M, Gaese BH. 2011. Stimulus-Specific Adaptation in the Gerbil Primary Auditory Thalamus Is the Result of a Fast Frequency-Specific Habituation and Is Regulated by the Corticofugal System. J Neurosci. 31:9708–9722.

Bosman LWJ, Houweling AR, Owens CB, Tanke N, Shevchouk OT, Rahmati N, Teunissen WHT, Ju C, Gong W, Koekkoek SKE, De Zeeuw CI. 2011. Anatomical pathways involved in generating and sensing rhythmic whisker movements. Front Integr Neurosci. 5:53.

Boyden ES, Zhang F, Bamberg E, Nagel G, Deisseroth K. 2005. Millisecond-timescale, genetically targeted optical control of neural activity. Nat Neurosci. 8:1263–1268.

Bruno RM, Sakmann B. 2006. Cortex Is Driven by Weak but Synchronously Active Thalamocortical Synapses. Science. 312:1622–1627.

Brunton BW, Botvinick MM, Brody CD. 2013. Rats and Humans Can Optimally Accumulate Evidence for Decision-Making. Science. 340:95–98.

Butovas S, Schwarz C. 2007. Detection psychophysics of intracortical microstimulation in rat primary somatosensory cortex. European Journal of Neuroscience. 25:2161–2169.

Carandini M, Churchland AK. 2013. Probing perceptual decisions in rodents. Nat Neurosci. 16:824–831.

Carandini M, Ferster D. 1997. A Tonic Hyperpolarization Underlying Contrast Adaptation in Cat Visual Cortex. Science. 276:949–952.

Cardin JA, Carlén M, Meletis K, Knoblich U, Zhang F, Deisseroth K, Tsai L-H, Moore CI. 2010. Targeted optogenetic stimulation and recording of neurons in vivo using cell-type-specific expression of Channelrhodopsin-2. Nat Protocols. 5:247–254.

Castro-Alamancos MA. 2002. Role of Thalamocortical Sensory Suppression during Arousal: Focusing Sensory Inputs in Neocortex. J Neurosci. 22:9651–9655.

Castro-Alamancos MA. 2004a. Absence of Rapid Sensory Adaptation in Neocortex during Information Processing States. Neuron. 41:455–464.

Castro-Alamancos MA. 2004b. Absence of Rapid Sensory Adaptation in Neocortex during Information Processing States. Neuron. 41:455–464.

Castro-Alamancos MA, Oldford E. 2002. Cortical sensory suppression during arousal is due to the activity-dependent depression of thalamocortical synapses. J Physiol. 541:319–331.

Chen I-W, Helmchen F, Lütcke H. n.d. Rare tones evoke specific early and late membrane potential responses in excitatory and inhibitory neurons of mouse auditory cortex. Neuron. Under revision.

Chung S, Li X, Nelson SB. 2002. Short-Term Depression at Thalamocortical Synapses Contributes to Rapid Adaptation of Cortical Sensory Responses In Vivo. Neuron. 34:437–446.

Dean I, Harper NS, McAlpine D. 2005. Neural population coding of sound level adapts to stimulus statistics. Nat Neurosci. 8:1684–1689.

Dhruv NT, Carandini M. 2014. Cascaded Effects of Spatial Adaptation in the Early Visual System. Neuron. 81:529–535.

Diamond ME, von Heimendahl M, Knutsen PM, Kleinfeld D, Ahissar E. 2008. “Where” and “what” in the whisker sensorimotor system. Nat Rev Neurosci. 9:601–612.

Douglas RJ, Martin KAC. 2004. Neuronal circuits of the neocortex. Annu Rev Neurosci. 27:419–451.

Dudai Y. 2004. Memory from A to Z: Keywords, Concepts, and Beyond. 1 edition. ed. Oxford: Oxford University Press.

Duque D, Pérez-González D, Ayala YA, Palmer AR, Malmierca MS. 2012. Topographic distribution, frequency, and intensity dependence of stimulus-specific adaptation in the inferior colliculus of the rat. J Neurosci. 32:17762–17774.

Eriksson J, Villa AEP. 2005. Event-related potentials in an auditory oddball situation in the rat. BioSystems. 79:207–212.

Erzurumlu RS, Murakami Y, Rijli FM. 2010. Mapping the face in the somatosensory brainstem. Nat Rev Neurosci. 11:252–263.

Ewert TAS, Vahle-Hinz C, Engel AK. 2008. High-Frequency Whisker Vibration Is Encoded by Phase-Locked Responses of Neurons in the Rat’s Barrel Cortex. J Neurosci. 28:5359–5368.

Fairhall AL, Lewen GD, Bialek W, de Ruyter Van Steveninck RR. 2001. Efficiency and ambiguity in an adaptive neural code. Nature. 412:787–792.

Fanselow EE, Nicolelis MAL. 1999. Behavioral Modulation of Tactile Responses in the Rat Somatosensory System. J Neurosci. 19:7603–7616.

Fanselow EE, Sameshima K, Baccala LA, Nicolelis MA. 2001. Thalamic bursting in rats during different awake behavioral states. Proc Natl Acad Sci USA. 98:15330–15335.

Farley BJ, Quirk MC, Doherty JJ, Christian EP. 2010. Stimulus-Specific Adaptation in Auditory Cortex Is an NMDA-Independent Process Distinct from the Sensory Novelty Encoded by the Mismatch Negativity. J Neurosci. 30:16475–16484.

Fishman YI. 2013. The Mechanisms and Meaning of the Mismatch Negativity. Brain Topogr. 27:500–526.

Fishman YI, Steinschneider M. 2012. Searching for the Mismatch Negativity in Primary Auditory Cortex of the Awake Monkey: Deviance Detection or Stimulus Specific Adaptation? J Neurosci. 32:15747–15758.

Fox K, Wright N, Wallace H, Glazewski S. 2003. The origin of cortical surround receptive fields studied in the barrel cortex. J Neurosci. 23:8380–8391.

Fraser G, Hartings JA, Simons DJ. 2006. Adaptation of trigeminal ganglion cells to periodic whisker deflections. Somatosens Mot Res. 23:111–118.

Ganmor E, Katz Y, Lampl I. 2010a. Intensity-Dependent Adaptation of Cortical and Thalamic Neurons Is Controlled by Brainstem Circuits of the Sensory Pathway. Neuron. 66:273–286.

Ganmor E, Katz Y, Lampl I. 2010b. Intensity-dependent adaptation of cortical and thalamic neurons is controlled by brainstem circuits of the sensory pathway. Neuron. 66:273–286.

Garcia-Lazaro JA, Ho SSM, Nair A, Schnupp JWH. 2007. Shifting and scaling adaptation to dynamic stimuli in somatosensory cortex. Eur J Neurosci. 26:2359–2368.

Gerdjikov TV, Bergner CG, Stüttgen MC, Waiblinger C, Schwarz C. 2010. Discrimination of Vibrotactile Stimuli in the Rat Whisker System: Behavior and Neurometrics. Neuron. 65:530–540.

Gescheider GA, Santoro KE, Makous JC, Bolanowski SJ. 1995. Vibrotactile forward masking: effects of the amplitude and duration of the masking stimulus. J Acoust Soc Am. 98:3188–3194.

Gilbert CD, Wiesel TN. 1979. Morphology and intracortical projections of functionally characterised neurones in the cat visual cortex. Nature. 280:120–125.

Gil Z, Connors BW, Amitai Y. 1999. Efficacy of Thalamocortical and Intracortical Synaptic Connections: Quanta, Innervation, and Reliability. Neuron. 23:385–397.

Goble AK, Hollins M. 1993. Vibrotactile adaptation enhances amplitude discrimination. J Acoust Soc Am. 93:418–424.

Gold JI, Shadlen MN. 2007. The Neural Basis of Decision Making. Annual Review of Neuroscience. 30:535–574.

Green DM, Swets JA. 1989. Signal Detection Theory and Psychophysics. Los Altos, Calif., USA: Peninsula Pub.

Grinvald A, Lieke E, Frostig RD, Gilbert CD, Wiesel TN. 1986. Functional architecture of cortex revealed by optical imaging of intrinsic signals. Nature. 324:361–364.

Guo ZV, Li N, Huber D, Ophir E, Gutnisky D, Ting JT, Feng G, Svoboda K. 2014. Flow of Cortical Activity Underlying a Tactile Decision in Mice. Neuron. 81:179–194.

Gutfreund Y. 2012. Stimulus-specific adaptation, habituation and change detection in the gaze control system. Biol Cybern. 106:657–668.

Hanks TD, Kopec CD, Brunton BW, Duan CA, Erlich JC, Brody CD. 2015. Distinct relationships of parietal and prefrontal cortices to evidence accumulation. Nature. advance online publication.

Harms L, Fulham WR, Todd J, Budd TW, Hunter M, Meehan C, Penttonen M, Schall U, Zavitsanou K, Hodgson DM, Michie PT. 2014. Mismatch Negativity (MMN) in Freely-Moving Rats with Several Experimental Controls. PLoS ONE. 9:e110892.

Hartings JA, Simons DJ. 2000. Inhibition suppresses transmission of tonic vibrissa-evoked activity in the rat ventrobasal thalamus. J Neurosci. 20:RC100.

Hartings JA, Temereanca S, Simons DJ. 2003. Processing of periodic whisker deflections by neurons in the ventroposterior medial and thalamic reticular nuclei. J Neurophysiol. 90:3087–3094.

Harvey MA, Saal HP, Dammann JF 3rd, Bensmaia SJ. 2013. Multiplexing Stimulus Information through Rate and Temporal Codes in Primate Somatosensory Cortex. PLoS Biol. 11:e1001558.

Hawken MJ, Shapley RM, Grosof DH. 1996. Temporal-frequency selectivity in monkey visual cortex. Visual Neuroscience. 13:477–492.

Hentschke H, Haiss F, Schwarz C. 2006. Central Signals Rapidly Switch Tactile Processing in Rat Barrel Cortex during Whisker Movements. Cerebral Cortex. 16:1142–1156.

Hershenhoren I, Taaseh N, Antunes FM, Nelken I. 2014. Intracellular Correlates of Stimulus-Specific Adaptation. J Neurosci. 34:3303–3319.

Higley MJ, Contreras D. 2007. Cellular Mechanisms of Suppressive Interactions Between Somatosensory Responses In Vivo. Journal of Neurophysiology. 97:647–658.

Hill DN, Mehta SB, Kleinfeld D. 2011. Quality metrics to accompany spike sorting of extracellular signals. J Neurosci. 31:8699–8705.

Hirata A, Aguilar J, Castro-Alamancos MA. 2009. Influence of subcortical inhibition on barrel cortex receptive fields. J Neurophysiol. 102:437–450.

Huber D, Petreanu L, Ghitani N, Ranade S, Hromádka T, Mainen Z, Svoboda K. 2008. Sparse optical microstimulation in barrel cortex drives learned behaviour in freely moving mice. Nature. 451:61–64.

Ikeda R, Cha M, Ling J, Jia Z, Coyle D, Gu JG. 2014. Merkel Cells Transduce and Encode Tactile Stimuli to Drive Aβ-Afferent Impulses. Cell. 157:664–675.

Imada A, Morris A, Wiest MC. 2012. Deviance detection by a P3-like response in rat posterior parietal cortex. Front Integr Neurosci. 6:127.

Jacobsen T, Schröger E. 2001a. Is there pre-attentive memory-based comparison of pitch? Psychophysiology. 38:723–727.

Jacobsen T, Schröger E. 2001b. Is there pre-attentive memory-based comparison of pitch? Psychophysiology. 38:723–727.

Jadhav SP, Wolfe J, Feldman DE. 2009. Sparse temporal coding of elementary tactile features during active whisker sensation. Nat Neurosci. 12:792–800.

Katz Y, Heiss JE, Lampl I. 2006. Cross-Whisker Adaptation of Neurons in the Rat Barrel Cortex. J Neurosci. 26:13363–13372.

Khatri V, Hartings JA, Simons DJ. 2004a. Adaptation in thalamic barreloid and cortical barrel neurons to periodic whisker deflections varying in frequency and velocity. J Neurophysiol. 92:3244–3254.

Khatri V, Hartings JA, Simons DJ. 2004b. Adaptation in Thalamic Barreloid and Cortical Barrel Neurons to Periodic Whisker Deflections Varying in Frequency and Velocity. J Neurophysiol. 92:3244–3254.

Kim J-N, Shadlen MN. 1999. Neural correlates of a decision in the dorsolateral prefrontal cortex of the macaque. Nat Neurosci. 2:176–185.

Klapoetke NC, Murata Y, Kim SS, Pulver SR, Birdsey-Benson A, Cho YK, Morimoto TK, Chuong AS, Carpenter EJ, Tian Z, Wang J, Xie Y, Yan Z, Zhang Y, Chow BY, Surek B, Melkonian M, Jayaraman V, Constantine-Paton M, Wong GK-S, Boyden ES. 2014. Independent optical excitation of distinct neural populations. Nat Meth. 11:338–346.

Kwegyir-Afful EE, Bruno RM, Simons DJ, Keller A. 2005. The role of thalamic inputs in surround receptive fields of barrel neurons. J Neurosci. 25:5926–5934.

Lak A, Arabzadeh E, Harris JA, Diamond ME. 2010. Correlated physiological and perceptual effects of noise in a tactile stimulus. Proc Natl Acad Sci USA. 107:7981–7986.

Landisman CE, Connors BW. 2007. VPM and PoM Nuclei of the Rat Somatosensory Thalamus: Intrinsic Neuronal Properties and Corticothalamic Feedback. Cereb Cortex. 17:2853–2865.

Laskin SE, Spencer WA. 1979. Cutaneous masking. I. Psychophysical observations on interactions of multipoint stimuli in man. J Neurophysiol. 42:1048–1060.

Leiser SC, Moxon KA. 2006. Relationship between physiological response type (RA and SA) and vibrissal receptive field of neurons within the rat trigeminal ganglion. J Neurophysiol. 95:3129–3145.

Loebel A, Nelken I, Tsodyks M. 2007. Processing of sounds by population spikes in a model of primary auditory cortex. Front Neurosci. 1:197–209.

Lumpkin EA, Marshall KL, Nelson AM. 2010. The cell biology of touch. J Cell Biol. 191:237–248.

Luna R, Hernández A, Brody CD, Romo R. 2005. Neural codes for perceptual discrimination in primary somatosensory cortex. Nat Neurosci. 8:1210–1219.

Malina KC-K, Jubran M, Katz Y, Lampl I. 2013. Imbalance between Excitation and Inhibition in the Somatosensory Cortex Produces Postadaptation Facilitation. J Neurosci. 33:8463–8471.

Malmierca MS, Cristaudo S, Pérez-González D, Covey E. 2009. Stimulus-specific adaptation in the inferior colliculus of the anesthetized rat. J Neurosci. 29:5483–5493.

Maravall M, Petersen RS, Fairhall AL, Arabzadeh E, Diamond ME. 2007. Shifts in Coding Properties and Maintenance of Information Transmission during Adaptation in Barrel Cortex. PLoS Biol. 5:e19.

May PJC, Tiitinen H. 2010. Mismatch negativity (MMN), the deviance-elicited auditory deflection, explained. Psychophysiology. 47:66–122.

Mayrhofer JM, Skreb V, Behrens W von der, Musall S, Weber B, Haiss F. 2013. Novel two-alternative forced choice paradigm for bilateral vibrotactile whisker frequency discrimination in head-fixed mice and rats. J Neurophysiol. 109:273–284.

Mayrhofer JM, Skreb V, von der Behrens W, Musall S, Weber B, Haiss F. 2013. Novel two-alternative forced choice paradigm for bilateral vibrotactile whisker frequency discrimination in head-fixed mice and rats. J Neurophysiol. 109:273–284.

Mease RA, Krieger P, Groh A. 2014. Cortical control of adaptation and sensory relay mode in the thalamus. PNAS. 111:6798–6803.

Meyer HS, Wimmer VC, Hemberger M, Bruno RM, Kock CPJ de, Frick A, Sakmann B, Helmstaedter M. 2010. Cell Type–Specific Thalamic Innervation in a Column of Rat Vibrissal Cortex. Cereb Cortex. 20:2287–2303.

Mill R, Coath M, Wennekers T, Denham SL. 2011. A Neurocomputational Model of Stimulus-Specific Adaptation to Oddball and Markov Sequences. PLoS Comput Biol. 7:e1002117.

Mill R, Coath M, Wennekers T, Denham SL. 2012. Characterising stimulus-specific adaptation using a multi-layer field model. Brain Res. 1434:178–188.

Minnery BS, Simons DJ. 2003. Response Properties of Whisker-Associated Trigeminothalamic Neurons in Rat Nucleus Principalis. Journal of Neurophysiology. 89:40–56.

Miyashita T, Shao YR, Chung J, Pourzia O, Feldman DE. 2013. Long-term channelrhodopsin-2 (ChR2) expression can induce abnormal axonal morphology and targeting in cerebral cortex. Front Neural Circuits. 7.

Mohar B, Katz Y, Lampl I. 2013. Opposite Adaptive Processing of Stimulus Intensity in Two Major Nuclei of the Somatosensory Brainstem. J Neurosci. 33:15394–15400.

Moore CI, Nelson SB, Sur M. 1999. Dynamics of neuronal processing in rat somatosensory cortex. Trends Neurosci. 22:513–520.

Morlet D, Fischer C. 2013. MMN and Novelty P3 in Coma and Other Altered States of Consciousness: A Review. Brain Topogr. 27:467–479.

Mountcastle VB, LaMotte RH, Carli G. 1972. Detection thresholds for stimuli in humans and monkeys: comparison with threshold events in mechanoreceptive afferent nerve fibers innervating the monkey hand. J Neurophysiol. 35:122–136.

Movshon JA, Lennie P. 1979. Pattern-selective adaptation in visual cortical neurones. Nature. 278:850–852.

Müller JR, Metha AB, Krauskopf J, Lennie P. 1999. Rapid adaptation in visual cortex to the structure of images. Science. 285:1405–1408.

Musall S, von der Behrens W, Mayrhofer JM, Weber B, Helmchen F, Haiss F. 2014. Tactile frequency discrimination is enhanced by circumventing neocortical adaptation. Nat Neurosci. 17:1567–1573.

Musall S, von Pföstl V, Rauch A, Logothetis NK, Whittingstall K. 2014. Effects of neural synchrony on surface EEG. Cereb Cortex. 24:1045–1053.

Näätänen R. 1992. Attention and Brain Function. Psychology Press.

Näätänen R. 2009. Somatosensory mismatch negativity: a new clinical tool for developmental neurological research? Dev Med Child Neurol. 51:930–931.

Näätänen R, Jacobsen T, Winkler I. 2005. Memory-based or afferent processes in mismatch negativity (MMN): a review of the evidence. Psychophysiology. 42:25–32.

Näätänen R, Paavilainen P, Rinne T, Alho K. 2007. The mismatch negativity (MMN) in basic research of central auditory processing: A review. Clinical Neurophysiology. 118:2544–2590.

Nakamura T, Michie PT, Fulham WR, Todd J, Budd TW, Schall U, Hunter M, Hodgson DM. 2011. Epidural Auditory Event-Related Potentials in the Rat to Frequency and duration Deviants: Evidence of Mismatch Negativity? Front Psychol. 2:367.

Nelken. 2007. Mismatch negativity and stimulus-specific adaptation in animal models. J Psychophysiol.

Nelken I. 2014. Stimulus-specific adaptation and deviance detection in the auditory system: experiments and models. Biol Cybern. 1–9.

Netser S, Zahar Y, Gutfreund Y. 2011. Stimulus-Specific Adaptation: Can It Be a Neural Correlate of Behavioral Habituation? J Neurosci. 31:17811–17820.

O'Connor DH, Hires SA, Guo ZV, Li N, Yu J, Sun Q-Q, Huber D, Svoboda K. 2013. Neural coding during active somatosensation revealed using illusory touch. Nat Neurosci. 16:958–965.

Ohzawa I, Sclar G, Freeman RD. 1982. Contrast gain control in the cat visual cortex. Nature. 298:266–268.

Ollerenshaw DR, Zheng HJV, Millard DC, Wang Q, Stanley GB. 2014. The Adaptive Trade-Off between Detection and Discrimination in Cortical Representations and Behavior. Neuron. 81:1152–1164.

Patterson CA, Wissig SC, Kohn A. 2014. Adaptation disrupts motion integration in the primate dorsal stream. Neuron. 81:674–686.

Pellicano E, Jeffery L, Burr D, Rhodes G. 2007. Abnormal Adaptive Face-Coding Mechanisms in Children with Autism Spectrum Disorder. Current Biology. 17:1508–1512.

Pettersen KH, Devor A, Ulbert I, Dale AM, Einevoll GT. 2006. Current-source density estimation based on inversion of electrostatic forward solution: Effects of finite extent of neuronal activity and conductivity discontinuities. Journal of Neuroscience Methods. 154:116–133.

Pincze Z, Lakatos P, Rajkai C, Ulbert I, Karmos G. 2001. Separation of mismatch negativity and the N1 wave in the auditory cortex of the cat: a topographic study. Clin Neurophysiol. 112:778–784.

Pinto DJ, Brumberg JC, Simons DJ. 2000. Circuit dynamics and coding strategies in rodent somatosensory cortex. J Neurophysiol. 83:1158–1166.

Rankin CH, Abrams T, Barry RJ, Bhatnagar S, Clayton D, Colombo J, Coppola G, Geyer MA, Glanzman DL, Marsland S, McSweeney F, Wilson DA, Wu C-F, Thompson RF. 2009.

Habituation Revisited: An Updated and Revised Description of the Behavioral Characteristics of Habituation. Neurobiol Learn Mem. 92:135–138.

Reches A, Netser S, Gutfreund Y. 2010. Interactions between Stimulus-Specific Adaptation and Visual Auditory Integration in the Forebrain of the Barn Owl. J Neurosci. 30:6991–6998.

Ritt JT, Andermann ML, Moore CI. 2008. Embodied Information Processing: Vibrissa Mechanics and Texture Features Shape Micromotions in Actively Sensing Rats. Neuron. 57:599–613.

Romo R, Hernández A, Zainos A, Salinas E. 1998. Somatosensory discrimination based on cortical microstimulation. Nature. 392:387–390.

Roy NC, Bessaih T, Contreras D. 2011. Comprehensive mapping of whisker-evoked responses reveals broad, sharply tuned thalamocortical input to layer 4 of barrel cortex. Journal of Neurophysiology. 105:2421–2437.

Sachidhanandam S, Sreenivasan V, Kyriakatos A, Kremer Y, Petersen CCH. 2013. Membrane potential correlates of sensory perception in mouse barrel cortex. Nat Neurosci. 16:1671–1677.

Salinas E, Hernández A, Zainos A, Romo R. 2000. Periodicity and Firing Rate As Candidate Neural Codes for the Frequency of Vibrotactile Stimuli. J Neurosci. 20:5503–5515.

Sams M, Alho K, Näätänen R. 1984. Short-term habituation and dishabituation of the mismatch negativity of the ERP. Psychophysiology. 21:434–441.

Sanchez-Vives MV, Nowak LG, McCormick DA. 2000. Cellular Mechanisms of Long-Lasting Adaptation in Visual Cortical Neurons In Vitro. J Neurosci. 20:4286–4299.

Schwarz C, Hentschke H, Butovas S, Haiss F, Gerdjikov MCSTV, Bergner CG, Waiblinger C. 2010. The head fixated behaving rat - procedures and pitfalls. Somatosensory and Motor Research. 27:131–148.

Sherman SM. 2001. Tonic and burst firing: dual modes of thalamocortical relay. Trends in Neurosciences. 24:122–126.

Simons DJ, Carvell GE. 1989. Thalamocortical response transformation in the rat vibrissa/barrel system. J Neurophysiol. 61:311–330.

Squires NK, Squires KC, Hillyard SA. 1975a. Two varieties of long-latency positive waves evoked by unpredictable auditory stimuli in man. Electroencephalogr Clin Neurophysiol. 38:387–401.

Squires NK, Squires KC, Hillyard SA. 1975b. Two varieties of long-latency positive waves evoked by unpredictable auditory stimuli in man. Electroencephalogr Clin Neurophysiol. 38:387–401.

Stefanics G, Kremláček J, Czigler I. 2014. Visual mismatch negativity: a predictive coding view. Front Hum Neurosci. 8:666.

Strömmer JM, Tarkka IM, Astikainen P. 2014. Somatosensory mismatch response in young and elderly adults. Front Aging Neurosci. 6:293.

Stüttgen MC, Schwarz C. 2010. Integration of Vibrotactile Signals for Whisker-Related Perception in Rats Is Governed by Short Time Constants: Comparison of Neurometric and Psychometric Detection Performance. The Journal of Neuroscience. 30:2060–2069.

Sussman ES, Shafer VL. 2014. New perspectives on the mismatch negativity (MMN) component: an evolving tool in cognitive neuroscience. Brain Topogr. 27:425–427.

Szymanski FD, Garcia-Lazaro JA, Schnupp JWH. 2009. Current Source Density Profiles of Stimulus-Specific Adaptation in Rat Auditory Cortex. Journal of Neurophysiology. 102:1483–1490.

Taaseh N, Yaron A, Nelken I. 2011. Stimulus-Specific Adaptation and Deviance Detection in the Rat Auditory Cortex. PLoS ONE. 6:e23369.

Talbot WH, Darian-smith I, H H, Mountcastle VB. 1968. The sense of flutter-vibration: Comparison of the human capacity with response patterns of mechanoreceptive afferents from the monkey hand. Journal of Neurophysiology. 301–304.

Tannan V, Holden JK, Zhang Z, Baranek GT, Tommerdahl MA. 2008. Perceptual metrics of individuals with autism provide evidence for disinhibition. Autism Research. 1:223–230.

Tannan V, Simons S, Dennis RG, Tommerdahl M. 2007. Effects of adaptation on the capacity to differentiate simultaneously delivered dual-site vibrotactile stimuli. Brain Research. 1186:164–170.

Tannan V, Whitsel BL, Tommerdahl MA. 2006. Vibrotactile adaptation enhances spatial localization. Brain Res. 1102:109–116.

Temereanca S, Brown EN, Simons DJ. 2008. Rapid Changes in Thalamic Firing Synchrony during Repetitive Whisker Stimulation. J Neurosci. 28:11153–11164.

Tervaniemi M, Maury S, Näätänen R. 1994. Neural representations of abstract stimulus features in the human brain as reflected by the mismatch negativity. Neuroreport. 5:844–846.

Thompson RF. 2009. Habituation: a history. Neurobiol Learn Mem. 92:127–134.

Todd J, Harms L, Schall U, Michie PT. 2013. Mismatch negativity: translating the potential. Front Psychiatry. 4:171.

Tommerdahl M, Hester KD, Felix ER, Hollins M, Favorov OV, Quibrera PM, Whitsel BL. 2005. Human vibrotactile frequency discriminative capacity after adaptation to 25 Hz or 200 Hz stimulation. Brain Res. 1057:1–9.

Trevelyan AJ, Jack J. 2002. Detailed passive cable models of layer 2/3 pyramidal cells in rat visual cortex at different temperatures. J Physiol (Lond). 539:623–636.

Ulanovsky N, Las L, Farkas D, Nelken I. 2004. Multiple Time Scales of Adaptation in Auditory Cortex Neurons. J Neurosci. 24:10440–10453.

Ulanovsky N, Las L, Nelken I. 2003. Processing of low-probability sounds by cortical neurons. Nat Neurosci. 6:391–398.

Umbricht D, Krljes S. 2005. Mismatch negativity in schizophrenia: a meta-analysis. Schizophrenia Research. 76:1–23.

Umbricht D, Vyssotki D, Latanov A, Nitsch R, Lipp H-P. 2005. Deviance-related electrophysiological activity in mice: is there mismatch negativity in mice? Clinical Neurophysiology. 116:353–363.

Von der Behrens W, Bäuerle P, Kössl M, Gaese BH. 2009. Correlating Stimulus-Specific Adaptation of Cortical Neurons and Local Field Potentials in the Awake Rat. J Neurosci. 29:13837–13849.

Von Heimendahl M, Itskov PM, Arabzadeh E, Diamond ME. 2007. Neuronal Activity in Rat Barrel Cortex Underlying Texture Discrimination. PLoS Biol. 5:e305.

Waiblinger C, Brugger D, Schwarz C. 2013. Vibrotactile Discrimination in the Rat Whisker System is Based on Neuronal Coding of Instantaneous Kinematic Cues. Cereb Cortex. bht305.

Wang Q, Webber RM, Stanley GB. 2010. Thalamic synchrony and the adaptive gating of information flow to cortex. Nat Neurosci. 13:1534–1541.

Wark B, Lundstrom BN, Fairhall A. 2007. Sensory adaptation. Curr Opin Neurobiol. 17:423–429.

Wichmann FA, Hill NJ. 2001. The psychometric function: I. Fitting, sampling, and goodness of fit. Perception & Psychophysics. 63:1293–1313.

Wilson DA. 1998. Synaptic Correlates of Odor Habituation in the Rat Anterior Piriform Cortex. J Neurophysiol. 80:998–1001.

Wolfe J, Hill DN, Pahlavan S, Drew PJ, Kleinfeld D, Feldman DE. 2008. Texture Coding in the Rat Whisker System: Slip-Stick Versus Differential Resonance. PLoS Biol. 6:e215.

Yang H, O'Connor DH. 2014. Cortical adaptation and tactile perception. Nat Neurosci. 17:1434–1436.

Yaron A, Hershenhoren I, Nelken I. 2012. Sensitivity to Complex Statistical Regularities in Rat Auditory Cortex. Neuron. 76:603–615.

Yppärilä H, Karhu J, Westerén-Punnonen S, Musialowicz T, Partanen J. 2002. Evidence of auditory processing during postoperative propofol sedation. Clin Neurophysiol. 113:1357–1364.

Yu X-J, Xu X-X, He S, He J. 2009. Change detection by thalamic reticular neurons. Nat Neurosci. 12:1165–1170.

Zhang F, Wang L-P, Boyden ES, Deisseroth K. 2006. Channelrhodopsin-2 and optical control of excitable cells. Nat Meth. 3:785–792.

Curriculum vitae

Personal information

Name	MUSALL
Forename	Simon
Date of birth	07.04.1985
Place of birth	Reutlingen
Nationality	German

Education

Since December 2010

PhD student in the lab of Prof. Fritjof Helmchen, Brain Research Institute, UZH Zürich

February 2009 – December 2010

Diploma student in the lab of Prof. Nikos Logothetis, Max Planck Institute for Biological Cybernetics, Tübingen, Germany

August 2007 – December 2008

Research assistant in the lab of Prof. Heinrich Bülthoff, Max Planck Institute for Biological Cybernetics, Tübingen, Germany

October 2004 – September 2010

Diploma in biology with a focus on neurophysiology, Eberhard-Karls-University Tübingen

April 2004

Matura (Abitur) at the Wildermuth-Gymnasium Tübingen

Publications

Articles

Musall S., vd Behrens W., Mayrhofer J., Weber B., Helmchen F. and Haiss F., "Tactile frequency discrimination is enhanced by circumventing neocortical adaptation." Nature Neuroscience (*September 21, 2014*).

Mayrhofer J., Skreb V., vdBehrens W., Musall S., Weber B. and Haiss F., "Novel Two-Alternative Forced Choice Paradigm for Bilateral Vibrotactile Whisker Frequency Discrimination in Head-Fixed Mice and Rats." Journal of Neurophysiology (*January 1, 2013*)

Musall S., vPfostl V., Rauch A., Logothetis N. K., and Whittingstall K., "Effects of Neural Synchrony on Surface EEG." Cerebral Cortex (*December 12, 2012*).

Oral presentations

"Sensory versus optogenetic stimulation of somatosensory cortex"
LS2 – Life Sciences Switzerland, Annual Meeting; Zürich, Switzerland *January 2015*

"Somatosensory stimulus perception is shaped by neocortical response adaptation"
Barrels XXVI, Annual meeting on barrel cortex function; La Jolla, USA *November 2013*

"Impact of response adaptation on stimulus perception
Institute for Brain Research, Ph.D. Symposium; Zürich, Switzerland *February 2013*

"Direct cortical stimulation improves frequency-discrimination in rodents"
INI – Hifo Symposium; Zürich, Switzerland *July 2012*

"Optogenetic control of neural activity in task-performing rodents"
Institute for Brain Research, Ph.D. Symposium; Zürich, Switzerland *February 2012*

Acknowledgements

I would like to express my most sincere gratitude to Professor Fritjof Helmchen for giving me the opportunity to work in an outstanding scientific environment, his support and valuable criticism as well as openness towards new questions and experimental approaches. In particular, I want to thank him for his personal interest and taking the time to ensure my academic success and the successful completion of my doctoral thesis.

I especially want to thank Professor Bruno Weber, who allowed me to spend a very valuable time in his exceptional lab and for his continuing support over the course of the project and beyond. Special thanks also to Dr. Florent Haiss for valuable discussions and his efforts to get me started in my PhD.

Many thanks also to my great collaborators, especially Dr. Wolfger von der Behrens for his invaluable help, great discussions and reliably sponsoring food and drinks in the middle of the night. I also thank Dr. Johannes Mayrhofer for his valuable advice and being a great colleague, Stefano Carta for being so very helpful in the beginning of my PhD, my amazing students Melek Durmaz and Colette Steinegger and to all those who helped to realize this project.

This work would not have been possible without the technical help and resourcefulness of Stefan Weber, Stefan Giger and the ingenious Fabian Voigt.

Also many thanks to all the members of the Helmchen and Weber labs and to all those who I should have but failed to mention.

Lastly, I thank my family for all their love and support. In particular, I would like thank my wonderful wife and daughter for the cheer and laughter and for reminding me to keep my head high in challenging times.